Two- and Three-Phase Flow Functions for Numerical Simulation of EOR Processes

Amir Jahanbakhsh
BSc., MSc.

Submitted for the degree of Doctor of Philosophy

Petroleum Engineering

Heriot-Watt University
School of Energy, Geoscience, Infrastructure and Society
Institute of Petroleum Engineering

June 2016

ABSTRACT

The understanding of governing mechanisms of multi-phase (oil, water, and gas) flow in porous media is of keen interest in petroleum and environmental engineering. In the petroleum engineering context, three-phase flow occurs in several important processes including in enhanced oil recovery (EOR). Recovery of a significant amount of the residual oil in reservoirs after primary recovery and secondary recovery (waterflooding) is important in order to tackle the increasing demand for the energy. EOR methods mainly involve two and three-phase flow in the reservoir. Relative permeability (k_r) and capillary pressure (P_c) are two important parameters in multiphase flow which describe the interaction of each fluid in porous media. The importance of these flow functions will be even more significant for three-phase flow systems.

This thesis attempts to address three key issues.

(i) Improved determination of multi-phase flow functions (k_r and P_c).

(ii) The impact of parameters affecting flow functions.

(iii) Prediction of multi-phase flow functions.

Relative permeability (k_r) can be measured in the laboratory using steady-state and unsteady-state methods, or estimated by mathematical correlations and pore-network models. As multi-phase flow experiments and in particular steady-state measurements are very time consuming and expensive, more often the unsteady-state method is used for multi-phase k_r measurements. In this thesis, a methodology has been devised for calculating k_r values and in particular three-phase k_r from unsteady-state experiments. The effort was extended to simultaneously calculating P_c from the same coreflood experiment.

There are different physical parameters which can affect flow functions. The effect of gas/oil interfacial tension ($IFT_{g/o}$) on two and three-phase k_r and also on residual saturation during alternative water and gas injections has also been studied.

Finally, two-phase k_r have been estimated for rock and fluid conditions where there is no previous data. This has been achieved by taking data from different conditions under which measurements were made.

DEDICATION

To my beloved wife and parents,

for their constant love, support and inspiration.

ACKNOWLEDGMENTS

This work would never be possible without the support and collaboration I found within the Centre for Enhanced Oil Recovery and CO_2 Solutions. First of all, I would like to express my profound gratitude to Prof. Mehran Sohrabi for providing me the opportunity, financial support and encouragement throughout my study. Your office was always open when I had any question or concern. I am also thankful to Dr. Hamidreza Shahverdi who was my second supervisor during the first year of my study before he left to Isfahan University of Technology. I am most grateful for your invaluable guidance and all the constructive discussions and also for supporting me and my family when we arrived in Edinburgh. Many thanks go to Prof. Dabir Tehrani for his practical comments, positive criticism and encouragement. I was very lucky to get to know Dr. Ahmed Elsheikh. Thank you for sharing your knowledge and expertise in application of ensemble-based optimization algorithms and also for helping me to build a collaborative research work. A big thanks to Dr. Gillian Pickup and Prof. Fabio Inzoli for accepting to be my examiners and for your invaluable comments.

During my PhD I was fortunate enough to work with other academic staff. Prof. Mahmoud Jamiolahmady, thank you for believing in my well testing expertise and providing me the opportunity to work as a tutor and marker for your Well Testing course. Prof. Eric Mackay and Dr. Karl Stephen, I have learned a lot from the ECLIPSE tutorials for Reservoir Simulation course. Dr. Asghar Shams, I have gained a great deal of knowledge from tutorials for Formation Evaluation course. Thank you all for letting me to be part of the support team for these tutorials.

Thanks to the IPE computer support for providing me with all softwares needed to do my research study. Special thanks to Debbie Ross for all her administrative supports. Thanks to the International Student Advisors Office for their help with visa applications and the career advisers for helpful tips.

Special thanks go to my friends and colleagues at the Centre for Enhanced Oil Recovery and CO_2 Solutions; Hassan Alzayer, Omid Shahrokhi, Usman Taura, Shokoufeh Aghabozorgi, Juliana Facanha, Pedram Mahzari, S. Amir Farzaneh, Mehdi Seyyedsar, Mojtaba Seyyedi, Bruno Pereira, Bashir Alkhazmi, Latifa Al-Nuaimi, Mohamed AlHammadi, Ali Almesmari, Odilla Vilhena, Adel Traki, Shaun Ireland, Kamran Ahmed, and Pantelis Tsolis. Thanks are also extended to my friends at Heriot-Watt

University; Ehsan Nikjoo, Mohammadreza Ameri, Rasoul Nazari Moghadam, Mohsen Hoopanah, Saeed Ghanbari, Edris Joonaki, Eltazy Khalid, S. Ramin Mousavi, Reza Haghi, Morteza AminNaji, Morteza Haghighat Sefat, Saleh Godarzian, Mojtaba Moradi, Caroline Johnson, Houra Mozaffar, Hamidreza Nasriani, Khosro Jarrahian, Pezhman Ahmadi, Mahmoud Nazeri, Michael Wise, Payam Alikhani, Aliakbar Hassanpour, Masoud Ghaderi, Dennis Obidegwu, Christian Onwunyili, Misfer Almarri, and Ibrahim Abdulwahab. Special appreciation also goes to those who left the University, Jalal Foroozesh, Jalal Fahimpour, S. Mobeen Fatemi, Yousef Rafiei, Hamid Bazargan, S. Mohamad Shariatipour, Heron Gachuz, Reza Felahat, Reza Malakooti, Babak Zarei, Saeed Mazloom, Mohamed Ahmed, Gamal Alusta and Mustafa Lamorde.

My beloved wife, your support was infinite! I simply can’t thank you enough for your endless support, patience, love, and encouragement. Special thanks to my son, Ali, for his understanding, constant love and support. I am heavily indebted to my parents for their love, care and support. Without them, I would have achieved nothing. My hope, is to make you happy and be pleased with me.

ACADEMIC REGISTRY
Research Thesis Submission

Name*:*	AMIR JAHANBAKHSH		
School/PGI:	EGIS/Institute of Petroleum Engineering		
Version: *(i.e. First, Resubmission, Final)*	Final	Degree Sought (Award **and** Subject area)	Ph.D. in Petroleum Engineering

Declaration

In accordance with the appropriate regulations I hereby submit my thesis and I declare that:

1) the thesis embodies the results of my own work and has been composed by myself
2) where appropriate, I have made acknowledgement of the work of others and have made reference to work carried out in collaboration with other persons
3) the thesis is the correct version of the thesis for submission and is the same version as any electronic versions submitted*.
4) my thesis for the award referred to, deposited in the Heriot-Watt University Library, should be made available for loan or photocopying and be available via the Institutional Repository, subject to such conditions as the Librarian may require
5) I understand that as a student of the University I am required to abide by the Regulations of the University and to conform to its discipline.

* *Please note that it is the responsibility of the candidate to ensure that the correct version of the thesis is submitted.*

Signature of Candidate*:*		Date:	

Submission

Submitted By *(name in capitals):*	
Signature of Individual Submitting:	
Date Submitted:	

For Completion in the Student Service Centre (SSC)

Received in the SSC by *(name in capitals):*			
Method of Submission *(Handed in to SSC; posted through internal/external mail):*			
E-thesis Submitted (***mandatory for final theses)***			
Signature:		Date:	

Please note this form should bound into the submitted thesis.

Updated February 2008, November 2008, February 2009, January 2011

TABLE OF CONTENTS

LISTS OF FIGURES

LIST OF PUBLICATIONS

The research material in this thesis was part of the research program of a joint industry project (JIP) referred to as "Improved Characterization of Two- and Three-Phase Flow for Reliable Reservoir Performance Prediction". The results of this research have been reported, presented and discussed every six months in the corresponding steering committee meetings during Sep.2012-April.2016.

Furthermore, parts of the results of this study have been submitted as technical papers in different international conferences and peer-reviewed journals.

A list of these publications is as follows:

- **Jahanbakhsh, A.**, Shahverdi, H. & Sohrabi, M. (2016): "Gas/Oil Relative Permeability Normalization- Effect of Permeability, Wettability and Interfacial tension", SPE Reservoir Evaluation & Engineering-Formation Evaluation, SPE-170796-PA. http://dx.doi.org/10.2118/170796-PA.

- **Jahanbakhsh, A**., Sohrabi, M., Fatemi, S. M. and Shahverdi, H. (2016): "A Comparative Study of the Effect of Gas/Oil IFT Variation on Two- and Three-Phase Relative Permeability and the Performance of WAG Injection at Laboratory Scale", SPE-179571-MS, SPE Improved Oil Recovery Conference, Tulsa, Oklahoma 2016. http://dx.doi.org/10.2118/179571-MS.

- **Jahanbakhsh, A.,** and Sohrabi, M. (2015): "A New Approach for Simultaneous Estimation of Relative Permeability and Capillary Pressure from Coreflood Experiments", SPE-175068-MS, Paper presented at the SPE Annual Technical Conference and Exhibition, Houston, Texas 2015. http://dx.doi.org/10.2118/175068-MS.

  Jahanbakhsh, A., Shahverdi, H. and Sohrabi, M. (2014): "Relative Permeability Normalization- Effect of Permeability, Wettability and Interfacial tension", SPE-170796-MS, Paper presented at the SPE Annual Technical Conference and Exhibition, Amsterdam 2014. http://dx.doi.org/10.2118/170796-MS.

- **Jahanbakhsh, A**., El Sheikh, A. and Sohrabi, M., (2016): "Application of Ensemble Smoother and Multiple-Data Assimilation for Estimating Relative Permeability from Coreflood Experiments", accepted for the 15th European Conference on the Mathematics of Oil Recovery (ECMOR XV), Amsterdam 2016.

Chapter 1– Introduction

Multi-phase flow and in particular three-phase flow in porous media is one of the very active research areas in both petroleum and environmental engineering. In the oil industry, two- and three-phase flow occurs in secondary recovery and Enhanced Oil Recovery (EOR) processes including waterflooding, gas injection, tertiary gas injection, water alternating gas injection, depressurization below the bubble point, gas cap expansion, solution gas drive, gravity drainage, steam injection and thermal flooding. In the environmental engineering context, multi-phase flow occurs when a non-aqueous phase liquid (NAPL) flows simultaneously with water and air through soils and also CO_2 storage in aquifers and geological formations.

In the petroleum engineering context, recovery of a significant amount of the residual oil in reservoirs after primary recovery and secondary recovery is important in order to tackle the growing world's demand for the energy. Therefore, there is a need to seek means of recovering more of the residual oil left in the reservoirs. Hence, several EOR techniques have been developed to recover economically a significant portion of this residual oil which maybe around 40 to 60% of the original oil in place. The majority of these methods mainly involve two and three-phase flow at different parts of the reservoir. Some of these methods have sequential drainage and imbibition processes such as Water-Alternating-Gas (WAG) injection which add the effect of hysteresis to the complexity of the fluid flow behaviour. Relative permeability (k_r) and capillary pressure (P_c) are two critical parameters in multiphase flow which describe the interaction of each fluid in porous media. The importance of these flow functions will be even more significant for three-phase flow systems. These are the input parameters to the reservoir simulation for modelling the fluid flow in porous media, history matching the recovery mechanisms and predicting the future performance of the reservoirs.

Extensive laboratory measurements and modelling efforts have been performed in two-phase flow area for several decades, but that is not the case for three-phase relative permeability (k_r). The fewer efforts in three-phase flow are mainly because three-phase flow experiments, and in particular steady-state measurements, are very complicated, labour intensive, time-consuming and expensive. Furthermore, the presence of three fluid phases at the same time, means two independent fluid saturations, produces an infinite number of saturation paths as possible candidates for fluid flow study and k_r

measurements. Therefore, it is not practical to measure k_r for all possible three-phase saturation paths.

Traditionally, two-phase relative permeabilities are measured in a Special Core Analysis (SCAL) program for some available core samples. Although this practice has been established in the oil and gas industry, it is still impractical to measure two-phase relative permeabilities for hundreds of core samples to cover difference regions of a reservoir or a field. Plausible and robust methods are required to estimate relative permeabilities for the regions where no core sample or measurement is available. The effect of different parameters such as absolute permeability, wettability, interfacial tension (IFT) on k_r should be properly included in such a predictive method. The k_r and P_c curves are conventionally measured separately and sometimes even from two different core samples. Capillary pressure is measured by: mercury porosimetry, the porous plate method or by the centrifuge method. Using these methods, P_c is measured at equilibrium conditions and it can be called static P_c. The equilibrium conditions may not be achievable during multi-phase flow in porous media. The fluid flow is a dynamic process, and there has been a question around the application of static P_c for modeling of this process. Moreover, it is not known whether there are any differences between static and dynamic P_c. Therefore, the simultaneous estimation of k_r and P_c from coreflood experiments to obtain dynamic P_c has gained more interest.

In the last three decades, more attentions has been paid to three-phase flow mechanisms and specially three-phase relative permeability. Leverett and Lewis (1941) measured the first three-phase relative permeabilities using the steady-state method. Alizadeh and Piri (2014) reviewed experimental studies on three-phase k_r since 1980.These studies were involved with investigating the effect of wettability, IFT, spreading, oil layer drainage and saturation history on three-phase flow functions. Some of these studies are highlighted in the following paragraphs.

A example of a research study on the effect of wettability at three-phase flow conditions is the extensive work by Oak (1990). He measured steady-state three-phase k_r for different wettability conditions of water-wet, oil-wet and intermediate-wet on Berea sandstone cores. DiCarlo et al. (1998) studied three-phase flow in sand packs for three wettability conditions of water-wet, oil-wet, and fractionally-wet. They used a CT scanning method to measure the oil and water relative permeabilities.

A limited number of studies have investigated the impact of IFT on three-phase relative permeabilities. Delshad et al. (1987) measured steady-state two- and three-phase k_r for low IFT mixture of brine/oil/surfactant/alcohol in Berea sandstone cores. Dria et al. (1993) reported steady-state three phase CO_2/oil/brine relative permeabilities in a water-wet dolomite core. Cinar and Orr (2004) and Cinar and Orr (2005) investigated the effect of IFT reduction on three-phase relative permeabilities for water-wet wettability condition using three-phase analogous liquid systems. Cinar et al. (2004) and (2007) reported three-phase k_r measurements that included the combined effects of IFT variation and wettability.

A research study on characterization of three-phase flow in porous media was initiated in 1997 at Heriot-Watt University. The experimental research work was started using micro-models. An extensive list of micromodel experiments in two-phase and mainly three-phase flow in the form of WAG injections were performed at different wettability conditions (water-wet, mixed-wet and oil-wet). The results of these micromodel experiments showed that the residual oil saturation to secondary water flooding or secondary gas injection decreases at three-phase flow conditions. Therefore, the experimental study was extended to the core scale displacement experiments (Sohrabi et al. (2000, 2005 and 2008)). The coreflood studies started with series of two-phase displacement experiments in water-wet and mixed-wet 1000 mD Clashach sandstone core at high (2.7 mNm^{-1}) and very low (0.04 mNm^{-1}) IFT conditions (Sohrabi et al. (2007)). A series of three-phase flow and WAG injections was performed on 1000 mD mixed-wet core at the IFT above values. The next set of coreflood experiments was conducted on 65 mD Clashach sandstone core. Similar to the 1000 mD corefloods, two different wettability of water-wet and mixed-wet and different gas/oil IFT conditions were considered in these series of experiments. In summary, the effect of rock permeability, wettability, and gas/oil IFT conditions were studied for two- and three-phase flow systems (Fatemi et al. (2011, 2012 and 2015)).

As it was mentioned before, it is not practical to measure k_r for all possible three-phase saturation paths. Furthermore, for the purpose of numerical simulation, it is preferred to have a correlation to estimate the three-phase relative permeabilities accurately. Stone (1970) introduced a probability method which uses two-phase k_r data for oil/water and gas/oil systems to predict the three-phase oil relative permeability. In 1973, Stone modified his first models by including two-phase gas and water k_r into the formulation. Both models were proposed for water-wet systems and assuming water and gas relative

permeabilities are only function of their saturations. Modification to the Stone's first model was suggested by Hustad and Holt (1992). They introduced an exponent to the saturation term of the correlation and used that exponent as a tuning parameter to obtain a better match between results of their numerical simulation and experiment.

Baker (1988) proposed an interpolation method to calculate three-phase k_r for all three phases (oil, water, and gas) using two-phase k_r data. In his method, three-phase k_r of each phase is assumed to be a function of saturations of two other phases. Hustad and Hansen (1995), proposed a model for three-phase relative permeabilities which had the basis of Baker's model. Later, Hustad and Browning (2010) proposed a formulation to calculate three-phase k_r and P_c and account for hysteresis for compositional simulation. Blunt (2000) introduced a model based on saturation-weighted interpolation between the two-phase relative permeabilities. The special feature of this model is accounting for oil layer drainage in the calculation of relative permeability. Other different models have been developed to predict three-phase k_r from two-phase k_r data, such as Jerauld (1997) and UTKR3P (2013).

Delshad et al. (1987); Delshad and Pope (1989), Pejic and Maini (2003), Petersen et al. (2008) and some other researchers have undertaken studies to evaluate the performance of the existing three-phase k_r models in predicting k_r values. The common conclusion from these assessment studies is that none of the models can predict the measured three-phase relative permeabilities from different sources. These studies showed that the three-phase k_r models are not capable of accounting for the effect of different wettability, interfacial tension, and saturation directions. Therefore, an extensive bank of three-phase experimental data and k_r is required to characterize three-phase flow in porous media and propose a robust predictive three-phase k_r model.

It is worth mentioning that the concept of P_c is still an ambiguous subject in three-phase flow systems, and more research should be performed to shed light on this area.

The general theme of the thesis is a characterization of multiphase flow in porous media. The overall purpose is to address some issues in two- and three-phase flow systems which are still outstanding. This research was carried out alongside extensive experimental research studies. The objective of the research is to (*i*) develop a methodology and a computer program to estimate flow functions (k_r and P_c) from the two- and three-phase coreflood experiments, (*ii*) Secondly, by having the developed program there is a facility to estimate k_r for different phases in multiphase flow

conditions and to characterize this flow function, (*iii*) as it is not always possible to perform either steady-state or unsteady state coreflood experiments for the purpose of measuring relative permeability, a normalization technique was introduced, evaluated and improved in order to estimate a k_r curve from already measured k_r curves obtained from another rock which might have different rock permeability, wettability and IFT conditions.

1.1. Structure of the Thesis

Chapter 1&2- The first chapter of the thesis highlights the motivations behind this work and introduces different aspects of the performed research study. The second chapter presents the experimental procedures and the facilities used in the Centre for Enhanced Oil Recovery and CO_2 Solutions at Heriot-Watt University for performing the coreflood preparations and experiments. The hydrocarbon fluids and brine and also rock properties are summarized. Different preparation procedures including establishing initial water saturation and alternating wettability to mixed-wet wettability have been elaborated in detail.

Chapter 3- This chapter is devoted to highlighting the importance of measuring three-phase k_r curves. We explain the methodology of estimating this flow function from measured unsteady-state coreflood experiments (two- and three-phase) results. Usually, the recovery of different phases and pressure drop across the core are measured during an experiment. The most common explicit method to calculate k_r from the measured results is the Johnson–Bossler–Naumann (JBN) method (Johnson et al. (1959)). In the implicit or parameter estimation method, k_r values are estimated using history matching technique. A functional form of k_r containing tuning parameters is selected for each phase, and an advanced optimization technique is used to match the experimental data to the simulation results. The process of history matching is an iterative process, and it is repeatedly attempted by changing the tuning parameters within the functional form of k_r until the closest match is obtained. The implicit method has been selected for estimating k_r and by using MATLAB a computer program developed and Genetic Algorithm implemented as the non-linear global optimizer. This program can estimate two- and three-phase k_r curves from two- and three-phase unsteady state coreflood experiments respectively.

Chapter 4- Chapter 4 is dedicated to simultaneous estimation of two critical flow functions of k_r and P_c from unsteady state coreflood experiments. These two flow

functions have been conventionally measured separately, and the measurements are not usually performed on the same rock sample. The drawback to determining k_r and P_c separately is that they may not be consistent with each other, and the measured P_c does not correspond to the k_r which is measured from a dynamic flow system. Therefore, simultaneous determination of P_c and k_r for a given system would be preferred. History matching techniques have been applied to estimate k_r and P_c simultaneously from unsteady state coreflood experiments. Some in-situ measurements such as saturation and pressure profiles may be included in the history matching data to reduce the associated non-uniqueness problem of history matching, but this information is rarely available. Conventionally, two independent functions were used to generate these two flow functions in the process of the history matching. A new methodology has been developed to honour a known relationship between the core k_r and the P_c curve and to improve the optimization process and the accuracy of the estimated P_c and k_r. Making the k_r function dependent on the P_c in the history matching process will reduce the number of tuning parameters and is expected to reduce the uncertainty associated with the history matching process.

Chapter 5- The effect of gas/oil IFT on two- and three-phase relative permeabilities has been studied in Chapter 5. Firstly we investigated the effects of gas/oil IFT reduction on two- and three-phase relative permeabilities according to the literature and the results of our experimental studies on 65 and 1000 mD cores at three different gas/oil IFT values of 0.04, 0.15 and 2.7 $mN.m^{-1}$. We used the developed computer program to estimate two- and three-phase relative permeabilities from the results of coreflood experiments. The general perception is that the IFT reduction results in an increase in k_r of existing phases at each saturation value. A significant amount of studies have been performed on the two-phase systems and although there is no single conclusion but more insight has been gained on the effect of IFT reduction on the two-phase k_r. However, for the three-phase system, there is still a long journey to take in, to appreciably understand and model the effect of IFT change on the three-phase k_r. The Second objective is to evaluate the frequently used Coats IFT scaling method against our two-phase experimental data. The common practice is that the two-phase k_r is usually measured at high IFT values and for simulating a process that has to change IFT value, towards miscible conditions, a modification is applied to the high IFT k_r data to calculate their value at lower values of IFT. Application of this method has been evaluated for two-phase data.

Chapter 6-The objective of Chapter 6 is to predict the gas/oil k_r for new rock/fluid conditions (i.e., permeability, wettability, IFT) using existing gas/oil k_r data measured at different conditions. Using measured data from coreflood experiments, we showed that by applying an appropriate normalization technique, one can adequately predict k_r of rocks with different permeability and wettability conditions in two-phase gas/oil flow. However, the results showed that the effect of IFT change cannot be captured by normalization techniques. A new hypothesis has been introduced and proposed here based on Dynamic Trap Saturation to improve the methodology. Finally, the aim is to devise ways and means of estimating relative permeabilities, using available k_r data of one set of rocks and relevant fluid conditions, for different rocks and conditions. We have measured two-phase gas/oil k_r for two Clashach sandstone cores with similar pore size distribution and absolute permeability of 65 and 1000 mD, under mixed-wet and water-wet conditions, with low and high gas/oil IFT.

Chapter 7- Finally in Chapter 7 the conclusions drawn from this research study are summarized. Moreover, recommendations for further and future works in the relevant research areas are presented.

1.2. References

Alizade, A. H. and Piri, M., 2014. Three-Phase Flow in Porous Media: A Review of Experimental Studies on Relative Permeability. Reviews of Geophysics, 2013RG000433.

Baker, L.E., 1988. Three-Phase Relative Permeability Correlations, paper SPE 17369, presented at the SPE Enhanced Oil Recovery Symposium, Tulsa, Oklahoma.

Beygi, M. R., Delshad, M., Pudugramam, V. S., Pope, G. A. and Wheeler, M. F., 2013. A New Approach to Model Hysteresis and Its Impact on CO2-EOR Processes with Mobility Control Strategies. SPE Western Regional & AAPG Pacific Section Meeting, 2013 Joint Technical Conference. Monterey, CA, USA: Society of Petroleum Engineers.

Blunt, M.J., 2000. An Empirical Model for Three-Phase Relative Permeability: SPE Journal, paper SPE 67950, (12).

Cinar, Y. & Orr Jr., F. M., 2005. Measurement of Three-Phase Relative Permeability with IFT Variation. SPE Reservoir Evaluation & Engineering, 8, pp. 33-43.

Cinar, Y., Marquez, S., and Orr J., F. M., 2004. Effect of IFT Variation and Wettability on Three-Phase Relative Permeability. SPE Annual Technical Conference and Exhibition. Houston, Texas: Society of Petroleum Engineers.

Cinar, Y., Marquez, S., and Orr J., F. M., 2007, Effect of IFT Variation and Wettability on Three-Phase Relative Permeability: SPE Reservoir Evaluation & Engineering, paper SPE 90572-PA, (06).

Delshad, M., and Pope, G.A., 1989, Comparison of the three-phase oil relative permeability models: Transport in Porous Media, 4(1), p. 59-83.

Delshad, M., Delshad, M., Pope, G.A., and Lake, L.W., 1987, Two- and Three-Phase Relative Permeabilities of Micellar Fluids: SPE Formation Evaluation, paper SPE 13581, (09).

DiCarlo, D.A., Sahni, A., and Blunt, M.J., 1998, The Effect of Wettability on Three-Phase Relative Permeability, paper SPE 49317, presented at the SPE Annual Technical Conference and Exhibition, New Orleans, Louisiana.

Daria, D., Pope, G. A. and Sepehrnoori, K., 1993. Three-Phase Gas/Oil/Brine Relative Permeabilities Measured Under CO2 Flooding Conditions. SPE Reservoir Engineering, 8, 143-150.

Fatemi, S. M. and Sohrabi, M., 2015. Mechanistic Study of the Effect of Gas/Oil IFT on the Performance of Gas, WAG and SWAG Injections in Mixed-Wet Systems. SPE Annual Technical Conference and Exhibition held in Houston, Texas, USA, 28–30 September 2015.

Fatemi, S. M., Sohrabi, M., Ireland, S. and Jamiolahmady, M. 2012. Recovery Mechanisms and Relative Permeability for Oil/Gas System at Near-miscible Conditions: Effects of Immobile Water Saturation, Wettability, Hysteresis and Permeability. SPE Improved Oil Recovery Symposium. Tulsa, Oklahoma, USA, Society of Petroleum Engineers.

Fatemi, S. M., Sohrabi, M., Jamiolahmady, M., Ireland, S. and Robertson, G., 2011. Experimental Investigation of Near-Miscible Water-Alternating-Gas (WAG) Injection Performance in Water-wet and Mixed-wet Systems. Presented at Offshore Europe,Aberdeen,6–8September.SPE-145191-MS. http://dx.doi.org/10.2118/145191-MS.

Hustad, O.S., and Browning, D.J., 2010. A Fully Coupled Three-Phase Model for Capillary Pressure and Relative Permeability for Implicit Compositional Reservoir Simulation: SPE Journal, paper SPE 125429-PA, (12).

Hustad, O.S., and Hansen, A.G., 1995. A Consistent Correlation for Three-Phase Relative Permeabilities and Phase Pressure Based on Three Sets of Two Phase Data, presented at the 8th European IOR Symposium, Vienna, Austria.

Hustad, O.S., and Holt, T., 1992. Gravity Stable Displacement of Oil by Hydrocarbon Gas after Waterflooding, paper SPE 24116, presented at the SPE/DOE Enhanced Oil Recovery Symposium, Tulsa, Oklahoma.

Jerauld, G., 1997. General Three-Phase Relative Permeability Model for Prudhoe Bay. SPE Res Eng 12 (4): 255–263. SPE-36178-PA. http://dx.doi.org/10.2118/36178-PA.

Johnson, E.F., Bossler, D.P., and Naumann, V.O., 1959. Calculation of Relative Permeability from Displacement Experiments, paper SPE 001023-G.

Leverett, M.C., and Lewis, W.B., 1941. Steady Flow of Gas-oil-water Mixtures through Unconsolidated Sands, paper SPE 941107-G.

Oak, M.J., 1990. Three-Phase Relative Permeability of Water-Wet Berea, paper SPE 20183, presented at the SPE/DOE Enhanced Oil Recovery Symposium, Tulsa, Oklahoma.

Pejic, D., and Maini, B.B., 2003. Three-Phase Relative Permeability of Petroleum Reservoirs, paper SPE 81021, presented at the SPE Latin American and Caribbean Petroleum Engineering Conference, Port-of-Spain, Trinidad and Tobago.

Petersen, E.B., Lohne, A., Vatne, K.O., Helland, J.O., G.Virnovsky, and P.Eric Øren, 2008. Relative Permeabilities for Two- And Three Phase Flow Processes Relevant to The Depressurization of the Statfjord Field, presented at the International Symposium of the Society of Core Analysts, Abu Dhabi, UAE.

Sohrabi, M., Henderson, G.D., Tehrani, D.H., and Danesh, A., 2000. Visualisation of Oil Recovery by Water Alternating Gas (WAG) Injection Using High Pressure Micromodels - Water-Wet System, paper SPE 63000, presented at the SPE Annual Technical Conference and Exhibition, Dallas, Texas.

Sohrabi, M., Danesh, A., and Tehrani, D.H., 2005. Oil Recovery by Near-Miscible SWAG Injection, paper SPE 94073, presented at the SPE Europec/EAGE Annual Conference, Madrid, Spain.

Sohrabi, M., Tehrani, D. H. and Al-Abri, M. 2007. Performance of Near-Miscible Gas and SWAG Injection in a Mixed-Wet Core. Oral presentation of paper SCA2007-26 given at the International Symposium of the Society of Core Analysts, Calgary, 10–12 September.

Sohrabi, M., Danesh, A., Tehrani, D., and Jamiolahmady, M., 2008. Microscopic mechanisms of oil recovery by near-miscible gas injection: Transp. Porous Media, 72, p. 351-367.

Stone, H.L., 1970. Probability Model for Estimating Three-Phase Relative Permeability, SPE Journal of Petroleum Technology, paper SPE 2116, (02).

Stone, H.L., 1973. Estimation of Three-Phase Relative Permeability and Residual Oil Data, paper SPE 73-04-06, (10-12).

Chapter 2-Coreflood Experiments

The characterization of three-phase flow in porous media and Water-Alternative-Gas injection (WAG) is a joint industrial project in Heriot-Watt University which started in 1997. The new phase of the project which has a wider scope was commenced in 2014 with the new title of "Improved Characterization of Two- and Three-Phase Flow for Reliable Reservoir Performance Prediction (Water Flooding, Gas Injection, and WAG Injection)". A comprehensive set of coreflood experiments including two- and three-phase experiments were performed using different sandstone cores with different permeability and wettability conditions and at various gas/oil interfacial tension ($IFT_{g/o}$) values. In the new phase of the project, different cores of carbonate rocks and low permeability sandstone have been used. The experiments utilized in this research for simulation, history matching and modelling purposes were conducted by other Ph.D. students (AlAbri, M., and Fatemi, S. M.), and the present author was not involved in performing experiments and the laboratory work.

In addition to experimental data which was obtained in Heriot-Watt University, some published experimental data in the literature has been utilized by the present author. More detail will be presented accordingly. This chapter describes the coreflood facilities, rock, and fluids used at Heriot-Watt laboratory to perform unsteady state coreflood experiments.

2.1 Coreflood Facilities

A high-pressure coreflood facility is used to perform two and three-phase experiments. The coreflood rig can take long core up to 3 feet with a large diameter up to 2 inches and it is equipped with an X-ray scanner. The X-ray scanner provides scans of the core before, during, and after the experiments which can be used to monitor the fluid distribution during the flow and to check the experimental artefacts, such as capillary end effect. The rig has been designed to work at high pressures up to 6000 psia, with all components and their content being kept at a controlled temperature of 38 °C. Figure 2-1 shows a schematic diagram of this coreflood rig. In all the displacement tests, the cores are oriented horizontally and to eliminate the effect of gravity; the cores are rotating along the horizontal axis.

The coreflood rig is equipped with six pumps which are used for the injection purposes. The test fluids are maintained in stainless steel piston cells, with brine being injected into or withdrawn from the base of the cells by the displacement pumps to circulate the fluids around the flow system. To allow circulation of fluids through the core, two cells are allocated for each fluid; one is initially full, and the other is empty. A large 100 cc sight glass is placed at the core outlet. The pressure drop across the core is measured using two high accuracy transducers located at the inlet and outlet of the core. The transducers provide stable differential pressure data with an accuracy of 0.01 psi during the tests.

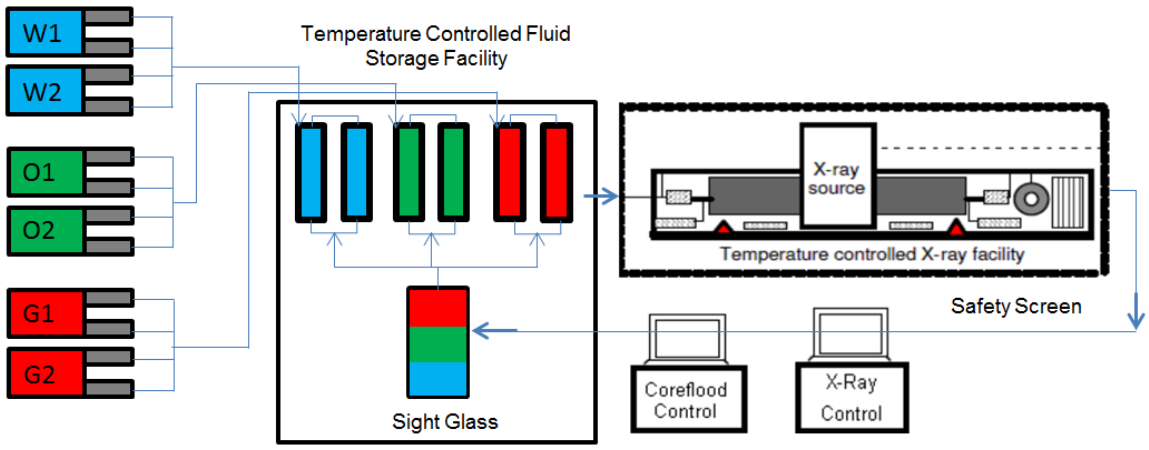

Figure 2-1: High-pressure coreflood facility used for displacement tests.

2.1.1 Porous Media (Cores) and Fluids

Two clean and homogenous Clashach sandstone cores with the different permeability were used for performing unsteady-state coreflood experiments. The physical properties

of these cores are given in Table 2-1. Porosity values have been measured using the Helium porosity method. The core was then saturated with 100% brine (the same brine that is utilized for the coreflood experiments), and permeability values were measured, using the brine. Before performing the coreflood tests, an X-ray scan was run, and the profile of porosity along the core was obtained. Figure 2-2 depicts the profile of the porosity along the length of the 65mD core. The average porosity from this profile is consistent for the measured porosity using Helium. Apart from some normal fluctuations in the profile, the porosity value is relatively the same along the core, which indicates that there are no major heterogeneities in the core. Both cores were chosen to be long enough to minimize the capillary end effect while performing flooding tests.

Table 2-1: Physical properties of the 65 and 1000 mD Clashach sandstone core samples.

Core	*Absolute Permeability/ mD*	*Porosity*	*Length/cm*	*Diameter/cm*
1	65	0.1818	60.5	5.08
2	1000	0.176	66.5	4.86

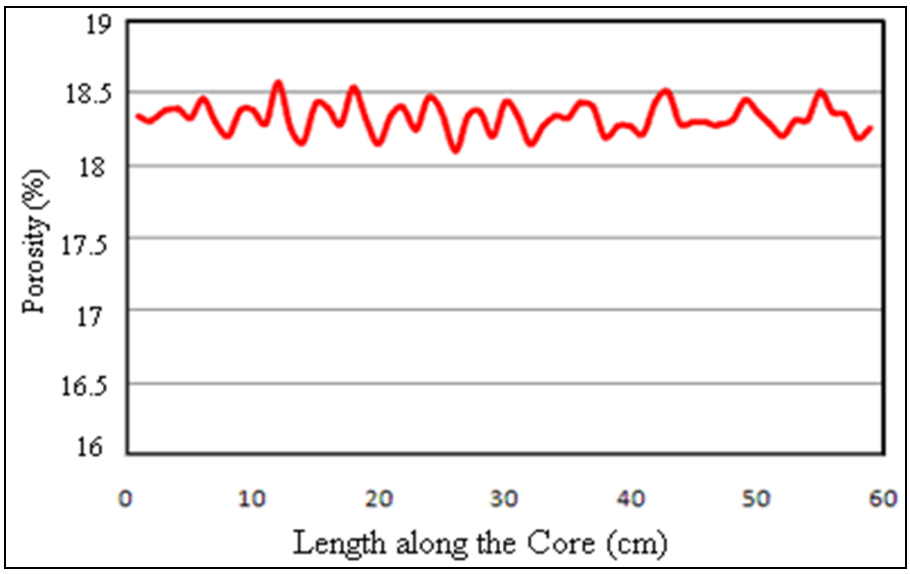

Figure 2-2: Porosity profile along the 65 mD Clashach sandstone core sample.

The pore size distribution for three Clashach sandstone core samples was examined using their mercury injection P_c curves of three samples with a broad range of permeabilities (140, 553 and 1000 mD). Figure 2-3 shows that the Clashach sandstone shows similar pore size distribution for different permeabilities.

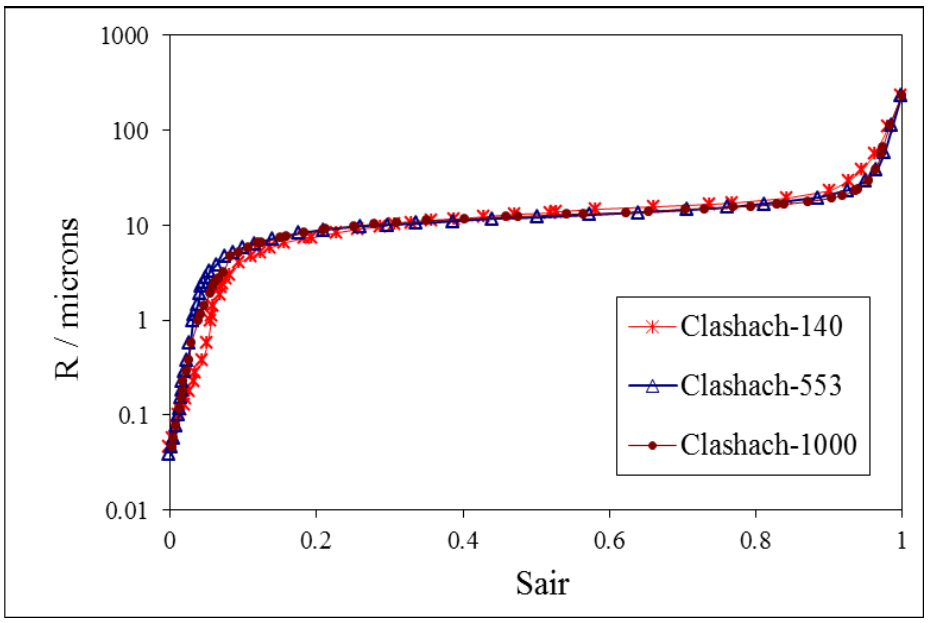

Figure 2-3: Pore size distribution of Clashach sandstone in a wide range of permeability.

The hydrocarbon fluid system used in the coreflood experiments was prepared from a binary mixture of methane (C1) and n-butane (nC4). The mixture has a composition of 73.6 mol% C1 and 26.4 mol% n-C4. Table 2-2 shows the measured properties of the hydrocarbon vapour (gas) and that of hydrocarbon liquid (oil), at the test temperature of 38 ^{o}C (100 ^{o}F), and different test pressures (corresponding to different gas/oil IFT values). As the critical pressure of this hydrocarbon system at 38 ^{o}C is about 1865 psia, the test pressure of 1840 psia is very close to the critical point, and hence, the gas and oil are nearly miscible. Therefore, the test pressure of 1840 psia (which is corresponding to very low gas/oil IFT value of 0.04 mNm^{-1}) will be considered as near-miscible conditions. At the test pressure of 1790 psia, gas/oil IFT is 0.15 mN.m$^{-1,}$ and this condition will be considered as intermediate IFT system, compared to the tests at a pressure of 1215 psia in which the gas/oil system will be seen as immiscible (gas/oil IFT = 2.7 mN.m^{-1}).

Table 2-2: measured fluid properties for C1-nC4 binary mixture at 38 ^{o}C.

Pressure /psia	***ρ_g /kg.m^{-3}***	***ρ_L /kg.m^{-3}***	***μ_g /mPa.s***	***μ_L /mPa.s***	***IFT /mN.m^{-1}***
1215	86.68	466.06	0.0141	0.0793	2.70
1790	184.8	345.10	0.0206	0.0474	0.15
1840	211.4	317.40	0.0249	0.0405	0.04

The immobile water phase and the brine used in the experiments were synthesized with small amounts of Sodium Chloride (NaCl) and Calcium Chloride ($CaCl_2$) dissolved in

distilled and degassed water. Table 2-3 shows the properties of the brine at 38 ^{o}C. The brine composition was designed to prevent possible adverse reaction between the brine and clay such as swelling and it was not supposed to be representative of any reservoir's brine.

Table 2-3: Properties of synthetic brine at an experimental temperature of 38 ^{o}C.

Salinity / mg.L^{-1}	***Density / g.L^{-1}***	***Viscosity /mPa.s***	***IFTo/w /mN.m^{-1}***	***IFTg/w /mN.m^{-1}***
1000	992.96	0.68	55	60

To minimize the mass transfer during the coreflood experiments, all the fluids (oil, gas, and brine) were pre-equilibrated at average test pressure and temperature. They were kept in equilibrium in the high-pressure transfer vessels, which were placed in a temperature controlled oven. The mixing process was repeated several times before each displacement test to ensure that phase equilibrium conditions were satisfied.

2.1.2 Establishing Irreducible Water Saturation

Establishing immobile water saturation was a long process of sequential displacements. First, the core was fully saturated with water after being cleaned. Then, water was displaced using viscous mineral oils, and the injection continued until no further water production. The mineral oils were displaced over a period of days using decane (C10). Decane was then displaced by injecting methane (C1) at high pressure, ensuring miscible displacement. Finally, C1 was displaced by equilibrated oil (C1-nC4) at test conditions to initialize the experiment. To make sure no vaporization of the water in the core occurred during the tests, C1 and C10 were maintained in equilibrium with water before the injection. The establishment process resulted in 8% and 18% irreducible water saturation for 1000mD and 65mD cores, respectively. The profile of the established irreducible water saturation along the core was also obtained using X-ray analysis. Figure 2-4 shows irreducible water saturation (18%) profiles along the 65mD core for both water-wet and mixed-wet samples, which are very close and indicate that the established irreducible water saturations for the two wettability conditions are the same.

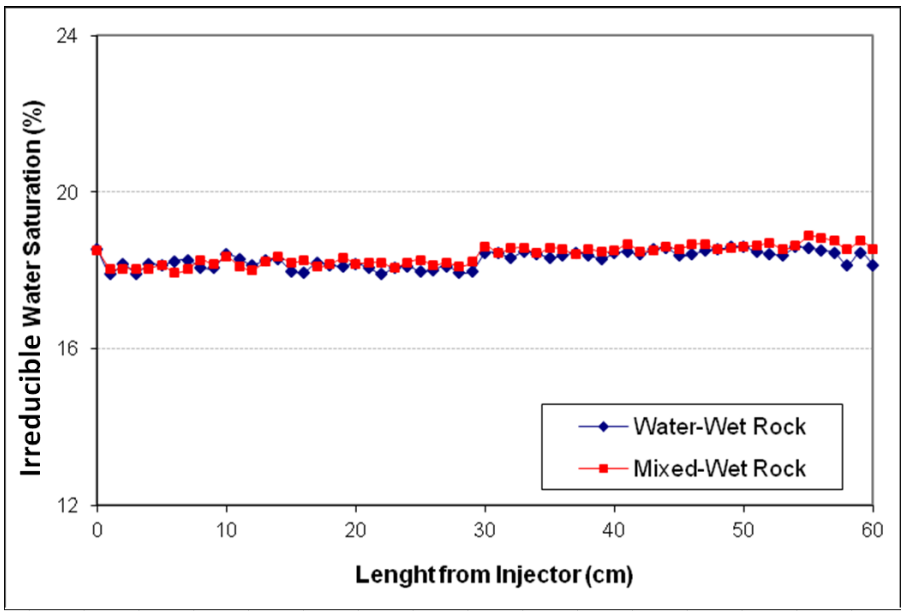

Figure 2-4: Established immobile water saturation along the core, obtained from X-ray for 65mD water-wet and mixed-wet cores.

2.1.3 Development of Mixed-Wettability

Core wettability can be altered by either suitable chemicals or aging in suitable crude oils. Although using chemicals for alternating the wettability is less time consuming and also has a relatively simpler procedure the stability of the wettability is poor. Aging in crude oils has a more difficult procedure and is longer. However, once the desired wettability condition has been achieved, it could be very stable and durable. A suitable crude oil was identified for wettability alteration. The procedure was tested on thin sections and small core plugs taken from the same rock before attempting to alter the wettability of the main rock. Wettability of the treated thin sections was evaluated by direct visualisation using Environmental Scanning Electron Microscope (ESEM) where the surface of thin sections was exposed to water condensation in an enclosed chamber. Figure 2-5 (a) shows a magnified picture of rock grains in a thin untreated section. Because the rock was strongly water-wet it was not possible for the condensing water to form droplets on the surface, the water would instead cover the grain surface with a spreading layer. This thin section was soaked in the crude oil and after four days, its surface was gradually exposed to water condensation. The water was observed to form droplets of varying size and contact angle on the surface which is shown in Figure 2-5 (b). This was the result of the surface being exposed to the crude oil and wettability alteration by adsorption of organic material to the grains surface (Fatemi et al. (2011)).

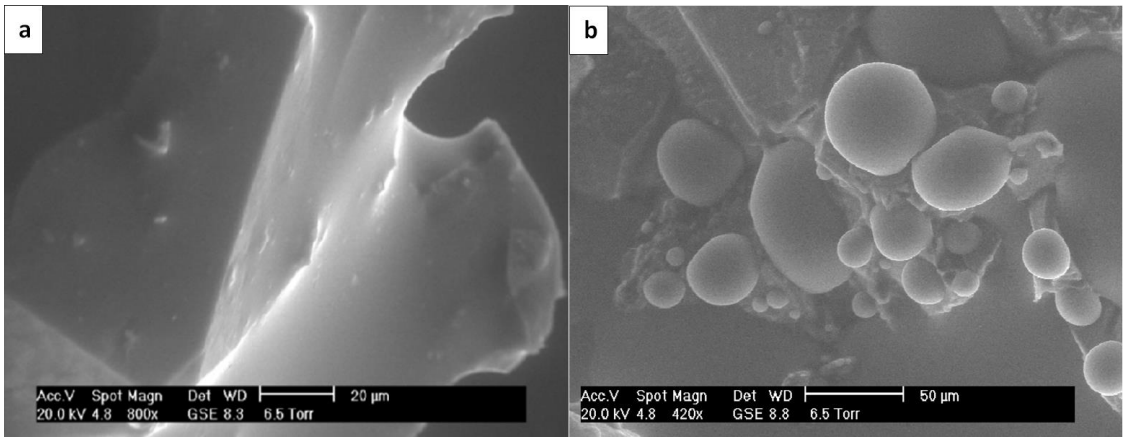

Figure 2-5: (a) ESEM picture for a thin section of water-wet rock: Water films were formed on the grains (b) ESEM picture for a thin section of mixed-wet rock: Water formed droplets on the grain surfaces rather than films.

Wettability of the treated core plug was evaluated by performing a US Bureau of Mines (USBM) test (Sohrabi et al. (2007)). USBM index of (-0.02) was determined by measuring the capillary pressure curves, using the centrifuge technique. The index value shows that the core wettability was mixed-wet with an average neutral wettability.

2.1.4 Capillary Pressure Data

Figure 2-6 and Figure 2-7 show the measured air/mercury P_c for 1000 mD water-wet core and oil/water P_c for 1093 mD mixed-wet core (obtained during USBM wettability determination test), respectively. Currently, these are the only available measured data for P_c. The Leverett J-function (Eq.2-1) is employed to convert these P_c data for the core and condition of interest.

$$J = \frac{P_c\sqrt{K/\varphi}}{\sigma\cos\theta} \qquad 2\text{-}1$$

P_c, K,φ, σ and θ are capillary pressure, absolute permeability, porosity, IFT and contact angle respectively. The similarity of their pore size distribution between two rocks is the main reason that justified use of the J-function to convert P_c data from one rock type to another. As it was shown in Figure 2-3, the Clashach sandstone shows similar pore size distribution for a broad range of permeabilities (140, 553 and 1000 mD). It has been assumed that the 65mD Clashach sandstone core also has a similar pore size distribution.

The interfacial tension between fluids and contact angle (θ) are required to apply the J-function method. The IFT values for water/oil (58 mNm^{-1}) and water/gas (60 mNm^{-1}) were extracted from published measured data (Hassan et al. (1953) and Danesh (1998)).

Contact angles of 0° and 37° were assumed for the water-wet and mixed-wet core samples respectively. The converted P_c data was then used as input information in the simulator when calculating the two-phase k_r curves by history matching the coreflood experiments.

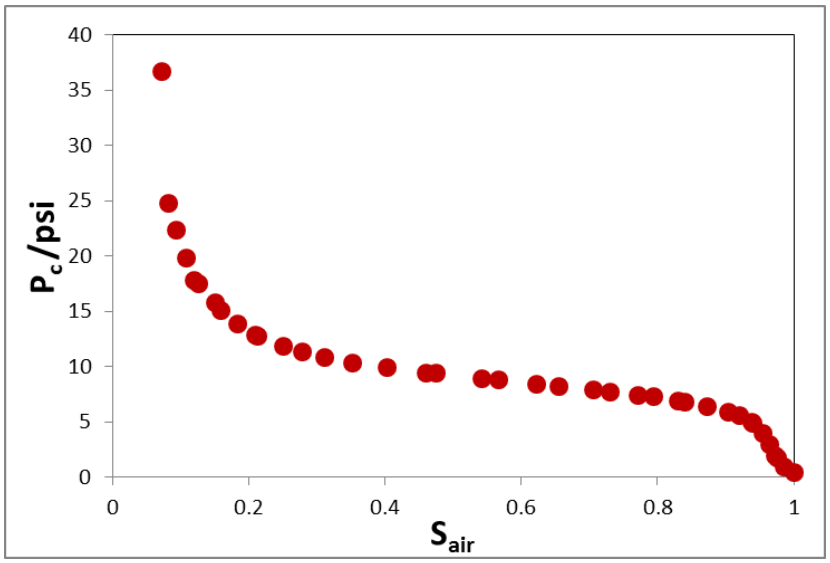

Figure 2-6: Measured air-mercury capillary pressure for 1000 mD water-wet core.

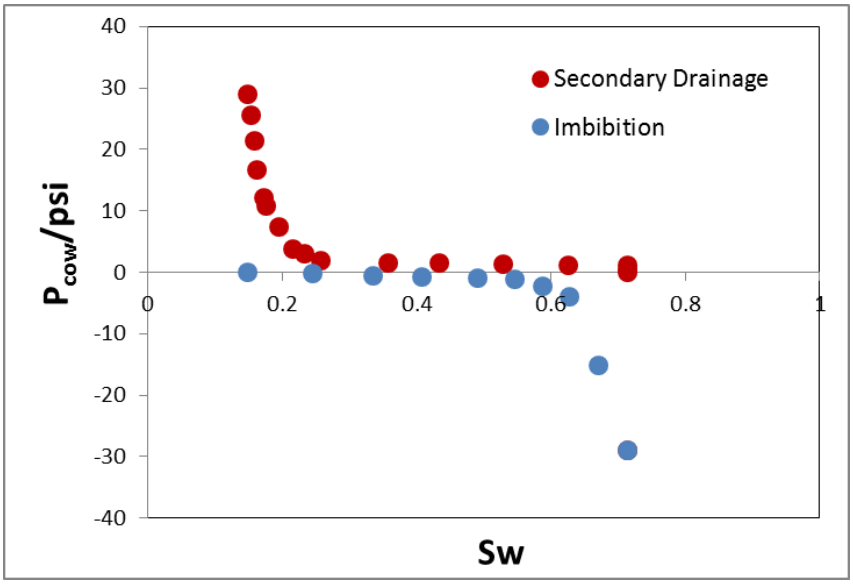

Figure 2-7: Measured oil/water capillary pressure obtained during USBM wettability determination test carried out on 1093 mD mixed-wet core (Sohrabi et al. 2007).

2.2 Coreflood Experiments

Relative permeability is measured in the laboratory using two methods of 'steady state' and 'unsteady state' experiments. It is possible to measure relative permeability directly for a wide saturation range using the steady state method, but it is very time-consuming. In the unsteady state method or 'displacement experiment' for a two-phase system, the core is initially saturated with one fluid (e.g. water) then another liquid (e.g. oil) is injected into the core to displace the first fluid, at a specific rate. Injection is continued

until residual saturation of the displaced fluid is achieved. The pressure drop across the core and production data are recorded during the experiment and used to calculate relative permeabilities. The unsteady state method is less time consuming than the steady state method, but the saturation range for relative permeability is limited.

To generate a reliable source of data for fluid flow characterization and simulation purposes, a high-quality set of coreflood experiments were conducted in 65 and 1000mD water-wet and mixed-wet Clashach sandstone cores. All the two- and three-phase coreflood experiments were performed using the unsteady-state method.

The effects of different parameters such as absolute rock permeability, wettability, and gas/oil IFT values on oil recovery, the performance of gas and water alternating gas (WAG) injections and also relative permeability were investigated. These experiments include two-phase and three-phase flow systems and were performed in the presence of irreducible (connate) water saturation. The results of the unsteady-state two- and three-phase displacement tests which have been used in this thesis will be introduced in the relevant sections, and more details of experiments including total injected fluid, injection rate, and initial fluid saturations will be presented accordingly.

2.3 References

Fatemi, S. M., Sohrabi, M., Jamiolahmady, M., et al. 2011. Experimental Investigation of Near-Miscible Water-Alternating-Gas (WAG) Injection Performance in Water-wet and Mixed-wet Systems. Presented at Offshore Europe, Aberdeen, 6–8 September. SPE-145191-MS. http://dx.doi.org/10.2118/145191-MS.

Sohrabi, M., Tehrani, D. H. and Al-Abri, M. 2007. Performance of Near-Miscible Gas and SWAG Injection in a Mixed-Wet Core. Oral presentation of paper SCA2007-26 given at the International Symposium of the Society of Core Analysts, Calgary, 10–12 September.

Chapter 3– Estimation of Three-Phase Relative Permeability (k_r) from Unsteady-State Coreflood Experiments

The understanding of governing mechanisms of simultaneous flow of different phases (oil, water, and gas) in porous media is of great interest in petroleum and environmental engineering. In the petroleum engineering context, three-phase flow occurs in EOR processes including tertiary gas injection, water alternating gas injection (WAG), depressurization below the bubble point, gas cap expansion, solution gas drive, gravity drainage, steam injection and thermal flooding. In the environmental engineering context, three-phase flow occurs when a non-aqueous phase liquid (NAPL) or dense non-aqueous phase liquids (DNAPL) flows simultaneously with water and air through soils and also CO_2 storage in geological formations.

Relative permeability (k_r) is an important flow function for understanding, describing and simulating multiphase flow through porous media. k_r can be measured in the laboratory using steady-state and unsteady-state methods, or be estimated by mathematical correlations and pore-network models. Extensive laboratory measurements and modelling were performed in two-phase flow area (Honarpour et al. (1986)), but three-phase k_r did not receive similar attention. This is mainly because three-phase flow experiments and in particular steady-state measurements are very complicated, labour intensive, time-consuming and expensive. Therefore, more often unsteady-state method as the less cumbersome method compared to the steady-state is used for three-phase k_r measurements. In this chapter, the devised methodology for estimating k_r values from unsteady-state coreflood experiments is demonstrated.

3.1 Introduction

Relative permeability (k_r), capillary pressure (P_c) and fluid saturations are important macroscopic properties for describing multiphase flow through porous media. To understand multiphase flow in porous media, the relationships among these properties should be understood. These relationships are dependent on the fluids' properties, the pore size distribution, and the saturation history and are used in diffusivity equations to describe the fluid flow in porous media.

The most common approach currently used to calculate the three-phase k_r to be employed in the numerical simulation of three-phase flow in porous media is based on available empirical correlations (models) which use laboratory-measured two-phase k_r data. These models have little or no physical basis, and the published evaluations on them (Cao & Siddiqui (2010), Delshad & Pope (1989), Baker (1988)) have demonstrated that calculating three-phase relative permeabilities by using measured two-phase k_r data may lead to erroneous results. Moreover, to characterize three-phase k_r and understand the effect of parameters, e.g., wettability, IFT, saturation history on flow function it is required to measure three-phase kr experimentally.

In steady state method for a two-phase system, the core is initially saturated with one fluid (e.g. water), and a specific ratio of the same fluid (water) with another fluid (e.g. oil) is injected into the core. The injection continues until the production rate for each fluid is the same as its injection rate and the pressure drop across the core is stabilized. For three-phase systems, all fluids are injected simultaneously at given ratios, until steady-state conditions are attained. It usually takes a more extended period to establish steady-state flow. Each experiment run gives one k_r point only. To obtain more k_r points, the experiment is run for several different ratios of injection fluids. Using steady-state method, it is possible to calculate k_r directly from Darcy's law for a wide saturation range, but it is very time-consuming.

In the unsteady-state method or 'displacement experiment' for a two-phase system, the core is initially saturated with one fluid (e.g. oil) then another fluid (e.g. water) is injected into the core to displace the first fluid, at a specific rate. Injection is continued until residual saturation of the displaced fluid is achieved. For a three-phase system, one fluid is injected to displace the other two existing fluids in the core (Figure 3-1). The pressure drop across the core and production data are recorded during the experiment and used to calculate relative permeabilities. The unsteady-state method is less time consuming than steady-state method but the saturation range for k_r is limited, and its

calculation is more complicated than for the steady-state method. The most common method to calculate k_r from production and pressure data obtained from the two-phase unsteady-state experiments is the JBN method (Johnson et al. 1959). It is an analytical method and is based on the Buckley–Leverett theory of two-phase flow in porous media. In this explicit method, the saturations and corresponding relative permeabilities at the end of the core sample are calculated directly. To apply the proposed analytical solution the following simplifying assumptions should be made; the fluids are incompressible and immiscible, the flow is one-dimensional, isothermal and the capillary pressure is neglected. Therefore, this method is not appropriate for low rate displacement in which the effects of capillary forces are not negligible. The other limitation of JBN method is that it is required to differentiate the experimental data, and this differentiation may exaggerate the errors in the measured data and affect the accuracy of calculated relative permeabilities (Kerig & Watson (1987)). JBN method can also be extended to three-phase flow systems. Virnovskii (1984) presented a method based on the JBN method to determine three-phase relative permeabilities from an unsteady-sate coreflood experiment. The required data are the same as for the standard JBN method.

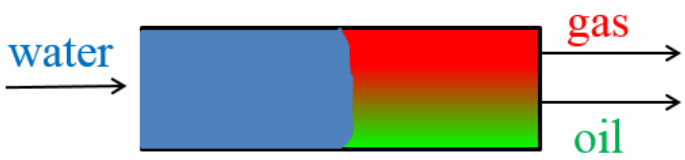

Figure 3-1: Three-phase unsteady-state coreflood experiment. One fluid displaces the resident phases.

The other approach is parameter estimation using numerical simulation and history matching the measured experimental data. For two-phase systems, Sigmund and McCaffery (1979) and later, Batycky et al. (1981) developed a procedure to characterize k_r curves by two unknown parameters. They used their parameterized k_r curves to simulate a displacement experiment while allowing for the capillary pressure effects in the simulation. A non-linear least square method was then applied to fit the calculated pressure drops and production data from the simulation with the measured data obtained from the experiment. They varied the parameters mentioned above, describing their relative permeabilities, in the simulation until the least square error was minimized. Kerig and Watson (1986) used the parameter estimation approach and presented the relative permeabilities by cubic spline functions. They used the Marquardt's modification of Gauss-Newton minimization algorithm to estimate the parameters.

Kulkarni et al. (1998) and Eleri et al. (1995) estimated k_r with a B-spline model and a modified Levenberg-Marquardt algorithm (1963).

Most of the optimization tools mentioned above are gradient-based techniques which require calculating the gradient of the objective function, and local optima may not be avoided. Global optimization methods, such as simulated annealing algorithm (SA), genetic algorithm (GA) and ensemble-based history matching have also been attempted to find the global optimum. Ucan et al. (1993) and Schembre and Kovscek (2006) used simulated annealing, Sun and Mohanty (2005) applied the genetic algorithm and Zhang et al. (2012) implemented Ensemble Kalman Filter (EnKF) to estimate flow functions from unsteady-state two-phase flow experiments.

Mejia et al. (1996) and Nordtvedt et al. (1997) extended the method originally introduced for two-phase systems by Kerig and Watson (1986) to three-phase flow displacement experiments. They used gradient-based optimization methods (e.g., Levenberg-Marquardt) to find appropriate values of the parameters for three-phase flow functions. This optimization method is adequate for obtaining two-phase k_r from two-phase coreflood experiments. For three-phase k_r calculation which has a larger number of unknown parameters this method may not be efficient, and the trapping in the local minima is unavoidable.

In the current research study, a computer program was developed as an optimization tool to obtain three-phase k_r from three-phase unsteady-state coreflood experiments. A Genetic Algorithm (GA) (Holland (1975)), was implemented as the optimization method to globally minimize the objective function through a process of a history matching. The objective function is simply defined as the differences between the experimental data and the results of numerical simulation. The main purpose is to provide an automatic history matching tool to researchers, practicing reservoir engineers and petrophysicists to obtain two- and three-phase relative permeabilities from the corresponding two- and three-phase coreflood experiments. To the best of our knowledge, the current commercial softwares work for two-phase experiments, and there is no commercial software in the oil industry for calculating three-phase relative permeabilities from unsteady-state coreflood experiments.

The performance of the automatic history matching depends on the simulator or the mathematical representation of the fluid flow in porous media, functional form of flow function (e.g., k_r) and the optimization method. The mathematical model should adequately represent the physical mechanisms happening during the displacement

experiment. The functional form of k_r curves should have enough flexibility and the generated k_r for any phase should increase as saturation of that phase increases. Global optimization methods are strongly recommended. Moreover type, quantity and quality of measured data have a significant impact on the accuracy of history matching results.

3.2 Automatic History Matching

The applied workflow for the automated history matching process is shown in Figure 3-2. The mathematical representation of the flow functions, the coreflood simulation, and the optimization algorithm have been demonstrated as the main components of the process. The process starts with an initial guess for the parameters of the k_r functions. The k_r values will be calculated according to the initial parameters and be provided to the numerical simulation. The difference between experimental and simulation results, referred to as objective function or misfit, is minimized iteratively by adjusting the parameters of k_r functions until a certain error tolerance is achieved.

An objective function is formulated as a sum of squared differences between the measured data and the corresponding values calculated from the mathematical model of the experiment. The measured data can be divided into two types of internal and external measurement. The in-situ saturation and pressure profile during the dynamic flow are examples of internal measurements. These data are rarely available as they need more sophisticated facilities to measure them. Moreover, most of the saturation measurement methods are indirect, and the measured data should be analysed and converted to the saturation values. The externally measured data includes cumulative productions and pressure drop across the core. These data are the most available data from a coreflood experiment. The definition of a misfit (objective) function can be altered according to a number of phases available in a coreflood experiment and also the type of available measured data. Equation 3-1 can be used as a misfit function for a three-phase flow system when the cumulative production of all phases, the pressure drop across the core and the water saturation at different cross sections and also at various times are available as the measured data.

$$Misfit = \sum_{i=1}^{N_t}\left[W_{Q_o}\left(Q_{oi}^{Exp}-Q_{oi}^{Sim}\right)^2+W_{Q_w}\left(Q_{wi}^{Exp}-Q_{wi}^{Sim}\right)^2+W_{Q_g}\left(Q_{gi}^{Exp}-Q_{gi}^{Sim}\right)^2+W_{\Delta P}\left(\Delta P_i^{Exp}-\Delta P_i^{Sim}\right)^2\right] + \sum_{i=1}^{N_{ts}}\sum_{j=1}^{N_{ls}} W_S\left(S_{ij}^{Exp}-S_{ij}^{Sim}\right)^2, \quad 3\text{-}1$$

where Q is the cumulative production of each phase, ΔP is the pressure drop across the core sample, S is the saturation, and W is the weighting factor. The superscripts Exp and

Sim represent the experimental and simulated quantities, respectively; the subscript *i* represents the value at time point *i*; and the subscript *j* represents the saturation value at the spatial location *j*. The subscripts *o*, *w* and *g* represent the oil, water and gas phases respectively. N_t and N_{ts} are the number of sampling time points for external data and internal data respectively. N_{ls} is the number of cross sectional slices.

The weighting factor for each data type, W_x, is defined as the combination of user defined weighting factor (w) and the maximum-likelihood weighting factor ($1/\sigma_x^2$) presented in Eq. 3-2. σ_x^2 is the variance of the experimental measurement errors for data type *x*. In this study, the mean squared value of each data type has been used instead of the variance and *w* is equal one.

$$W_x = \frac{w}{\sigma_x^2} \qquad 3\text{-}2$$

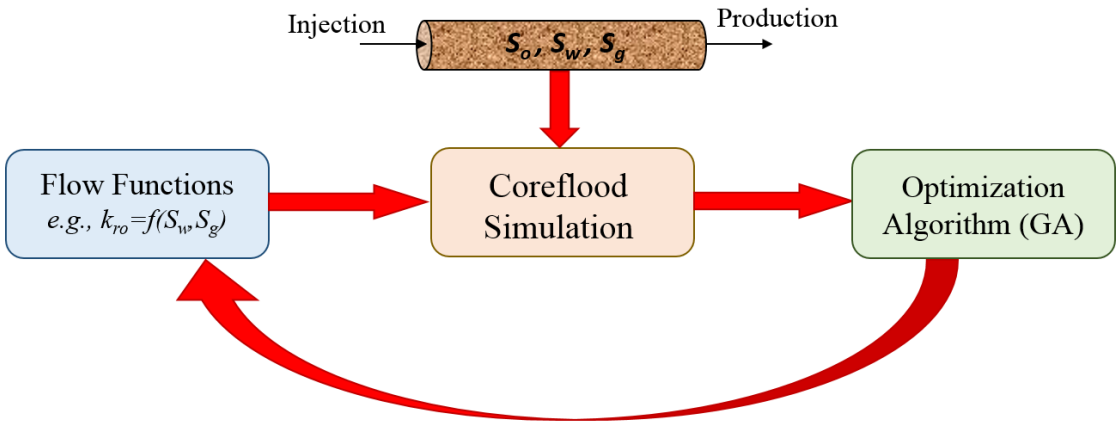

Figure 3-2: Workflow for determination of three phase k_r values from unsteady-state coreflood experiment

3.2.1 Mathematical Model (Coreflood Simulation)

The mathematical equations representing the immiscible three-phase flow in porous media (Eq.3-3 to 3-5) are obtained by substituting Darcy's Law into the mass conservation equation for each phase. The mass transfer between oil and gas has been neglected. For more details on the derivation, see Aziz and Settari (1979).

$$\nabla \cdot \left[\frac{k k_{ro}}{\mu_o} \nabla P_o \right] = \frac{\partial (\varphi S_o)}{\partial t} + q_o \qquad 3\text{-}3$$

$$\nabla \cdot \left[\frac{k k_{rg}}{\mu_g} \nabla P_g \right] = \frac{\partial (\varphi S_g)}{\partial t} + q_g \qquad 3\text{-}4$$

$$\nabla \cdot \left[\frac{k k_{rw}}{\mu_w} \nabla P_w \right] = \frac{\partial(\varphi S_w)}{\partial t} + q_w \qquad 3\text{-}5$$

Where k_r, μ, P, q, S are respectively the relative permeability, viscosity, pressure, injection or production rate and saturation of different phase of oil, gas and water. Permeability, porosity, and time are denoted by k, φ and t respectively. Eq.3-3 to 3-5 contain six dependent variables. Three additional relations are required to describe three-phase flow completely. The relationship among saturation values of the three phases is defined by the fact that the summation of the saturation values is always equal to one.

$$S_o + S_g + S_w = 1 \qquad 3\text{-}6$$

The relationship among the pressure values of existing phases can be defined by the capillary pressures between each pair of fluids.

$$P_{cgo} = P_g - P_o \qquad 3\text{-}7$$

$$P_{cow} = P_o - P_w \qquad 3\text{-}8$$

The multi-phase flow equations are so complex that it is not possible to solve them analytically, and practically these equations can only be solved numerically. The most common numerical method is based on finite difference approximation of the flow equations. Generally to simulate a coreflood experiment, the simultaneous one-dimensional (1D) flow of multiphase should be modelled. Therefore, Eq.3-3 to 3-5 is simplified to 1D and the initial and boundary conditions corresponding to the experiment are imposed and equations will be solved numerically. A core sample and its equivalent Cartesian model (discretised) is shown in Figure 3-3. The core sample and the Cartesian model have the same cross-sectional area. For a horizontal coreflood experiment, the flow is in the X direction, and as the diameter of the core is smaller than its length, the flow in the Y and Z directions is negligible. To ensure there is no gravity effect (flow in the Z direction) the core can be rotated during the experiment. For a vertical coreflood experiment, the flow is in the Z direction, and the flow in the X and Y directions is negligible. For the numerical simulation, Eclipse Black-oil simulator is used in this research study. Therefore, the 1D simulation model is built in Eclipse, and all physical features in this simulator can be used to model properly the mechanisms happening in the experiment. By applying numerical simulation, the capillary forces

between fluids and gravity effects can be included in the simulation, unlike the JBN method.

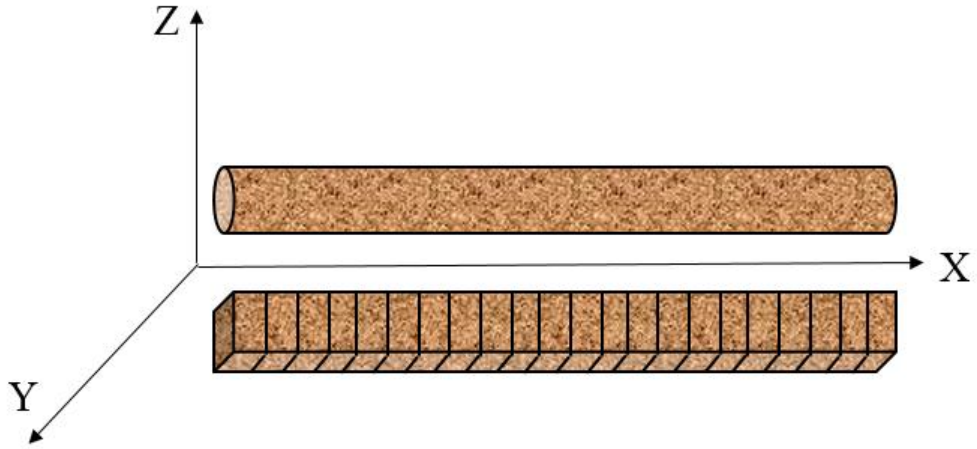

Figure 3-3: Horizontal core and equivalent 1D Cartesian gridding in X direction.

3.2.2 Functional Form of Relative Permeability (k_r)

There are two functional forms for representing the relative permeability; parametric and non-parametric representations. The parametric presentations are usually analytical correlations which define the relationship between k_r and saturation. The Corey (1954) model is a simple power law function with only one empirical parameter and is the most widely used model. It defines k_r curves by endpoints and exponential factors. The Corey model has limitations to exhibit the flexibility to capture the different observed shape of k_r curves. Chierici (1984) proposed an exponential formulation with two parameters for each k_r curve. This correlation is more flexible than the Corey model. However, as the results of studies by Lomeland et al. (2005) and Moghadasi et al. (2015) showed, the Corey and Chierici models are not flexible enough to capture the entire saturation range of k_r curves. Lomeland et al. (2005) proposed a three-parameter model which shows enough flexibility to capture different shapes of k_r over a wide saturation range. This model is known as LET model.

Unlike parametric models, the nonparametric models are more flexible. One of the most commonly used nonparametric models is B-spline. Although B-spline curves are very flexible and have more degree of freedom, they cannot always guarantee the monotonicity of k_r curves. Also, the estimated k_r curves may have one or several breaks (Eydinov et al. (2007)) and sometimes irregular shapes. It is worth mentioning that B-spline models may introduce more non-uniqueness to the estimation due to their numerous unknowns. The higher the number of unknowns in B-spline model, the more uncertainty will be associated to the solution.

In this study, a power-law model (Corey) which has the least number of parameters for history matching and also the flexible and versatile model of LET are used to represent the k_r curves as two separate options.

Corey Model

Corey (1954) introduced a simple power law function with only one empirical parameter. Using the Corey correlation for oil and water system, the oil and water relative permeabilities are as follow:

$$k_{row} = k^0_{rocw}(1 - S^*_w)^{now} \quad \text{3-9}$$

$$k_{rw} = k^0_{rw}(S^*_w)^{nw} \quad \text{3-10}$$

$$S^*_w = \frac{S_w - S_{wco}}{1 - S_{wco} - S_{orw}} \quad \text{3-11}$$

For two-phase gas/oil system at connate water saturation (irreducible water saturation) with gas injection, the k_r curves can be obtained using Corey model as follow:

$$k_{rog} = k^0_{rocw}(1 - S^*_g)^{nog} \quad \text{3-12}$$

$$k_{rg} = k^0_{rg}(S^*_g)^{ng} \quad \text{3-13}$$

$$S^*_g = \frac{S_g}{1 - S_{wco} - S_{org}} \quad \text{3-14}$$

The curvatures of the k_r curve are given by the parameter "*n*", e.g., *nw* for water k_r. S_{wco} is irreducible water saturation and S_{orw} and S_{org} are residual oil saturation after two-phase water flooding and gas injection respectively. The end point relative permeability for oil (at irreducible water saturation), water and gas are presented by k^0_{rocw}, k^0_{rw} and k^0_{rg} respectively.

S_{wco} and k^0_{rocw} are well determined while S_{orw}, S_{org}, k^0_{rw} and k^0_{rg} are uncertain due to lack of information. The "*n*" parameter for varying the curvature of all k_r curves (*now, nog, nw, and ng*), all end point relative permeabilities (k^0_{rocw}, k^0_{rw} and k^0_{rg}) and residual oil saturations (S_{orw}, S_{org}) are considered to be matching parameters to enhance the flexibility of the Corey curves.

LET Model

LET model was proposed by Lomeland et al. (2005) as a three-parameter model with more flexibility compared to the Corey model and can reconcile the measured experimental k_r data. The LET k_r curves for oil/water and gas/oil systems are as follow:

$$k_{row} = k^0_{rocw} \frac{(1-S^*_w)^{L^w_o}}{(1-S^*_w)^{L^w_o} + E^w_o (S^*_w)^{T^w_o}} \quad 3\text{-}15$$

$$k_{rw} = k^0_{rw} \frac{(S^*_w)^{L^o_w}}{(S^*_w)^{L^o_w} + E^o_w (1-S^*_w)^{T^o_w}} \quad 3\text{-}16$$

$$k_{rog} = k^0_{rocw} \frac{(1-S^*_g)^{L^g_o}}{(1-S^*_g)^{L^g_o} + E^g_o (S^*_g)^{T^g_o}} \quad 3\text{-}17$$

$$k_{rg} = k^0_{rg} \frac{(S^*_g)^{L^o_g}}{(S^*_g)^{L^o_g} + E^o_g (1-S^*_g)^{T^o_g}} \quad 3\text{-}18$$

The empirical model parameters are L, E, and T for each k_r curve. Values of T and L describe the shape of the upper and lower parts of the k_r curve respectively. The parameter E describes the position of slope or the elevation of k_r curve. As the value of E increases, the slope moves toward the high end of the curve and as it decreases the slope moves toward the lower end. Practical experience using this model indicated that $L \geq 1$, $E > 0$ and $T \geq 0.5$ (Lomeland et al. (2005)). The physically meaningful parameters of LET model are residual oil saturations (S_{orw}, S_{org}) and endpoint relative permeabilities (k^0_{rocw}, k^0_{rw} and k^0_{rg}).

Having these parameters, the LET model behaves flexibly and produces smooth and physically meaningful curves of k_r. The model can reconcile most of the measure k_r data and capture the variable behaviour of k_r curve across the entire saturation range (Moghadasi (2015), Ebeltoft et al. (2014), Lomeland et al., (2005)).

Three-phase relative permeability calculations

For the three-phase flow system, there are three k_r functions (k_{ro}, k_{rg} & k_{rw}) to be estimated. According to the research results of many researchers, the three-phase k_r of the most wetting and non-wetting phases in water-wet and mixed-wet rocks are only function of their own saturations. Therefore, the three-phase water k_r can be presented

as a function of water saturation. This is also similar for the three-phase gas k_r. For the intermediate phase, oil, the three-phase k_r is a function of the saturation of the other two phases, gas and water. Therefore, to estimate three-phase k_r from a coreflood experiment, the functional form of oil, gas and water will be presented as follows:

$k_{ro} = k_{ro}(S_w, S_g)$

$k_{rg} = k_{rg}(S_g)$

$k_{rw} = k_{rw}(S_w)$

For the gas and water functional form, the Corey and LET models are adequate. The functional form of k_{ro} should account for the effect of gas and water phases. Many empirical correlations have been proposed so far for estimation of three-phase k_r using two-phase gas/oil and oil/water k_r data. These correlations can be utilized sufficiently to define k_{ro} as a function of gas and water saturations. In general, most of these models can be divided into two categories, Stone type, and Baker type models. The two most widely used models in commercial simulators are Modified Stone 1 and Saturation-Weighted Interpolation models (Eclipse Technical Manual). These models have been used as the functional form of three-phase k_{ro} in the developed computer program.

STONE Type Models

Stone (1970) proposed a probability model using channel flow theory which is an interpolation between the two-phase gas/oil and oil/water relative permeabilities. k_{rog} and k_{row} are multiplied to each other in the following form to calculate three-phase k_{ro}:

$$k_{ro} = \frac{S_o^*}{(1-S_g^*)(1-S_w^*)} k_{rog} k_{row} \qquad 3\text{-}19$$

To calculate k_{ro} at the three-phase flow conditions, the two-phase gas/oil relative permeability (k_{rog}) should be looked up at its three-phase gas saturation value, and the two phase oil/water relative permeability (k_{row}) should be looked up at three-phase water saturation value.

A modified version of Stone's first (ST1) three-phase k_{ro} model, summarized by Aziz and Settari (1979) as follows. This modified version has been implemented in commercial simulators.

$$k_{ro} = k_{rocw} S_o^* F_w F_g \quad (3\text{-}20)$$

Where:

k_{rocw}: Relative permeability to oil at irreducible/connate water (S_{wc}),

$$S_o^* = \frac{S_o - S_{om}}{1 - S_{wco} - S_{om}} \quad \text{when } S_o > S_{om} \quad (3\text{-}21)$$

$$F_w = \frac{k_{row}}{k_{rocw}(1 - S_w^*)} \quad (3\text{-}22)$$

$$F_g = \frac{k_{rog}}{k_{rocw}(1 - S_g^*)} \quad (3\text{-}23)$$

$$S_w^* = \frac{S_w - S_{wco}}{1 - S_{wco} - S_{om}} \quad \text{When } S_w > S_{wco} \quad (3\text{-}24)$$

$$S_g^* = \frac{S_g}{1 - S_{wco} - S_{om}} \quad (3\text{-}25)$$

S_{om} is the minimum residual oil saturation in the presence of all three phases. In the other words, S_{om} is the minimum of the critical oil-to-water saturation and the critical oil-to-gas saturation.

Stone in 1973 modified his first model, incorporating water and gas relative permeabilities in the calculation of three-phase k_{ro}. The negative signs of k_{rw} and k_{rg} in this model may lead to negative values for three-phase k_{ro}.

$$k_{ro} = (k_{rog} + k_{rg})(k_{row} + k_{rw}) - k_{rg} - k_{rw} \quad (3\text{-}26)$$

BAKER Type Models

Baker (1988) developed an arithmetic averaging between two phase k_r to calculate three-phase k_r. This kind of model estimates three-phase k_r for all mobile phases as a function of two independent saturations. Unlike the Stone models, the two-phase oil relative permeabilities (k_{row} and k_{rog}) in the Baker model should be assigned at three-phase oil saturation. The three-phase k_{ro} is given by:

$$k_{ro} = \left(\frac{(S_w - S_{wc})}{(S_w - S_{wc}) + S_g} \right) k_{row} + \left(\frac{S_g}{(S_w - S_{wc}) + S_g} \right) k_{rog} \qquad 3\text{-}27$$

The Saturation-Weighted Interpolation (SWI) model is a different version of Baker model which has been implemented in the Eclipse reservoir simulator. In this model the three-phase k_{ro} is only calculated based on Baker's suggested model and the water and gas relative permeabilities were assumed to be a function of their saturations. The Saturation-Weighted interpolation model relies on an assumption of complete segregation of the water and gas within porous media while oil phase is uniformly distributed.

3.2.3 Optimization Algorithm (Genetic Algorithm)

J. Holland (1975) introduced Genetic Algorithm (GA) as an adaptive exploratory search algorithm based on the idea of evolution in nature. Although GA has a random search in its evolution, it uses historical information to control and guide the random search through the search space. Having a robust search methodology, GA has been used to solve search and optimization problems. Generally, the GA method was designed to simulate the process of "survival of the fittest" introduced by Charles Darwin. In nature, there is always a competition among individuals for resourcing over a generation and the fittest individuals survive over the weaker ones. In genetics, every single chromosome represents a point in a search space. During the evolution process, all individuals compete for being selected for resourcing. The healthy individuals will be mainly successful in each competition and produce more offspring, and their genes propagate throughout the population. This process will increase the chance of producing offspring which are better than their parents.

To implement the genetic algorithm, a group of individuals is created randomly. Each in the population is evaluated, and its fitness score is calculated. The higher the fitness score, the higher the chance of being selected in the next step of the algorithm. The individuals with higher fitness scores are selected randomly to create one offspring. The created offspring are mutated randomly and evaluated to obtain the fitness score. This process continuous until the best solution has been found.

To apply GA as an optimization tool for obtaining k_r from coreflood experiment, it is required to define its components properly.

Chromosomes (Individual): a set of oil, water and gas k_r (Figure 3-4) are considered as a chromosome.

k_{ro}^1	k_{rw}^1	k_{rg}^1

Figure 3-4: Chromosome1 which is a set of all three-phase relative permeabilities (k_{ro}, k_{rw}, and k_{rg}).

<u>*Genes*</u>: parameters in the mathematical representation of k_r curves are considered as genes. For example for k_{rw} with LET functional form the genes are shown in Figure 3-5.

k_{rw}^0	L_w^o	E_w^o	T_w^o	S_{orw}

Figure 3-5: Genes in the water relative permeability.

<u>*Population*</u> is a group of randomly created chromosomes. A certain number of different sets of oil, water and gas k_r curves are considered as the population.

Figure 3-6 shows the GA for the history matching process. The procedure that was followed in the GA used in this study can be broken down into the following steps:

1. Generate an initial random population of chromosomes (candidate solutions: 100 sets of k_r in this study).

2. Run the coreflood simulation for each chromosome and find the misfit or mismatch value between experimental and simulation results of each individual. The lower misfit value is equivalent to higher fitness score.

3. Sort the chromosomes based on their misfit and select two chromosomes from the population with better fitness (the lower the misfit value, the bigger the chance of being selected). The two chromosomes are selected randomly from the top fifty percent of the sorted chromosomes.

4. Generate one offspring using the two randomly selected chromosomes in step 3. This step includes crossover and mutation. The crossover probability (λ) is randomly selected between value of 0 and 1. The offspring can be created using Eq. 3-28. Mutation is a random change in the created offspring and prevents the optimization process to be trapped in local minimum. It can be performed by changing one of the parameters slightly.

$$\text{Offspring} = \lambda \times (Chromosome1) + (1-\lambda) \times (Chromosome2) \qquad 3\text{-}28$$

5. Run the coreflood simulation for the offspring and find the misfit value. If this misfit value is less than the maximum misfit in the initial population, then the offspring would be placed in the population and the chromosome with the highest misfit value will be removed from the population. If the offspring's misfit value is larger than the maximum misfit value in the population then this offspring will be discarded, and new offspring will be generated (step 4).

6. Continue the process, step 3 to 5, until a satisfactory misfit value is achieved. This process may continue with more than 1000 iterations in order to achieve the minimum global misfit.

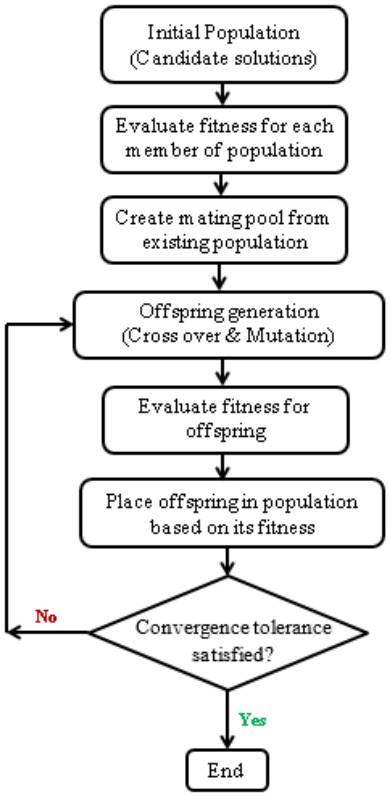

Figure 3-6: Genetic Algorithm for obtaining k_r from a coreflood experiment.

3.2.4 Application for Two-Phase Coreflood Experiments

The developed algorithm and computer code can be used for calculating two-phase k_r from two-phase coreflood experiments. For different combinations of two-phase flow e.g., gas/oil, oil/water and gas/water the misfit function is defined properly, and a similar procedure is taken. Corey and LET are the mathematical functional forms of the

two-phase relative permeabilities used in this project. The number of tuning parameters in two-phase flow problems is less than three-phase flow and history matching process will be much faster, and the optimization converges in a shorter time.

3.3 Experiments, Results, and Discussion

3.3.1 Experiments

Several WAG experiments, especially at near-miscible conditions, have been performed in the Centre for Enhanced Oil Recovery and CO_2 Solutions. These WAG experiments have been conducted on both water-wet and mixed-wet Clashach sandstone cores with the permeability of 65 and 1000 mD. Two WAG injection tests started with water flooding in the 65 mD water-wet, and mixed-wet cores. The 1st gas injection slug of these WAG injections had the widest range of saturation change in the oil phase and was used to demonstrate the performance of the proposed method for estimating three-phase k_r. Therefore, the results of these gas injections, e.g., pressure drop and production data were history matched to obtain the three-phase k_r for each phase during that period of injection.

Gas Injection in 65 mD, water-wet and mixed-wet cores at near-miscible conditions ($IFT_{g/o}$=0.04 mNm^{-1})

These experiments were studied the first gas injection after primary water flooding at near-miscible conditions at 1840 psia corresponding to the gas/oil IFT of 0.04 mN.m^{-1}. The residual oil after water flooding was 42% and 20% for water-wet and mixed-wet cores respectively. Gas was injected into the core at the rate of 25 cm^{3}h^{-1}, and then the injection rate was increased stepwise. Figure 3-7 compares the three-phase flow saturation path for the two gas injections between water-wet and mixed-wet cores. Figure 3-8 to Figure 3-11 show the cumulative oil productions and pressure drop across the core for the water-wet and mixed cores respectively.

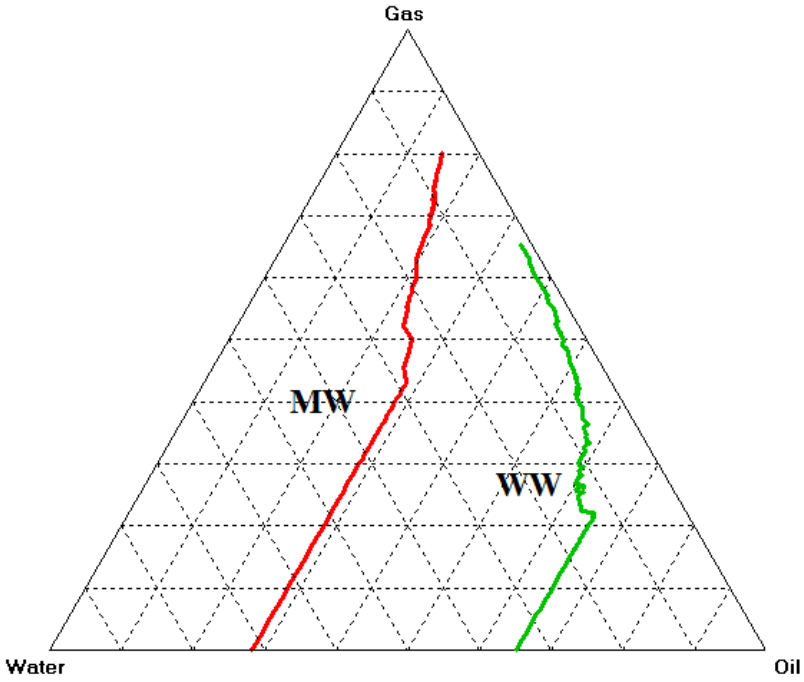

Figure 3-7: Comparison of three-phase saturation paths for first gas injections in 65 mD water-wet (green) and mixed-wet (red) cores.

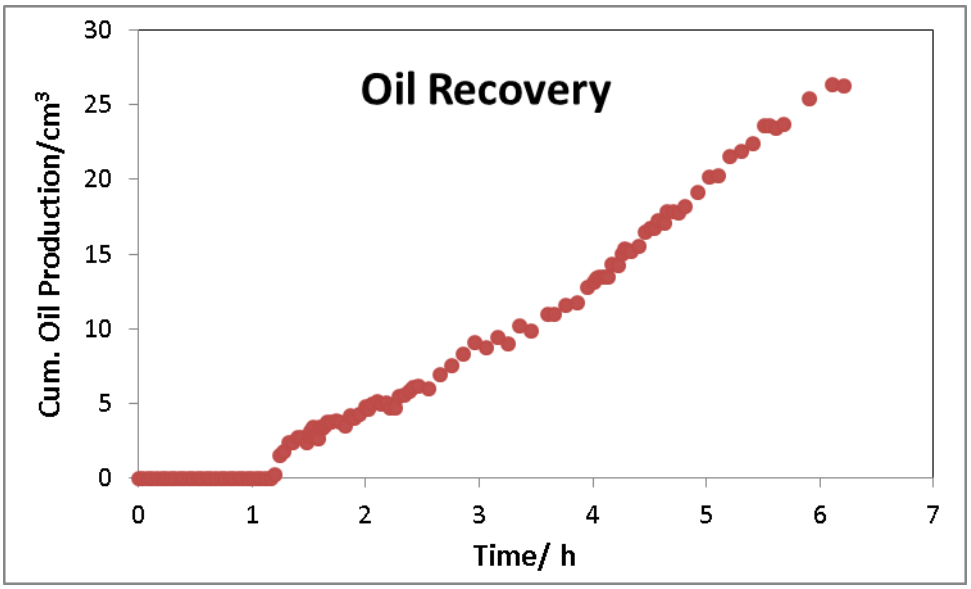

Figure 3-8: Cumulative Oil Production for first gas injection in 65 mD water-wet core.

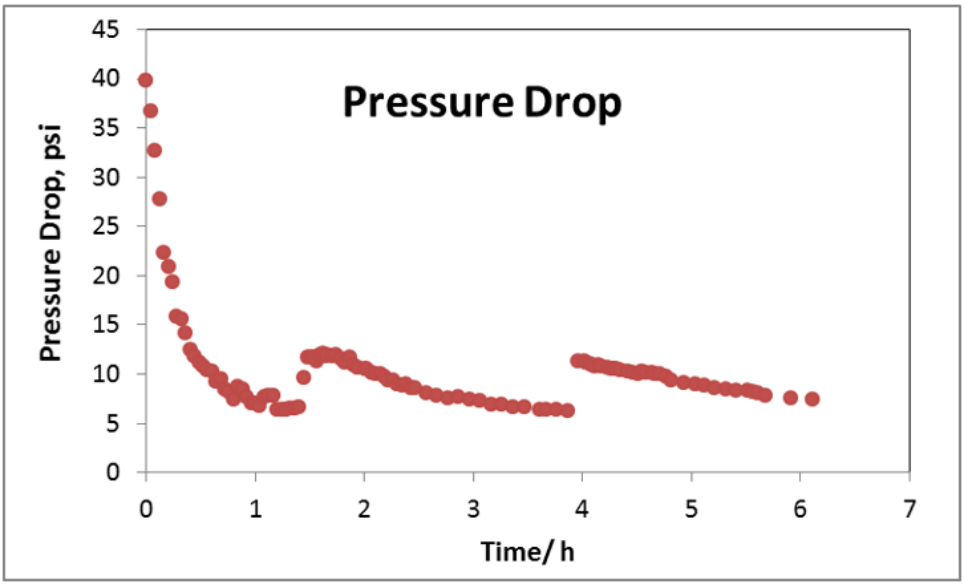

Figure 3-9: Pressure Drop across the core for first gas injection in 65 mD water-wet core.

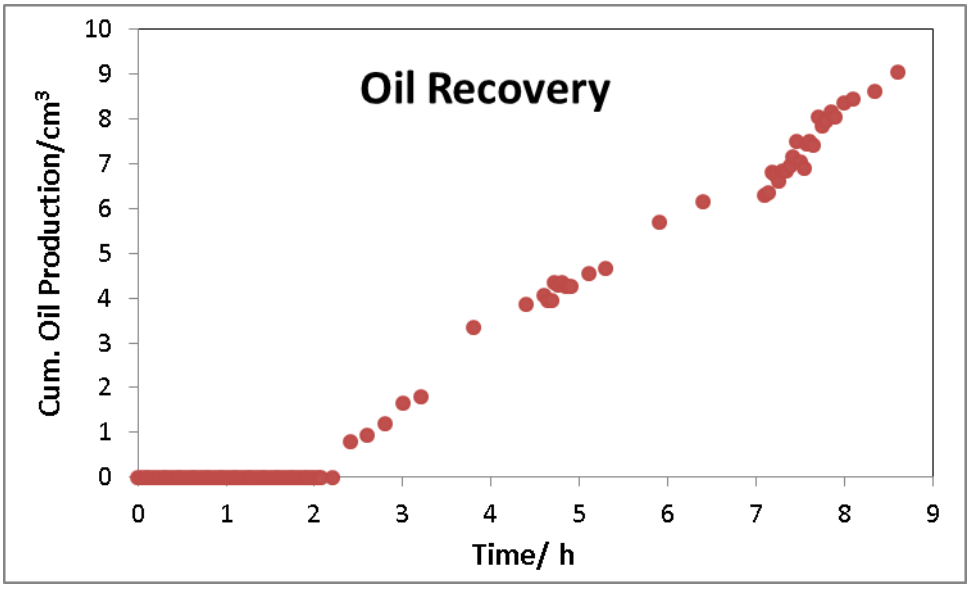

Figure 3-10: Cumulative Oil Production for first gas injection in 65 mD mixed-wet core.

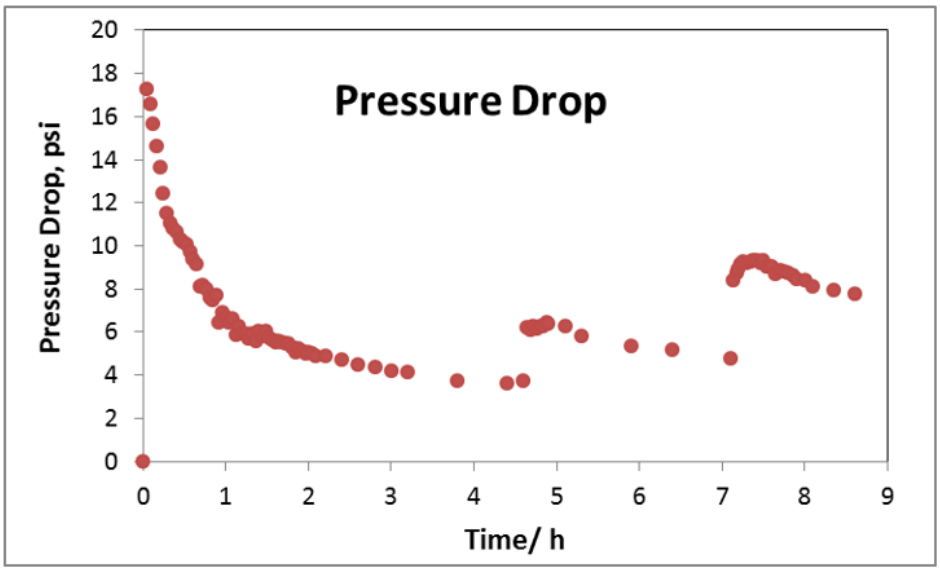

Figure 3-11: Pressure Drop across the core for first gas injection in 65 mD mixed-wet core

3.3.2 History Matching Results

The production of each fluid and pressure drop across the core for both the experimental and the history matched results of the first gas injection test are compared in Figure 3-13 to Figure 3-18 for both mixed-wet and water-wet cores, respectively. In order to insure the robustness of the history matching results, each experiment has been history matched for several times. For each individual history matching, more than 1000 (up to 5100) iterative runs have been performed to reach the minimum value for the objective function.

Figure ***3-12*** presents the progress of minimum misfit value and the average misfit value per 100 iterations throughout the history matching process for the first gas injection in 65 mD mixed-wet core. The history matching continued for 5100 iterations to make sure that the minimum misfit was reached. There are good agreements between the experimental, and the history matched data i.e. productions and pressure drop. For the history matching of gas injection in 65 mD, mixed-wet core both Baker (SWI) and Stone (Stone1) type models were used. As it is shown in Figure 3-13 to Figure 3-16, the former model had a better match in oil production while the latter model had a better match for pressure drop.

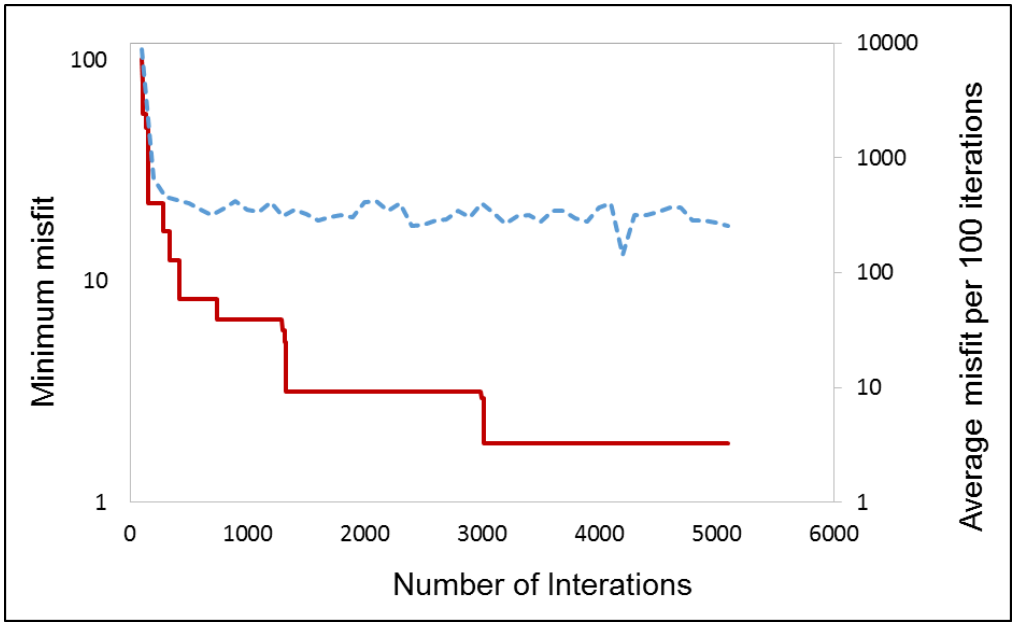

Figure 3-12: The minimum misfit and average misfit per 100 iterations for history matching of 1st gas injection in 65 mD mixed-wet core.

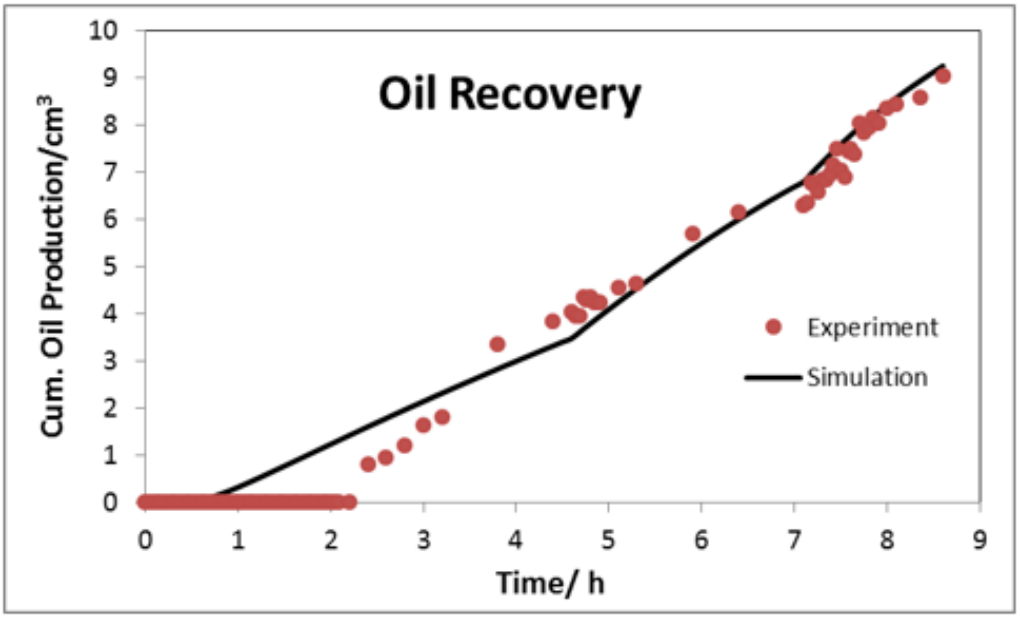

Figure 3-13: Comparison between history matching and experiment Cumulative Oil Production for 1st gas injection in 65 mD mixed-wet core. SWI three-phase k_{ro} function was used.

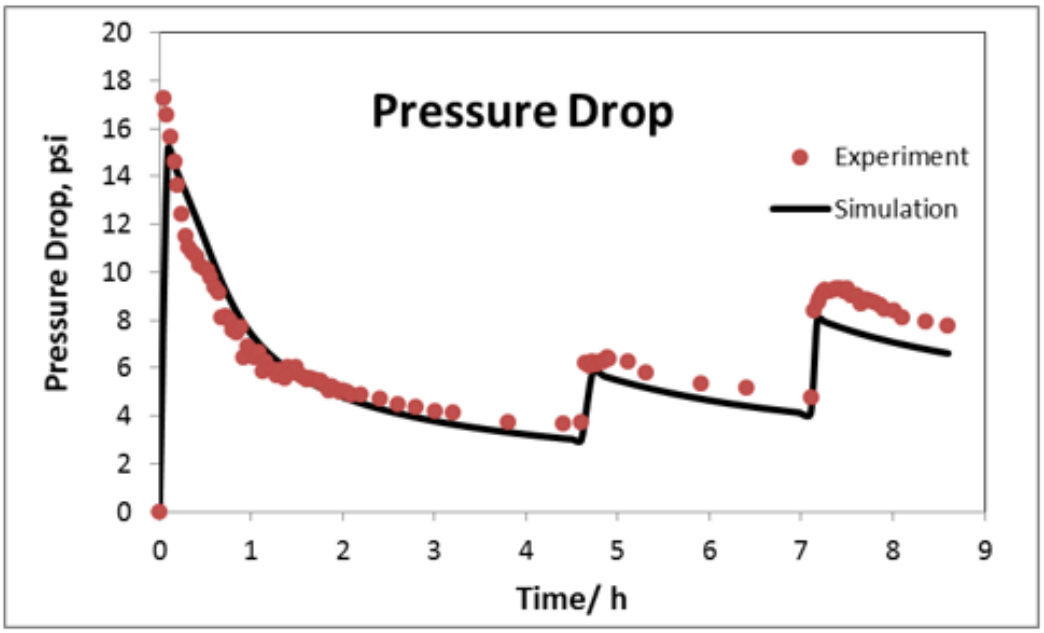

Figure 3-14: Comparison between history matching and experiment Pressure Drop for 1st gas injection in 65 mD mixed-wet core. SWI three-phase k_{ro} function was used.

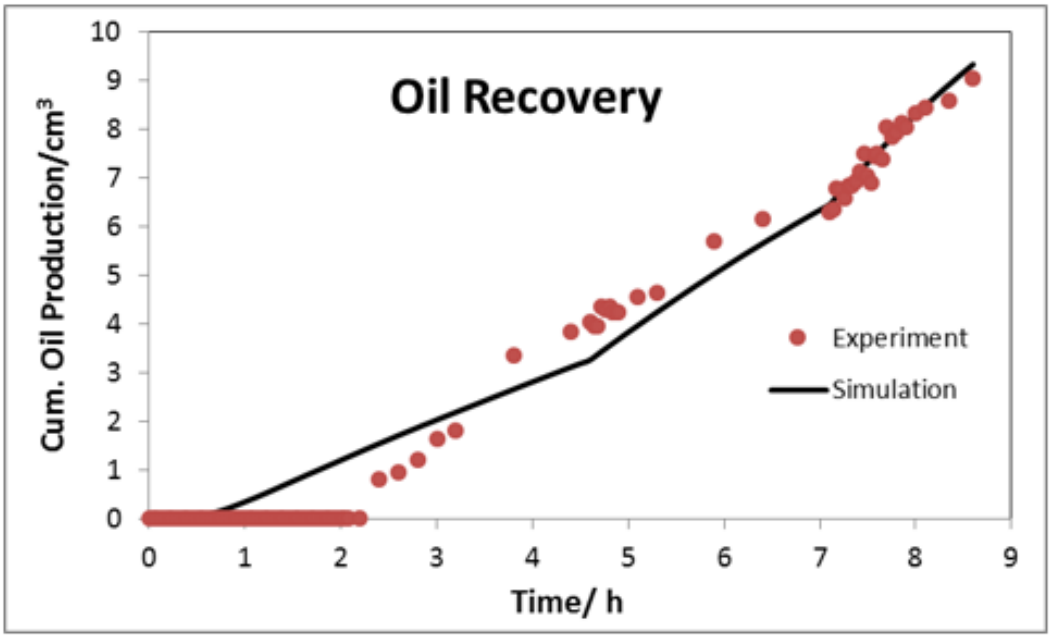

Figure 3-15: Comparison between history matching and experiment Cumulative Oil Production for 1st gas injection in 65 mD mixed-wet core. ST1 three-phase k_{ro} function was used.

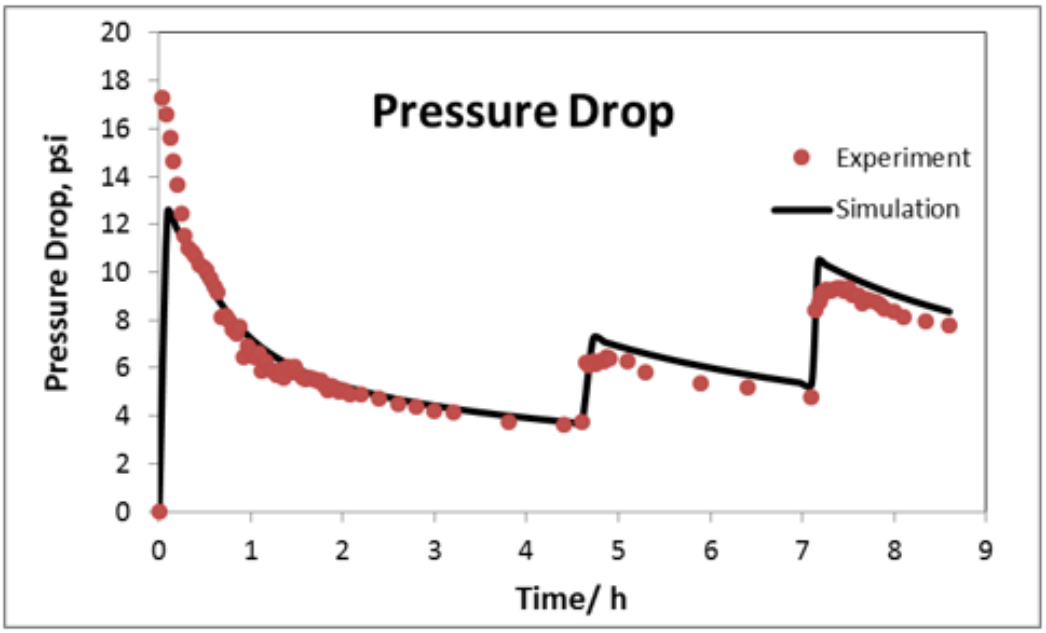

Figure 3-16: Comparison between history matching and experiment Pressure Drop for 1st gas injection in 65 mD mixed-wet core. ST1 three-phase k_{ro} function was used.

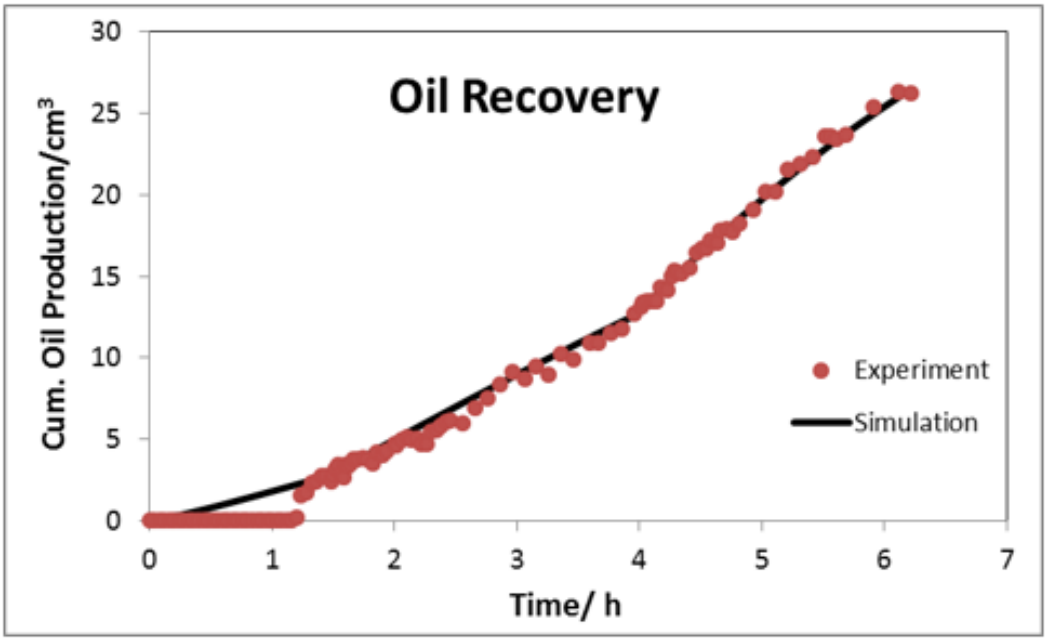

Figure 3-17: Comparison between history matching and experiment Cumulative Oil Production for 1st gas injection in 65 mD water-wet core. SWI three-phase k_{ro} function was used.

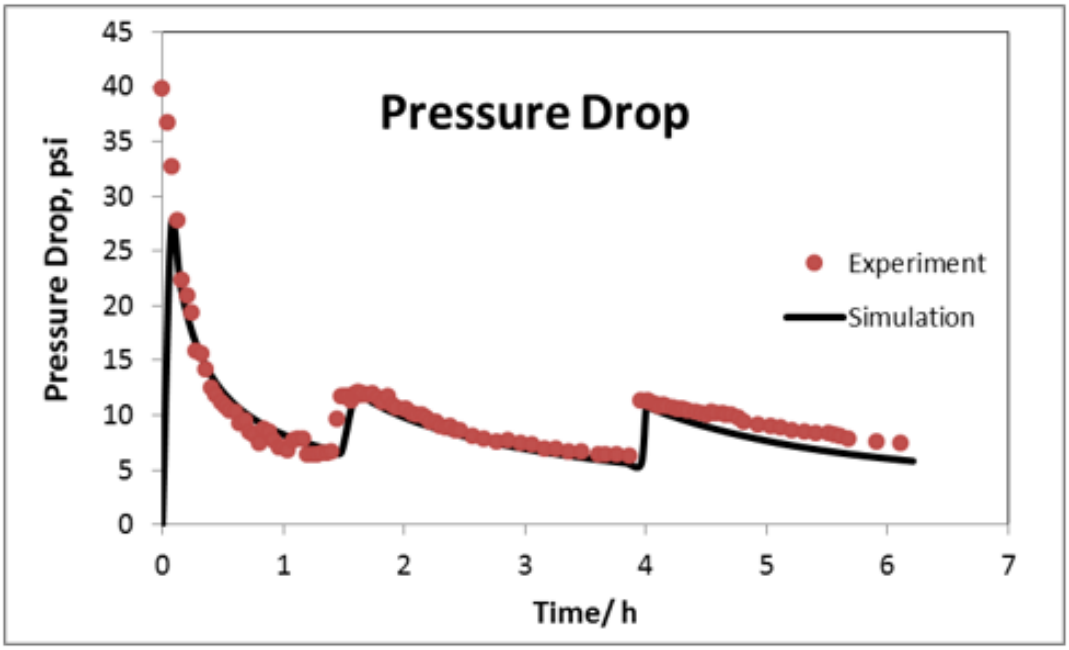

Figure 3-18: Comparison between history matching and experiment Pressure Drop for 1st gas injection in 65 mD water-wet core. SWI three-phase k_{ro} function was used.

The three-phase k_r values estimated from the history matching of these displacement experiments are representative for the three-phase saturation path which occurred in the experiments. The estimated three-phase k_{ro}, $k_{rw,}$ and k_{rg} versus their saturation for the experimental saturation path in mixed-wet and water-wet cores are shown in Figure 3-19 and Figure 3-20. The saturation ranges in these figures are mainly after the breakthrough of both gas and water phases.

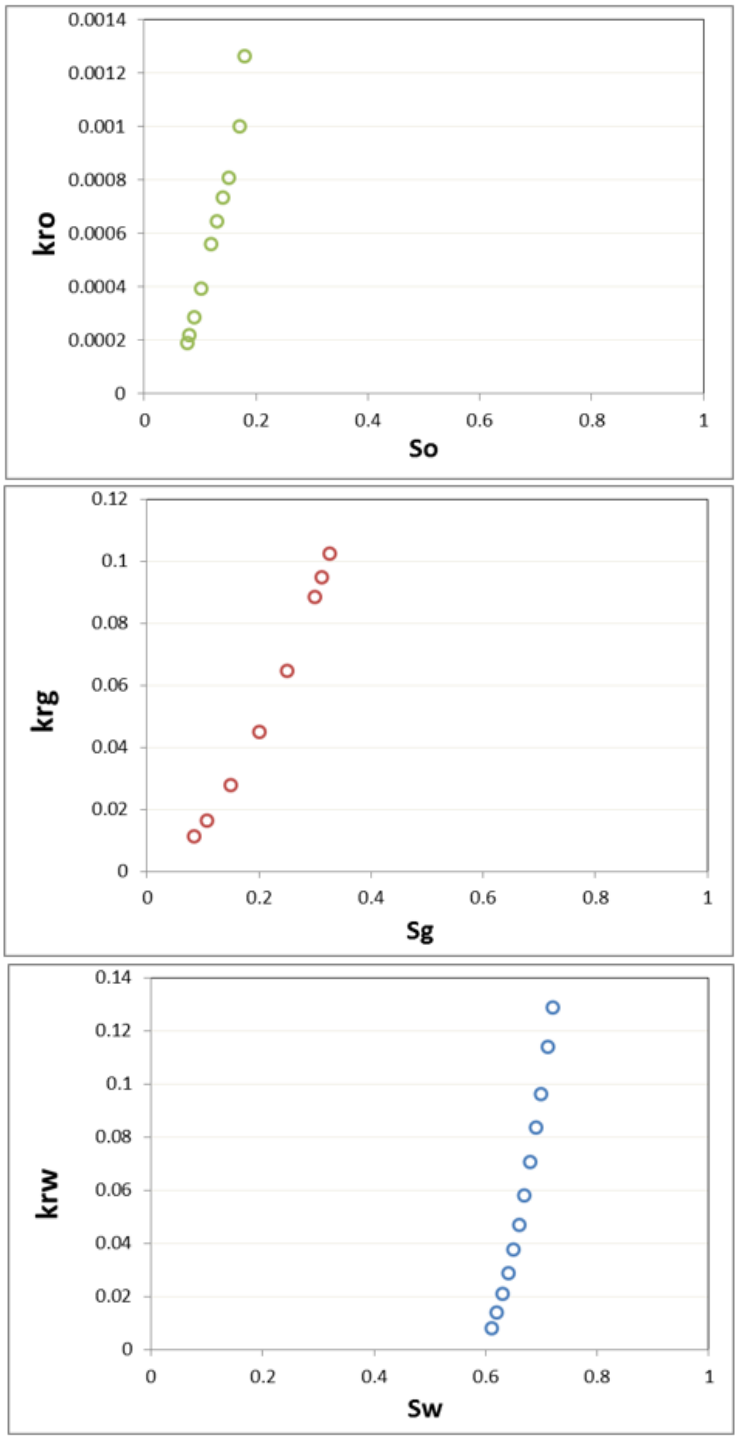

Figure 3-19: Estimated three-phase oil (top), gas (middle) and water (bottom) relative permeabilities from unsteady-state gas injection in 65 mD mixed-wet core.

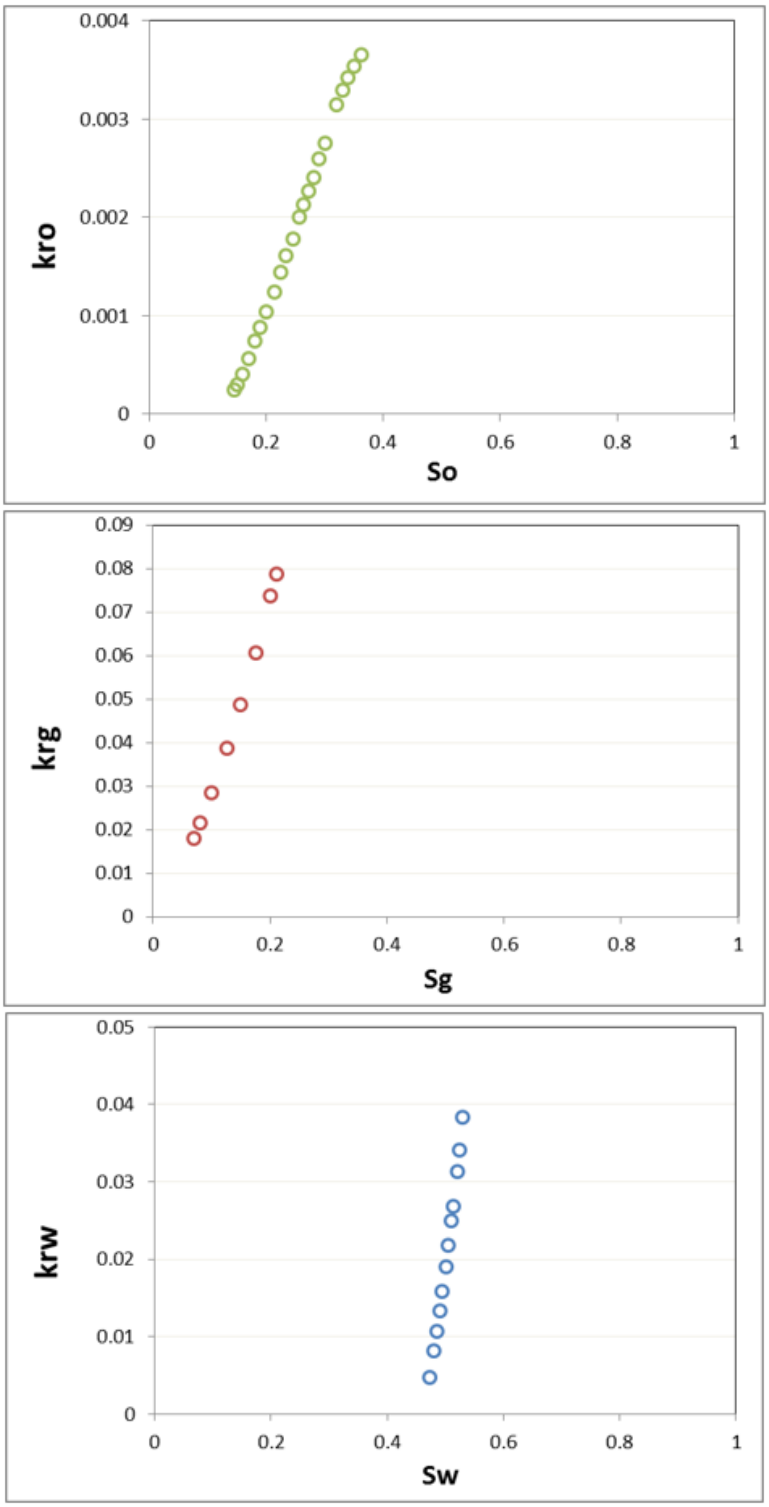

Figure 3-20: Estimated three-phase oil (top), gas (middle) and water (bottom) relative permeabilities from unsteady-state gas injection in 65 mD water-wet core.

3.4 Conclusions

The following conclusions can be drawn from this chapter:

1. A method has been proposed to obtain three-phase k_r curves by history matching three-phase coreflood displacements carried out in the laboratory.

2. A computer program has been developed to obtain three-phase k_r accurately from experimentally measured production and pressure drop data using unsteady-state coreflood displacements. This tool provides this opportunity to get three-phase k_r from different coreflood experiments performed at various rock and fluid properties and characterize three-phase flow in porous media.

3. Flexible parametric mathematical functions have been utilized for representing k_r curves in the optimization process. These functions produce k_r curves which reconcile most of the measured data published in the literature.

4. A global optimization algorithm, GA, has been employed in the estimation procedure of k_r. Applying GA minimizes the possibility of being in the local minimum solutions.

5. By using this approach, the limitations of analytical methods like JBN has been overcome. Capillary pressure can be included in the process of history matching. This approach is not limited to only immiscible conditions. For experiments with mass transfer, compositional simulation can be used for the coreflood simulation.

3.5 References

Aziz, K. and Settari, A., 1979. Petroleum Reservoir Simulation, London, UK, Applied Science Publishers (1979) 398.

Baker, L. E., 1988. Three-Phase Relative Permeability Correlations, paper SPE 17369, presented at the SPE Enhanced Oil Recovery Symposium, Tulsa, Oklahoma, USA.

Batycky, J. P., McCaffery, F. G., Hodgins, P. K. and Fisher, D. B., 1981. Interpreting Relative Permeability and Wettability from Unsteady-State Displacement Measurements. Society of Petroleum Engineers Journal, 21, 296-308.

Cao, P., and Siddiqui, S., 2010. Three-Phase Unsteady State Relative Permeability Measurement in Consolidated Cores Using Three Immiscible Liquids, presented at the International Symposium of the Society of Core Analysis, Halifax, Canada.

Chierici, G.L., 1984. Novel Relations for Drainage and Imbibition Relative Permeabilities. SPEJ, June 1984, pp. 275-276.

Corey, A.T., 1954. The Interrelation between Gas and Oil Relative Permeabilities. Prod. Monthly, 19 (1), pp. 38-41.

Danesh, A. (1998). PVT and Phase Behaviour of Petroleum Reservoir Fluids, Elsevier.

Delshad, M., and Pope, G.A., 1989. Comparison of the three-phase oil relative permeability models: Transport in Porous Media, 4(1), p. 59-83.

Ebeltoft, E., Lomeland, F., Brautaset, A., Haugen, A., 2014. Parameter based SCAL analysing relative permeability for full field application. In: Proceedings of International Symposium of the Society of Core Analysis. 8–11 September 2014, Avignon, France.

ECLIPSE Reservoir Simulation Software, Reference Manual/Technical Description, Version 2014.1, Schlumberger.

Eleri, O. O., Graue, A., Skauge, A. and Larsen, J. A., 1995. Calculation of Three-Phase Relative Permeabilities from Displacement Experiments with Measurements of in-situ Saturation. SCA Conference.

Eydinov, D., Gao, G., Li, G., and Reynolds, A.C., 2007. Simultaneous Estimation of Relative Permeability and Porosity/Permeability Fields by History Matching Production Data. Paper CIPC 2007-143 presented at the 8th Canadian International Petroleum Conference, Calgary, 12–14 June. http://dx.doi.org/10.2118/2007-143.

Hassan, M. E., Nielsen, R. F. and Calhoun, J. C., 1953. Effect of Pressure and Temperature on Oil-Water Interfacial Tensions for a Series of Hydrocarbons.

Holland, J., 1975. Adaptation in Natural and Artificial Systems, University of Michigan.

Honarpour, M., Koederitz, L., and Harvey, A.H., 1986. Relative permeability of petroleum reservoirs. C.R.C. Press, Boca Raton.

Johnson, E.F., Bossler, D.P., and Naumann, V.O., 1959. Calculation of Relative Permeability from Displacement Experiments, paper SPE 001023-G.

Kerig, P. D. and Watson, A. T., 1987. A New Algorithm for Estimating Relative Permeabilities from Displacement Experiments. SPE Reservoir Engineering, 2, 103-112.

Kerig, P., Watson, A., 1986. Relative-permeability estimation from displacement experiments: an error analysis. SPE Reservoir Eng. 1 (02), 175–182.

Kulkarni, R., Watson, A.T., Nordtvedt, J.E., Sylte, A., 1998. Two-Phase Flow in Porous Media: Property Identification and Model Validation“, AIChE Journal, Vol. 44, No. 11.

Lomeland, F., Ebeltoft, E, and Thomas, W.H., 2005. A new versatile relative permeability correlation. In: Proceedings of International Symposium of the Society of Core Analysts. Toronto, Canada, pp. 21–25.

Marquardt, D.W., 1963. An Algorithm for Least-Square Estimation of Nonlinear Parameters: Soc. Industrial Applied Math Journal, 11, p. 431-441.

Mejia, G.M., Watson, A.T., and Nordtvedt, J.E., 1996, Estimation of Three-phase Functions in Porous Media: AIChE Journal, 42(7).

Moghadasi, L., Guadagnini, A., Inzoli, F. and Bartosek, M., 2015. Interpretation of two-phase relative permeability curves through multiple formulations and Model Quality criteria. Journal of Petroleum Science and Engineering, 135, 738-749.

Nordvedt, J.E., Mejia, G., Yang, P., and Watson, A.T., 1997. Estimation of Capillary Pressure and Relative Permeability Functions from Centrifuge Experiments. SPE Reservoir Engineering, Vol. 8, No. 4, pp. 292-298.Press.

Schembre, J.M. and Kovscek, A.R., 2006.Estimation of dynamic relative permeability and capillary pressure from counter current imbibition experiment. Transp. Porous Med. 65(1), 31–51.

Sigmund, P. and McCaffery, F., 1979. An improved unsteady-state procedure for determining the relative permeability characteristics of heterogeneous porous media (includes associated papers 8028 and 8777). SPEJ. 19 (01), 15–28.

Stone, H.L., 1970. Probability Model for Estimating Three-Phase Relative Permeability, SPE Journal of Petroleum Technology, paper SPE 2116, (02).

Stone, H.L., 1973. Estimation of Three-Phase Relative Permeability and Residual Oil Data, paper SPE 73-04-06, (10-12).

Sun, X., and Mohanty, K.K., 2005, Estimation of Flow Functions during Drainage Using Genetic Algorithm: SPE Journal, paper SPE 84548-PA, (12).

Ucan, S., Civan, F. and Evans, R. D., 1993. Simulated Annealing for Relative Permeability and Capillary Pressure From Unsteady-State Non-Darcy Displacement. Society of Petroleum Engineers.

Virnovskii, G. A., 1984. Determination of Relative Permeabilities in a Three-Phase Flow in a Porous Media. Translated from Izvestiya Akademii Nauk SSSR, Mekhanika Zhidkosti i Gaza, No.5, pp. 187-189.

Zhang, Y., Li, H. and Yang, D., 2012. Simultaneous Estimation of Relative Permeability and Capillary Pressure Using Ensemble-Based History Matching Techniques. Transport in Porous Media, 94, 259-276.

Chapter 4 - Simultaneous Estimation of Relative Permeability and Capillary Pressure from Coreflood Experiments

Relative Permeability (k_r) and capillary pressure (P_c) curves are conventionally measured separately. k_r is usually measured using two methods of 'steady state' and 'unsteady state' experiments. P_c is measured by: mercury porosimetry, the porous plate method or by centrifuge method. The drawback of determining k_r and P_c separately is that they may not be consistent with each other, and the measured P_c does not correspond to the k_r which is measured from a dynamic flow system. Therefore, simultaneous determination of P_c and k_r for a given system would be preferred. In previous attempts for simultaneous estimation of k_r and P_c, two independent functions were used to generate k_r and P_c in the process of the history matching. To reduce the associated non-uniqueness problem of history matching, some in-situ measurements such as saturation and pressure profiles may be included in the history matching data. The objective of this part of the study is to develop a methodology to estimate k_r and P_c simultaneously when in-situ measurements are not available.

4.1 Introduction

More often P_c has been neglected in the process of obtaining k_r from coreflood experiments. However, it is well known that P_c could, in some cases affect the flow significantly. Therefore, methods were developed to simulate mathematically, and history match the experiment while accounting for the P_c effects, and estimate the set of phase relative permeabilities that are consistent with the real flow and result in the best match between calculated and measured pressure and production data. All published methods in which the authors have aimed to account for the effect of P_c have used separately measured P_c curves together with k_r curves for simulation purposes.

Conventionally, P_c is measured by: mercury porosimetry, the porous plate method or by centrifuge method. P_c measurement using mercury porosimetry involves injecting mercury into a core sample under vacuum. This method is very fast and covers a broad range of saturation and P_c. The volume of injected mercury at each pressure step determines the non-wetting phase saturation. The mercury injection is performed on a dry evacuated sample assuming mercury is a non-wetting phase, and air (or mercury vapour) is the wetting phase. Therefore, one of the disadvantages of this method is the lack of a true wetting and non-wetting phase during the test. The conversion should be made from the test conditions to the reservoir conditions, which requires contact angle and interfacial tension information on reservoir fluids as well as mercury/air, or mercury/mercury vapour. Moreover, this method was developed for a strongly water-wet system, while it is now well recognized that most of the reservoirs are not strongly water-wet.

In the porous plate method, the flat face of a rock sample that is first saturated with one fluid, e.g., water, is pressed against a flat porous plate (or membrane) in a chamber filled with the second fluid, e.g., gas. The porous plate is also saturated with water which is the displaced phase in the core. Then, the pressure in the gas phase is increased by a small step, forcing gas to displace the water in the sample. When the displacement stops and there is no further water production, the difference in pressure between the gas in the chamber and the water on the lower side of the porous plate is the P_c corresponding to the saturation of remaining water in the sample. Next, the pressure of the gas is increased again, and the pressure difference is measured at the end of displacement, and this process is repeated, yielding the P_c relationship for decreasing water saturation. The porous plate method can provide relatively more accurate (compared to the mercury injection) P_c measurements because it could use reservoir

'native' fluids and 'native-state' rocks (Newsham et al. (2004)). The primary disadvantage of this method is a limitation on the highest P_c that can be measured and this is related to the porous plate (membrane) properties. Another significant disadvantage of the porous plate method is the long times required to reach equilibrium at each saturation level. Furthermore, the porous plate method is difficult to operate at high pore pressure and temperature.

The centrifuge method imposes a centrifugal force on the sample which is saturated by one phase e.g. water and is immersed in another phase, e.g., oil in specially designed holders. At each particular rpm (revolutions per minute) the amount of water expelled from the core is measured, and the average P_c is calculated. The rate is then increased in steps, and the P_c is calculated at the corresponding water saturation and, therefore, a full drainage curve is produced. The main advantage of the centrifuge is the ability to obtain P_c data very quickly compared to the porous plate method. Furthermore, this method can now be operated at reservoir pressure and temperature conditions. Similar to the porous plate method, the main disadvantage of the centrifuge method is the limited maximum pressure which is around 1000 psi.

One of the disadvantages of determining k_r and P_c separately is that they are not consistent with each other, and the measured P_c does not correspond to the k_r that is measured from dynamic flow system. As Kalaydjian (1992) and Bentsen (1998) pointed out the dynamic P_c may be different from the static P_c. Factors such as flow rate affect the dynamic P_c. Therefore, simultaneous determination of P_c and k_r for a given system is preferred. Jennings et al. (1988) presented a new method of measuring P_c and k_r that involves history matching of the transient response of a porous-plate experiment. Lenormand et al. (1993) developed a semi-dynamic method for measurement of all cycles of P_c (drainage and imbibition for both positive and negative P_c) and any wettability. This technique can be used at high pressure and high temperature in a modified Hassler cell and can be automated. In Lenormand method, one fluid is injected at a constant rate or constant pressure into the core, while the second fluid is flushed across the core outlet. When steady-state conditions are achieved, P_c at the injection face of the core is calculated as the difference between the upstream and downstream pressures. The saturation at the inlet face should be measured during the test, and X-ray CT scanning can be used for this purpose. Additional points are gained by stepwise changing of the injection rate or injection pressure. A similar technique to the one introduced by Lenormand was reported by Pini and Benson (2013) to measure P_c and k_r

simultaneously from core flood experiments. Virnovsky et al. (1995) presented a new method to interpret multi-rate steady-state flow experiments for k_r and P_c simultaneously eliminating errors caused by the capillary end-effect. Other researchers applied history matching techniques to estimate k_r and P_c simultaneously from unsteady state core flood experiments. Ucan et al. (1993) used simulated annealing (an optimization method), Sun and Mohanty (2005) applied the genetic algorithm and Zhang et al. (2012) implemented ensemble-based history matching techniques to estimate k_r and P_c at the same time from unsteady state experiments. In previous research studies, two independent functions were used to generate k_r and P_c in the process of the history matching. To reduce the associated non-uniqueness problem of history matching, some in-situ measurements such as saturation and pressure profiles may be included in the history matching data.

In this study, the developed computer program which has been presented in Chapter 3, is extended to automated history matching on unsteady state two-phase core flood experiments and compute k_r and P_c simultaneously.

In the new methodology, the objective is to honour a known physical relationship between the core k_r and the P_c curve. Making the k_r function dependent on the P_c in the history matching process will reduce the number of tuning parameters and is expected to reduce the uncertainty associated with the history matching process. Although this is not the ultimate solution to the non-uniqueness problem of history matching process, it can improve the optimization process and the accuracy of the estimated P_c and k_r. This methodology can be useful in the absence of any in-situ measurements.

4.2 New Methodology

4.2.1 Theoretical Background

Existing calculation methods of k_r curves from P_c data are based on the model originally proposed by Purcell (1949) for calculating absolute core permeability from mercury injection data. He was the first researcher who presented the derivation of permeability from P_c measurement using mercury injection and postulated that porous rocks can be approximated by a bundle of (tortuous) capillary tubes with various pore diameters. The contribution of flow from various pore diameters is considered in Purcell formulation by integrating the squared inverse of the P_c versus mercury saturation curve as follows:

$$K = 0.5(\sigma_{Hg-air}\cos\theta)^2 Fp\phi \int_0^1 dSw/Pc^2 \quad 4\text{-}1$$

Where K is permeability in m^2, Fp is dimensionless Purcell lithology factor, σ_{Hg-air} is mercury/air interfacial tension in N /m, θ is wetting phase contact angle in radians, ϕ and S_w are porosity and wetting phase saturation in fraction of pore volume, P_c is capillary pressure in Pascal and 0.5 is units' consistency factor.

Later Purcell equation was extended to k_r calculation by Gates and Leits (1950). They calculated the effective and absolute permeability based on the Purcell model and suggested the following equations for the k_r of the wetting and non-wetting phase k_r:

$$k_{rw} = \frac{\int_0^{Sw} \frac{1}{Pc^2} dSw}{\int_0^1 \frac{1}{Pc^2} dSw} \quad 4\text{-}2$$

$$k_{rnw} = \frac{\int_{Sw}^1 \frac{1}{Pc^2} dSw}{\int_0^1 \frac{1}{Pc^2} dSw} \quad 4\text{-}3$$

Burdine (1953) introduced a tortuosity factor as a function of wetting phase saturation to the k_r correlations developed by Gates and Leits. He proposed the following k_r relations for the wetting and non-wetting phases:

$$k_{rw} = (\lambda_{rw})^2 \frac{\int_0^{Sw} \frac{1}{Pc^2} dSw}{\int_0^1 \frac{1}{Pc^2} dSw} \quad 4\text{-}4$$

$$k_{rnw} = (\lambda_{rnw})^2 \frac{\int_{Sw}^0 \frac{1}{Pc^2} dSw}{\int_0^1 \frac{1}{Pc^2} dSw} \quad 4\text{-}5$$

where λ_{rw} and λ_{rnw} are the tortuosity factors of the wetting and non-wetting phases which can be obtained by:

$$\lambda_{rw} = \frac{\tau_w(1)}{\tau_w(S_w)} = \frac{Sw - Swi}{1 - Swi} \quad 4\text{-}6$$

$$\lambda_{rnw} = \frac{\tau_{nw}(1)}{\tau_{nw}(S_w)} = \frac{1 - Sw - Se}{1 - Swi - Se} \qquad 4\text{-}7$$

where S_{wi} is the minimum wetting phase saturation from the P_c curve and S_e is the residual saturation of the non-wetting phase. $\tau_w\ (1.0)$ and $\tau_w\ (S_w)$ are the tortuosities of the pores containing the wetting phase when the wetting phase saturation is equal to 1 and S_w, respectively. τ_{nw} is the tortuosity of the pores containing the non-wetting phase. In Burdine's equations, the integrals ratio and the tortuosity ratio present the change in flow volume and path length of each phase respectively.

Mualem (1976) proposed an analytical model, with the similar concept of the one introduced by Purcell, which predicts the relative permeabilities using the P_c curve.

$$k_{rw} = S_e^n \left[\frac{\int_0^{S_e} \frac{1}{Pc} dSw}{\int_0^1 \frac{1}{Pc} dSw} \right]^2 \qquad 4\text{-}8$$

$$k_{rnw} = (1 - S_e)^n \left[\frac{\int_{S_e}^1 \frac{1}{Pc} dSw}{\int_0^1 \frac{1}{Pc} dSw} \right]^2 \qquad 4\text{-}9$$

$$S_e = \frac{Sw - Swr}{1 - Swr - Snwr} \qquad 4\text{-}10$$

where S_{wr} and S_{nwr} are the residual saturations of the wetting and non-wetting phases. According to his study on the available data in the literature, he suggested the value of 0.5 for "n" exponent in the k_r equations.

The Integral terms of Purcell, Burdine, and Mualem models can be solved either analytically or numerically. The mathematical expression between P_c and S_w is necessary for the analytical solution. Most of the models proposed for k_r estimation from P_c data differ in their mathematical expression for P_c data in the integral term.

Li and Horne ((2002), (2006)) compared the calculated k_r curves from Gates and Leits and Burdine models with the measured k_r curves. They concluded that the Gates and Leits model gives the best fit to the experimental data for wetting phase k_r while Burdine model gives the best fit for the non-wetting phase k_r. Therefore, in the current

study, the Gates and Leits model was used to calculate the wetting phase k_r and the Burdine model for the non-wetting phase k_r.

4.2.2 Estimation Procedure

The methodology consists of three principal components. First, a mathematical model is used to represent the fluid flow through porous media. The model should be adequately comprehensive so that all the relevant physical effects within the displacement experiments can be represented. The Eclipse simulator was chosen for this purpose and used as the core flood simulator. The second element is functional representation for k_r and P_c curves that need to be estimated, and the third one is an optimization tool which is utilized to minimize the misfit (objective) function.

The P_c was defined as a function of saturation (with some tuning parameters), and the k_r was linked to P_c. In the simulation, the tuning parameters were adjusted during history matching by ensuring that the results of simulation match the results of the coreflood experiment. For the P_c function, the model introduced by Li (2004) was used, which is defined as:

$$P_c = P_{\max}\left(1 - bS_w^*\right)^{\frac{-1}{\lambda}} \qquad 4\text{-}11$$

$$b = 1 - \left(\frac{P_e}{P_{\max}}\right)^{-\lambda} \qquad 4\text{-}12$$

Where P_{max} is the maximum value of P_c at residual wetting phase saturation, P_e is the threshold (entry) pressure; λ is the pore size distribution index, and b is a constant which is calculated from Eq 4-12. As suggested by Li and Horne (2006), the Gates and Leits model was used to derive the wetting phase k_r and the Burdine model for the non-wetting phase k_r. Therefore, the wetting and non-wetting k_r values were calculated using the following equations:

$$k_{rw} = k_{rw}^0\left[\frac{\int_0^{S_e}\frac{1}{P_c^2}dSw}{\int_0^1\frac{1}{P_c^2}dSw}\right] \qquad 4\text{-}13$$

$$k_{rnw} = k_{ro}^{0}(1-S_e)^2 \left[\frac{\int_{S_e}^{1} \frac{1}{P_c^2} dSw}{\int_{0}^{1} \frac{1}{P_c^2} dSw} \right] \qquad 4\text{-}14$$

$$S_e = \frac{S_w - S_{wc}}{1 - S_{wc} - S_{orw}} \qquad 4\text{-}15$$

Where k_{rw}^{0} and k_{ro}^{0} are the endpoint relative permeabilities for water (wetting phase) and oil (non-wetting phase), respectively. Therefore, the tuning parameters are P_{max}, P_e, λ, k_{rw}^{0}, k_{ro}^{0}.

A computer program was developed for this purpose based on the Genetic Algorithm (GA) which provides best estimates of k_r and P_c simultaneously by minimizing the error between experimental results and estimated ones. GA is one of the possible choices for finding global optimum and avoiding getting trapped in a local optimum. The misfit value as the objective function in history matching is given by:

$$Misfit = \sum_{t=1}^{N_t} \left[W_{Q_i} \left(Q_{it}^{Exp} - Q_{it}^{Sim} \right)^2 + W_{Qj} \left(Q_{jt}^{Exp} - Q_{jt}^{Sim} \right)^2 + W_{\Delta P} \left(\Delta P_t^{Exp} - \Delta P_t^{Sim} \right)^2 \right] \qquad 4\text{-}16$$

Where W is a weighting factor which was introduced in Chapter 3 and can be adjusted for each type of measured data. In this study, the mean squared value of each data type has been used instead of the variance and w is equal one.

Figure 4-1 shows the GA for the history matching process. The procedure that is followed in the GA used in this study can be broken down into the following steps:

1. Generate an initial random population of chromosomes (candidate solutions). For the conventional method: a set of P_c and k_r and for new method: a set of P_c and then the k_r is calculated from P_c.
2. Run the coreflood simulation for each chromosome and find the misfit value between experimental and simulated data of each individual.
3. Sort the chromosomes based on their misfit and select two chromosomes from the population with better fitness (the better bigger the chance of being selected).
4. Generate the offspring using the two selected chromosomes in step 3. This step includes crossover and mutation.
5. Run the coreflood simulation for the offspring and find the misfit value. If this misfit value is less than the maximum misfit in the initial population, then the offspring would be placed in the population and the chromosome with the highest misfit value will be

removed from the population. If the offspring's misfit value is larger than the maximum misfit value in the population then this offspring will be discarded, and new offspring will be generated (step 4).

6. Continue the process, using steps 3 to 5, until a satisfactory misfit value is achieved.

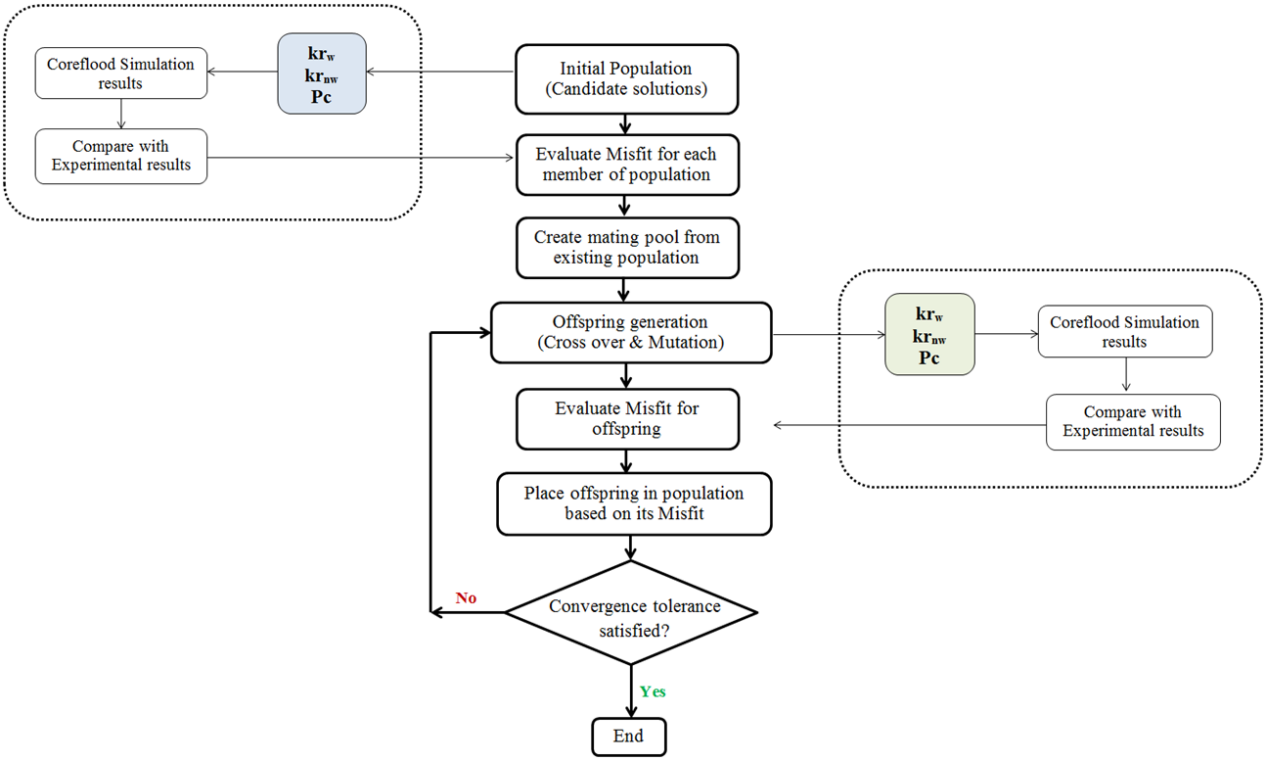

Figure 4-1: Genetic Algorithm for Simultaneous computation of k_r and Pc from a coreflood experiment

4.3 Verification of Methodology, Results, and Discussion

4.3.1 Experimental Data

The data published by Sun and Mohanty (2005) which were obtained from an unsteady-state primary drainage experiment have been used in this study. Water-wet Berea sandstone was used as the core sample. The core was 24.13 cm long with the diameter of 5 cm. The permeability and porosity of the rock were 157.8 mD and 22%, respectively. Brine (5% NaCl) was used as the wetting phase, and a mixture of Soltrol 130 was used as the non-wetting phase fluid. The core was oriented vertically, and the non-wetting phase (oil) was injected, at a constant rate of 22.5 cm^3/h, from top to the core which was fully saturated with the wetting phase (water). The injection was continued until no further brine was produced. The core was X-ray scanned slice by slice at a series of time points. The in-situ saturation profiles were obtained using ten

equally distributed slices in the axial direction. Figure 4-2, Figure 4-3 and Figure 4-4 present the cumulative water production, pressure drop across the core and the in-situ oil saturation profiles respectively.

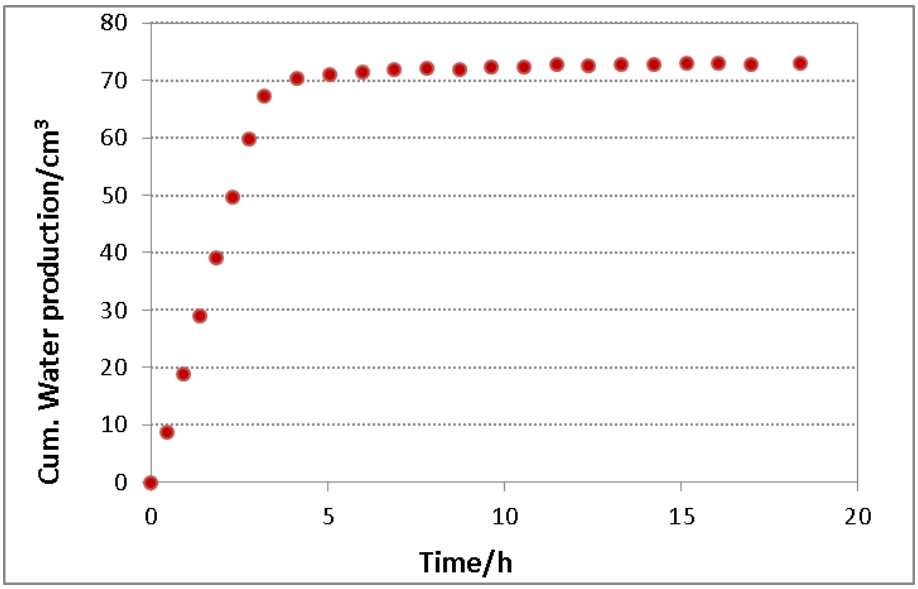

Figure 4-2: Cumulative water production (cm^3) for unsteady-state coreflood experiment (Sun & Mohanty (2005)).

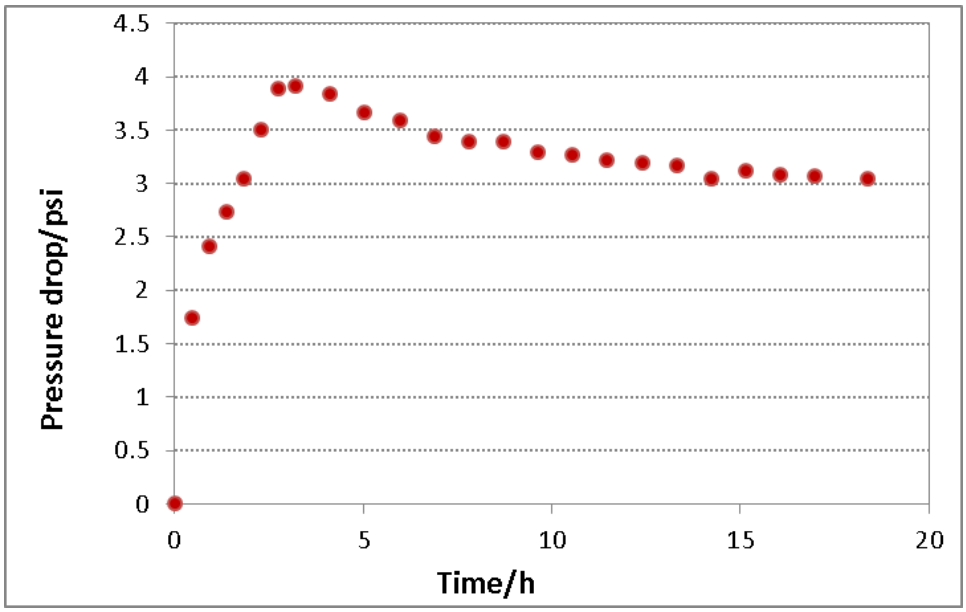

Figure 4-3: Pressure drop (psi) across for unsteady-state coreflood experiment (Sun & Mohanty (2005)).

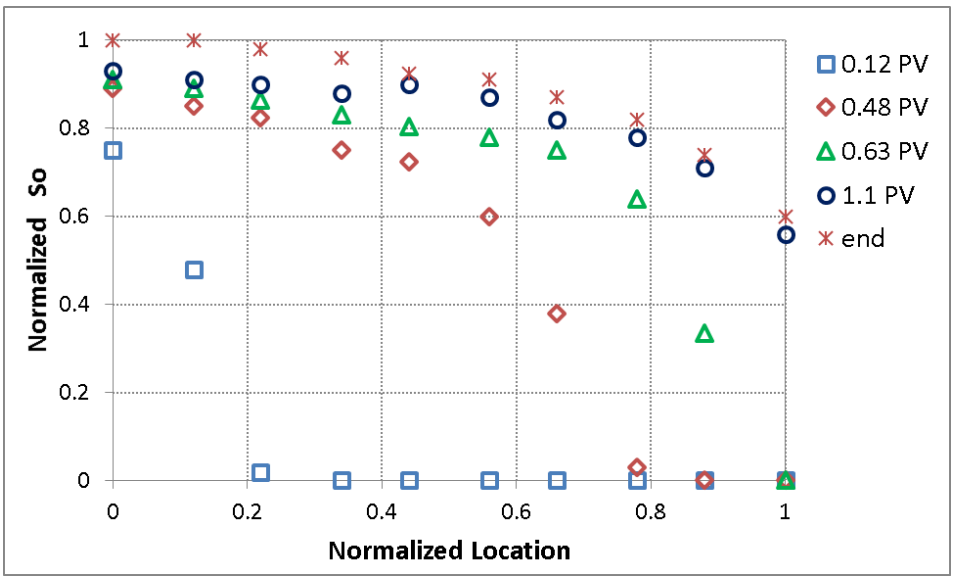

Figure 4-4: In-situ saturation profiles at different times during the unsteady-state coreflood experiment (Sun & Mohanty (2005)).

Sun and Mohanty (2005) used production and pressure drop data and the in-situ saturation profiles to perform the history match and calculate k_r and P_c for this rock and fluid system. They have applied a genetic algorithm as the optimization tool. They obtained a good match to the pressure drop, but there was some mismatch in the saturation profiles and the water production data. Later Zhang et al. (2012) used the results of this experiment with an optimization tool based on Ensemble Kalman Filter methods and simultaneously calculated k_r and P_c from this unsteady-state experiment. Similar to Sun and Mohanty (2005), there was some mismatch for the saturation profiles, but they obtained a better match for water production data. In both studies above k_r and P_c were calculated independently. Although there is no direct measurement of their P_c curve since they used the in-situ saturation profiles in history matching, which helped to reduce the uncertainty in their results, it can be assumed that their computed k_r and P_c are reliable and could be used as the reference. Figure 4-5 and Figure 4-6 show the estimated two-phase oil/water k_r and P_c obtained by Zhang et al. (2012) by history matching the unsteady-stated coreflood experiment accounting for the measured in-situ saturation profiles.

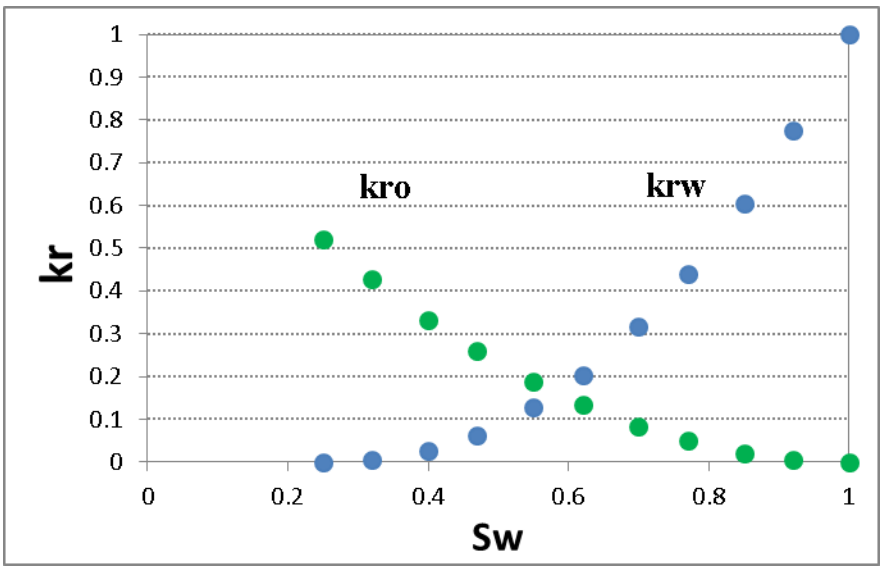

Figure 4-5: Estimated oil/water relative permeability from the unsteady-state coreflood experiment (Zhang et al. (2012)).

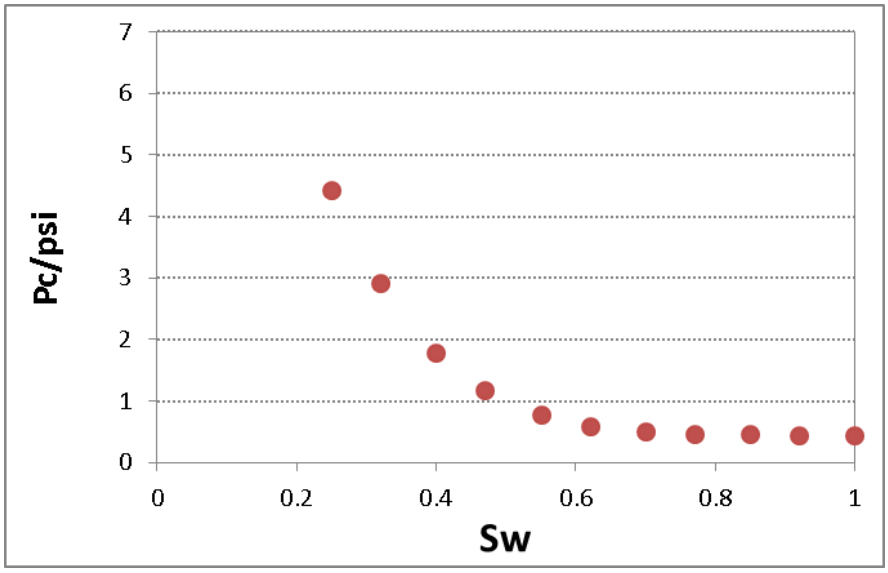

Figure 4-6: Estimated P_{cow} from the unsteady-state coreflood experiment (Zhang et al. (2012)).

In the new method it is assumed that as in-situ saturation profiles are not the type of data that is usually available, production and pressure drop data are used as the only measured data. The k_r and P_c were estimated from this coreflood experiment once considering the two flow functions are independent of each other and in another case as interdependent.

4.3.2 Approach A- New Method: Interdependent k_r & P_c Functions

As described before, in this approach the P_c curve is computed first using Eq.4-11 and then the wetting and non-wetting phase k_r values are calculated from P_c curve and Equations 4-13 and4-14. As the core was water-wet and initially saturated with 100%

water, it was assumed that the k_{rw}^{0} (endpoint water relative permeability) is equal to one. The number of parameters which should be estimated in the process of history matching has been reduced to four parameters; k_{ro}^{0}, P_{max}, P_e, λ. The connate (irreducible) water saturation was assumed to be known, i.e., the value given in the Sun and Mohanty's paper as 0.25 (S_{wc}=0.25). The history matching was run for a sufficient number of iterations to find the global optimum. Figure 4-7 and Figure 4-8 show the simulation results for water production and pressure drop compared with the experimental data. Excellent matches have been obtained for these two observation data. The computed k_r and P_c curves are presented in Figure 4-9 and Figure 4-10.

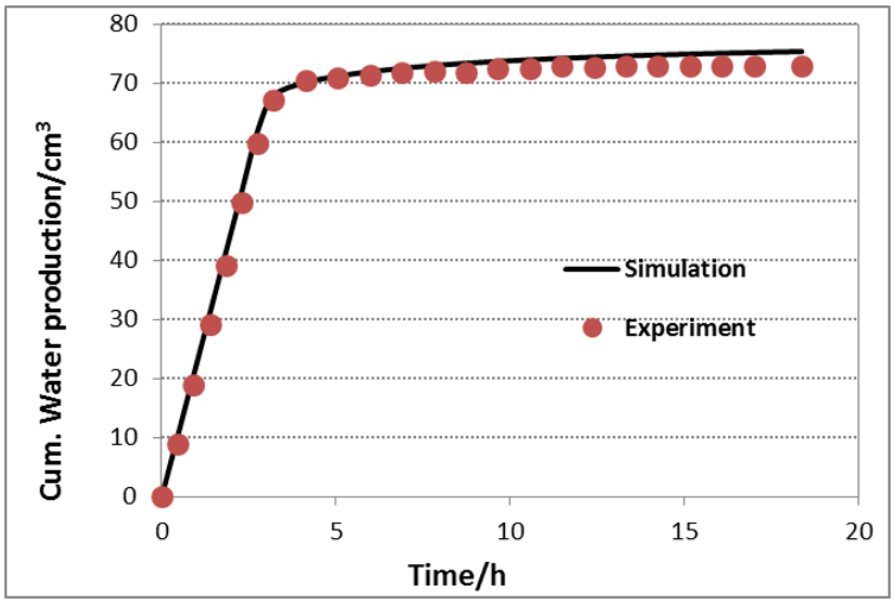

Figure 4-7: Comparison of cumulative water production versus injection time for simulation and experimental data, when k_r and P_c are related.

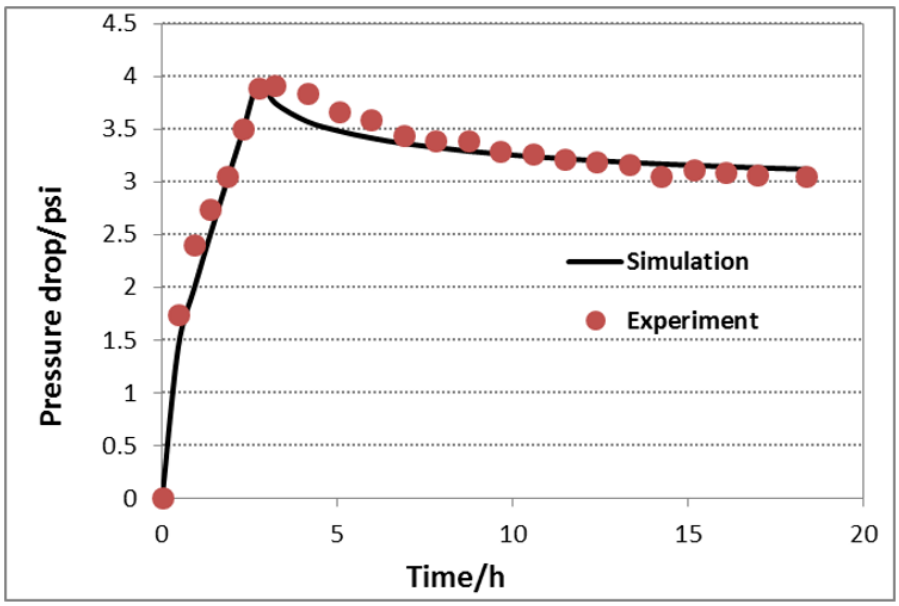

Figure 4-8: Comparison of pressure drop versus injection time for simulation and experimental data, when k_r and P_c are related.

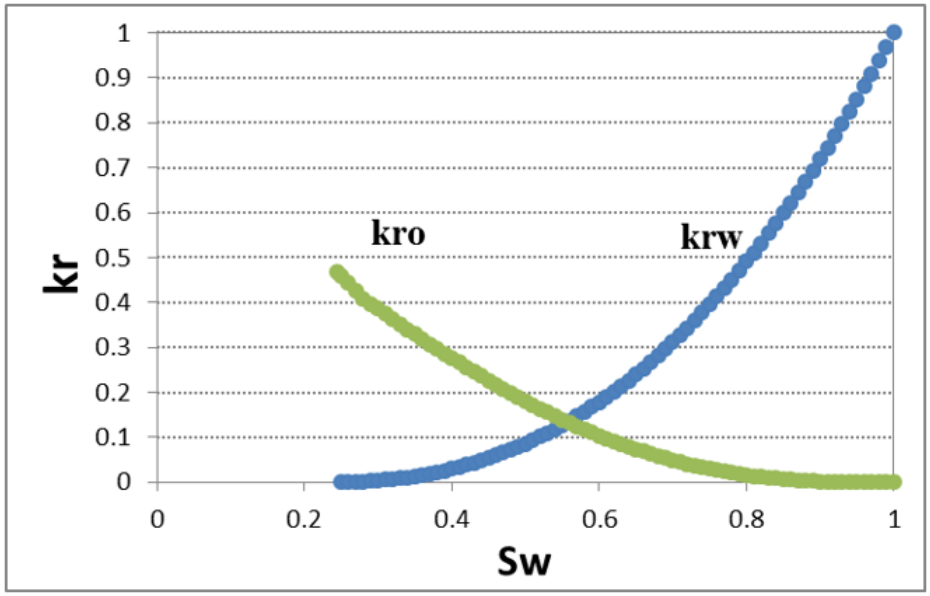

Figure 4-9: Computed oil and water k_r from coreflood experiment, when k_r and P_c are related.

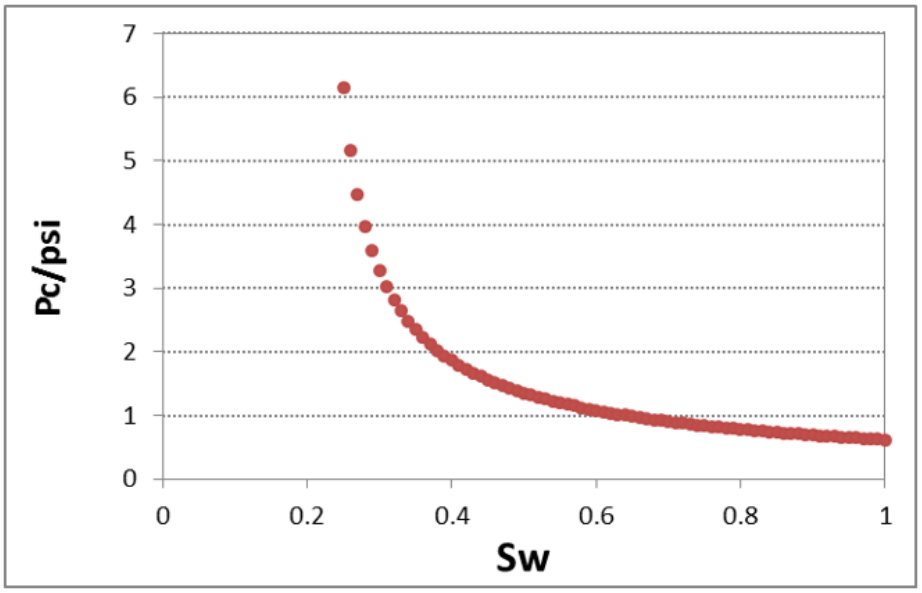

Figure 4-10: Computed capillary pressure (psi) from coreflood experiment when k_r and P_c are related.

4.3.3 Approach B- Conventional Method without in-situ Saturation: Independent kr & P_c Functions

In the conventional method, during the process of history matching, the k_r and P_c are generated independently in which each of them has its tuning parameters and in the course of the history matching, those parameters are adjusted in the way that the results of numerical simulation match with the results of the experiment. To reduce the degree of uncertainty in this approach, more often some in-situ measurements (saturation, pressure) are included in the process of history matching. In this part of the study, the conventional method was applied without including in-situ saturation profiles and the

estimated k_r and P_c compared with the ones obtained from Zhang et al. (2012) (saturation profiles were included) and a new method (approach A).

To represent the two-phase wetting and non-wetting k_r a power-law (Corey type) model was used, Eq.4-17. To represent P_c, the correlation (Eq.4-11) introduced by Li (2004) was used.

$$k_{ri} = k_{ri}^{0}(S_i^*)^{ni} \qquad i = oil, gas, water\ phase \qquad 4\text{-}17$$

k_{rw}^{0} was assumed to be one and therefore the six parameters which should be adjusted are k_{ro}^{0}, n_w, n_o, P_{max}, P_e, λ. Similar to the previous approach, the irreducible water saturation was assumed to be known and equal to 0.25. In this work, the k_r and P_c curves are re-calculated by matching the fluid recoveries and differential pressure data. It should be highlighted that the saturation profiles obtained from the displacement tests have not been used as the measured data in the process of history matching. Determination of the coefficients of the functional forms of k_r and P_c is carried out by the utilization of the GA mentioned above method. Figure 4-11 and Figure 4-12 show the simulation results for water production and pressure drop compared with the experimental data. The computed oil/water k_r and P_c curves are presented in Figure 4-13 and Figure 4-14.

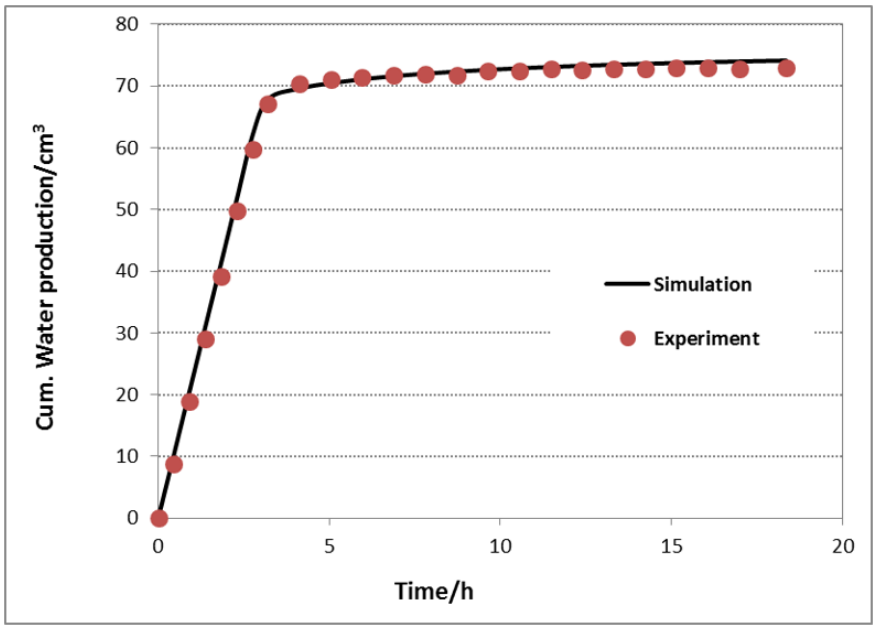

Figure 4-11: Comparison of cumulative water production versus injection time for simulation and experimental data, when k_r and P_c are two independent functions.

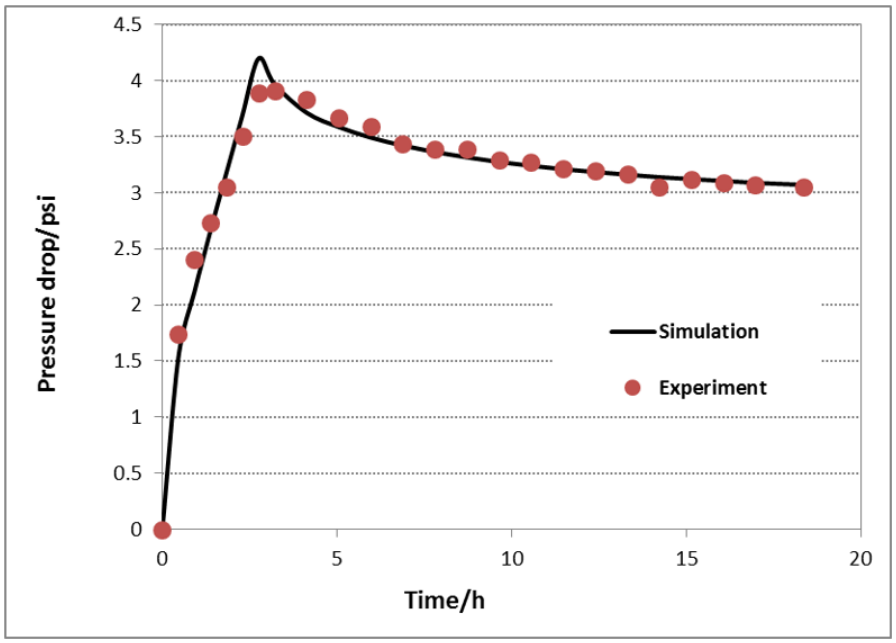

Figure 4-12: Comparison of pressure drop versus injection time for simulation and experimental data, when k_r and P_c are two independent functions.

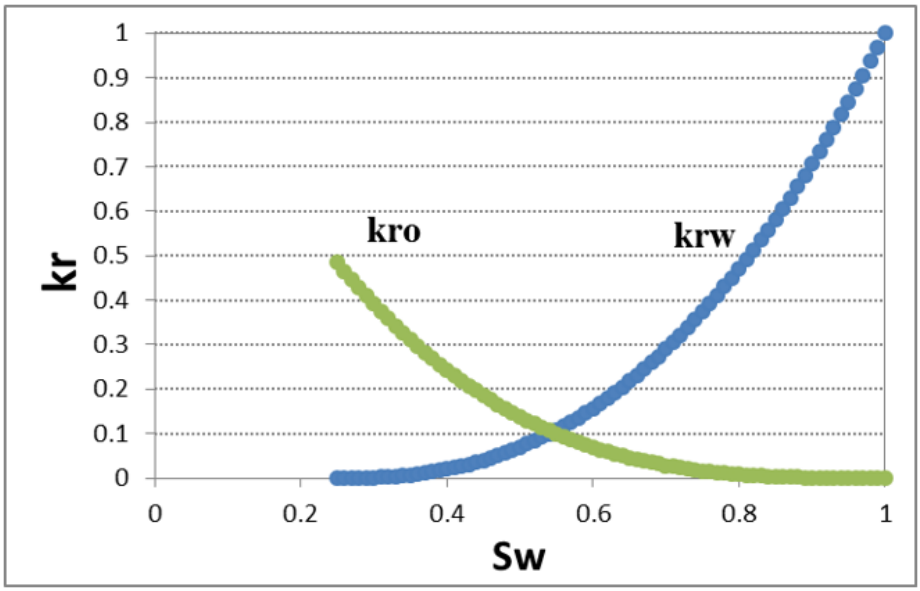

Figure 4-13: Estimated oil/water k_r from coreflood experiment when k_r and P_c are two independent functions.

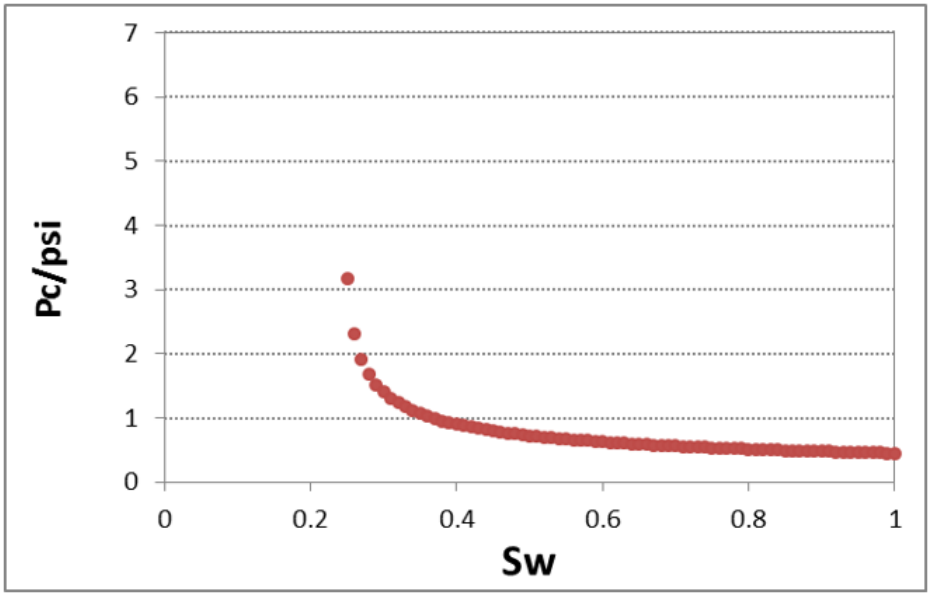

Figure 4-14: Estimated capillary pressure (psi) from coreflood experiment when k_r and P_c are two independent functions.

4.3.4 Discussion

The computed relative permeabilities from the two approaches and the one obtained by Zhang et al. (2012) were normalized and plotted against their normalized water saturation. Figure 4-15 and Figure 4-16 compare the relative permeabilities and capillary pressures respectively. It is recalled that Zhang et al. used production, pressure drop and in-situ saturation profiles for the history matching. It was assumed that their computed k_r and P_c could be utilized as a valid reference. There is a good agreement between the reference relative permeabilities and those obtained from the new method (Approach A) whereas the oil k_r obtained from Approach B is significantly different from the reference points. The estimated P_c obtained from the new method and that of Approach B exhibit different trends and different maximum P_c values, nevertheless our estimated values have a more similar trend to the reference P_c. Despite using fewer tuning parameters in the new method compared to approach B and the reference study, and also not including the in-situ saturation profiles in the history matching, the results in approach A are closer to the reference results compared to Approach B where P_c and k_r had been obtained separately.

For the case that k_r and P_c were estimated independently, although a perfect match was obtained for water production and pressure drop across the core, the estimated P_c may not be a unique curve for the joint estimated k_r unless some internal data such as in-situ saturation and pressure profiles are included in the history matching. As the number of tuning parameters in the flow functions increases, the flexibility of the flow functions

increases and a better match to the experimental results can be obtained. However, obtaining a good match will not necessarily guarantee that the estimated flow functions are true functions. Evaluating the estimated k_r and P_c curves shows that a portion of pressure drop which should be the contribution of capillary pressure between the oil and water phases has not been correctly represented in the simulation by the estimated P_c curve. Therefore, that portion of pressure drop was covered by a reduction in k_{ro} values. As a result, the estimated k_{ro} using method B is less than the reference k_{ro} values.

It should be mentioned that in this study, there was no direct measurement for P_c to compare with the estimated values. To further verify the new method introduced in the thesis, it is recommended that a set of consistent experimental data, including a coreflood experiment, measured P_c and k_r for a system of rock and fluids be obtained. Moreover, this study was performed for a drainage process and a water-wet core, and the validity of this method should be evaluated for imbibition process and other wettability conditions.

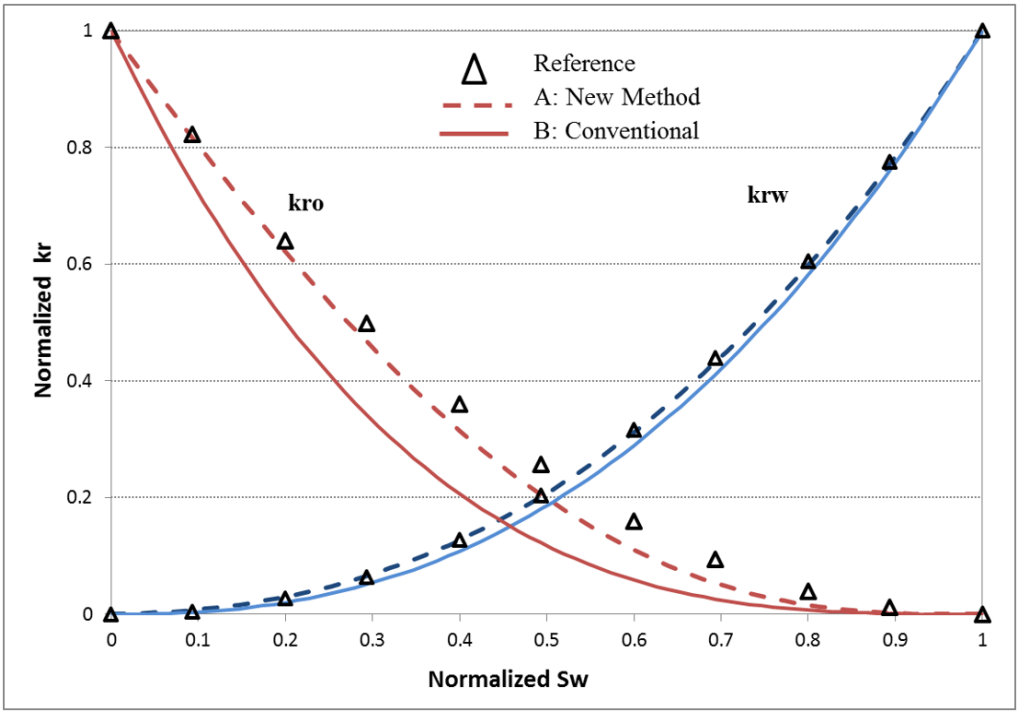

Figure 4-15: Comparison of computed normalized k_r by Zhang et al. (2012) (marker points) and those using two methods of:
(A) k_r and P_c being related (dashed lines and) (B) k_r and P_c being independent (solid lines).

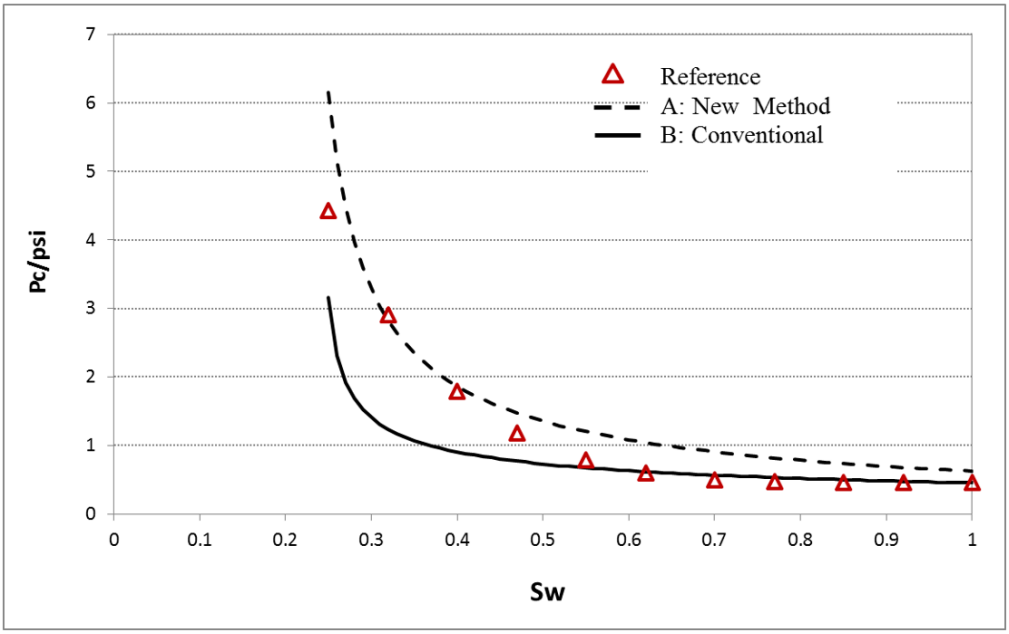

Figure 4-16: Comparison of computed P_c (psi) by Zhanget al. (2012) (marker points) and those using the two methods of:
(A) k_r and P_c being related (dashed lines and) (B) k_r and P_c being independent (solid lines).

4.4 Conclusions

In this study, k_r and P_c were estimated from the results of a coreflood experiment and assuming that k_r was interrelated with P_c. A known physical relationship was honoured between the core k_r and P_c. The P_c was defined as a function of saturation with some tuning parameters, and the k_r was then calculated from this P_c. The results of this method were compared with the approach where k_r and P_c are obtained independently, in the history matching for the unsteady-state primary drainage experiment. The following conclusions can be drawn from this study:

- The results demonstrate that simultaneous P_c and k_r estimation through the interrelated approach introduced in this work improves the accuracy of estimated k_r and P_c,
- The number of tuning parameters decreased in the history matching when k_r is assumed to be related to P_c,
- Although in the new method, fewer measured data (i.e., no measured saturation points) was used, as the results show, it still is capable of producing reliable results,
- Having fewer tuning parameters in the history matching may help to reduce the non-uniqueness problem associated with the history matching process,

- In the conventional method for simultaneous estimation of P_c and k_r it is highly recommended to include in-situ measurement (saturation and or pressure profiles) in the history matching. Ignoring such a practice will result in erroneous estimations.
- The simultaneous estimation of k_r and P_c has a high degree of uncertainty and to reduce it the application of any observed data would be recommended.
- The application of this method should be evaluated for imbibition processes and different wettability conditions as well.

4.5 References

Bentsen, R.G., 1998. Influence of hydrodynamic forces and interfacial momentum transfer on the flow of two immiscible phases. Journal of Petroleum Science and Engineering,19(3–4),pp.177–190. http://www.sciencedirect.com/science/article/pii/S0920410597000211.

Burdine, N T. 1953. Relative Permeability Calculations From Pore Size Distribution Data. Society of Petroleum Engineers. doi:10.2118/225-G.

Gates, J. I., and Lietz, W. T., 1950. Relative Permeabilities of California Cores by the Capillary - Pressure Method. American Petroleum Institute.

Jennings, J. W., McGregor, D. S., and Morse, R. A., 1988. Simultaneous Determination of Capillary Pressure and Relative Permeability by Automatic History Matching.

Kalaydjian, F. J.-M., 1992. Performance and Analysis of Three-Phase Capillary Pressure Curves for Drainage and Imbibition in Porous Media. SPE Annual Technical Conference and Exhibition. Washington, D.C., 1992 Copyright 1992, Society of Petroleum Engineers Inc.

Lenormand, R., Eisenzimmer, A. and Zarcone, C., 1993. A Novel Method for the Determination of Water/Oil Capillary Pressures of Mixed Wettability Samples. Symposium of SCA.

Li, Kewen, and Roland N Horne, 2002. Experimental Verification of Methods to Calculate Relative Permeability Using Capillary Pressure Data. Society of Petroleum Engineers. doi:10.2118/76757-MS.

Li, Kewen, and Roland N Horne, 2006. Comparison of Methods to Calculate Relative Permeability from Capillary Pressure in Consolidated Water-Wet Porous Media. Water Resources Research 42 (6): W06405. doi:10.1029/2005WR004482.

Li, Kewen, 2004. Generalized Capillary Pressure and Relative Permeability Model Inferred from Fractal Characterization of Porous Media. Society of Petroleum Engineers. doi:10.2118/89874-MS.

Mualem, Y., 1976. A New Model for Predicting the Hydraulic Conductivity of Unsaturated Porous Media. Water Resources Research 12 (3): 513–22. doi:10.1029/WR012i003p00513.

Newsham, K. E., Rushing, J. A., Lasswell, P. M., Cox, J. C. and Blasingame, T. A., 2004. A Comparative Study of Laboratory Techniques for Measuring Capillary Pressures in Tight Gas Sands, Society of Petroleum Engineers.

Pini, R. and Benson, S.M., 2013. Simultaneous determination of capillary pressure and relative permeability curves from core-flooding experiments with various fluid pairs. Water Resources Research, 49(6), pp.3516–3530. Available at: http://dx.doi.org/10.1002/wrcr.20274.

Purcell, W R., 1949. Capillary Pressures - Their Measurement Using Mercury and the Calculation of Permeability Therefrom. Society of Petroleum Engineers. doi:10.2118/949039-G.

Sun, X. and Mohanty, K. K., 2005. Estimation of Flow Functions during Drainage Using Genetic Algorithm. SPE Journal

Ucan, S., Civan, F. and Evans, R.D., 1993. Simulated Annealing for Relative Permeability and Capillary Pressure From Unsteady-State Non-Darcy Displacement.

Ucan, S., Civan, F. and Evans, R.D., 1997. Uniqueness and Simultaneous Predictability of Relative Permeability and Capillary Pressure by Discrete and Continuous Means.

Virnovsky, G.A.; Guo Y.; Skaeveland S. M., 1995. Relative Permeability and Capillary Pressure Co-currently Determined from Steady-State Flow Experiments. 8th European IOR Symposium. Vienna, Austria.

Zhang, Y., Li, H. and Yang, D., 2012. Simultaneous Estimation of Relative Permeability and Capillary Pressure Using Ensemble-Based History Matching Techniques. Transport in Porous Media, 94(1), pp.259–276. Available at: http://dx.doi.org/10.1007/s11242-012-0003-3.

Chapter 5– Effect of Gas/Oil IFT on Two- and Three-Phase Relative Permeability and Residual Oil Saturation

In some of the EOR processes such as gas and WAG injections, near-miscible conditions may be met or the interfacial tension (IFT) between a pair of existing fluids, e.g., gas and oil, can be subjected to change due to mass transfer between the phases. The general perception is that IFT reduction results in an increase in k_r of existing phases at each saturation value. A significant number of studies have been performed on two-phase systems, and more insight has been gained on the effect of IFT reduction on k_r. However, for a three-phase system, there is still a long journey to take in, to appreciably understand and model the effect of IFT change on the three-phase k_r. To model the above EOR processes, the flow functions, e.g., relative permeability (k_r) are required to represent fluid flow behaviour at different IFT conditions. The common practice is that the two-phase k_r is usually measured at high IFT values and for simulating a process that has to change IFT value, towards miscible conditions, the appropriate modification is applied to the high IFT k_r data to calculate their value at lower values of IFT.

The objective is firstly to investigate the effects of gas/oil IFT reduction on two- and three-phase relative permeabilities according to the literature and the results of the experimental studies at Heriot-Watt University on 65 and 1000 mD cores at three different gas/oil IFT values of 0.04, 0.15 and 2.7 $mN.m^{-1}$. Secondly, to evaluate the frequently used Coats IFT scaling method against the two-phase experimental data. Finally to investigate the effect of changing gas/oil IFT value on the reduction of residual oil saturation in WAG injections at laboratory scale.

5.1 Introduction

5.1.1 Effect of IFT on Two-Phase Relative Permeability

Variation of gas/oil IFT during gas injection processes from immiscible to miscible conditions has been observed in lab and field experiences. The possible effects of variation of IFT on k_r have been investigated by several researchers. Although there is some conflict with the findings of different researchers, in general, all agree that any reduction in IFT causes an increase in k_r. It has been observed that as IFT decreases toward zero, the k_r increases, its curvature reduces, and less hysteresis effect is observed. Also, most of the research studies have introduced a critical IFT value above which there are no significant effects of IFT variations on relative permeabilities while below the critical value IFT significant changes are observed in relative permeabilities. A summary of the literature review is presented in the following paragraphs.

Bardon and Longeron (1980) performed a series of coreflood (gas injection) experiments on Fontainebleau sandstone core using a binary mixture of two pure hydrocarbons (C1-nC7/C1-nC10). The IFT was controlled by varying the equilibrium pressure of the mixture. For the range of IFT from 0.001 to 12.6 mNm^{-1}, they introduced a critical IFT value of 0.04 mNm^{-1}. As shown in Figure 5-1, for the IFT values greater than the critical IFT, they obtained a single curve for gas relative permeability (k_{rg}) but a family of curves for oil relative permeability (k_{ro}) with k_{ro} increasing with decreasing IFT. However, for the IFT values less than the critical IFT, there is a great variation in the shapes of both k_{ro} and k_{rg} curves. The variation is mainly in the k_{ro} and k_{rg} curvature towards a straight-line as IFT decreases. i.e., both k_{ro} and k_{rg} increase, as IFT decreases.

Harbert (1983) performed coreflood experiments on outcrop and reservoir rock samples using an alcohol, brine, and oil fluid system to investigate the effect of low IFT on oil and water relative permeabilities. They found that IFT reduction had more pronounced effect on the non-wetting phase k_r than on the wetting phase k_r.

Fulcher (1985) conducted a series of steady-state oil/water k_r measurements on fired Beria sandstone, to determine whether the capillary number or its constituents cause any changes in the two-phase relative permeabilities. They introduced a critical oil/water IFT value of 2 mNm^{-1}, below which value both oil and water relative permeabilities increased with decreasing IFT, and the curves straightened out at very low IFT values.

Moreover, the increase in oil (non-wetting) k_r was observed to be more significant than the increase in water (wetting) k_r as IFT reduced.

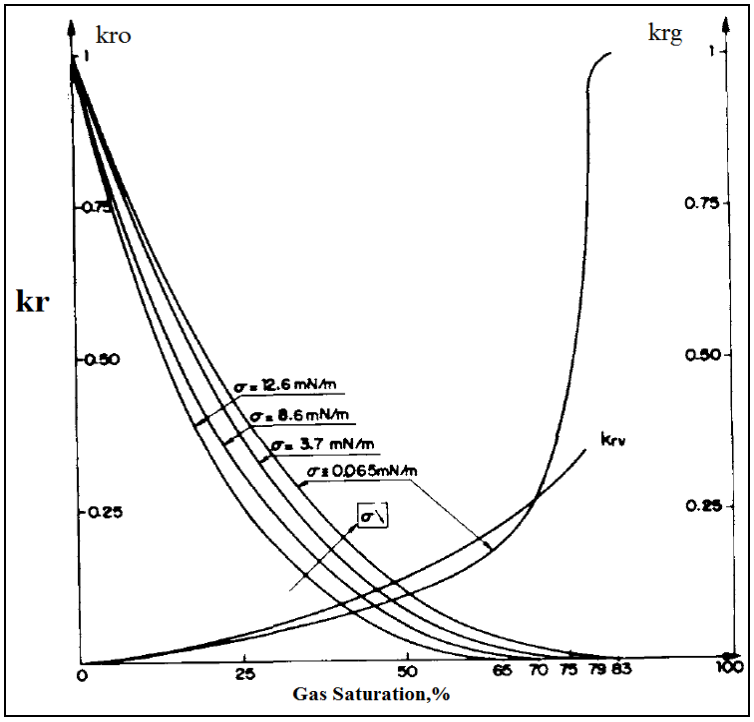

Figure 5-1: Oil and gas relative permeabilities for IFT values greater than 0.04 mNm^{-1}(after Bardon and Longeron (1980)).

Asar and Handy (1988) carried out a study similar to Bardon and Longeron (1980) but for a narrower IFT range of 0.03 to 0.82 mNm^{-1}. They used a methane/propane mixture to represent a gas-condensate system and performed steady-state core flood experiment to measure oil and gas k_r curves. They also concluded that the oil and gas k_r curves tend to straighten and residual oil saturation decreases to zero as IFT approaches zero. In their experiments, the shape of k_{ro} and k_{rg} curves deviated from high IFT curvature only at conditions close to the fluid critical point. Moreover, k_{ro} increases more rapidly than k_{rg} as IFT decreases.

McDougall et al. (1997) developed an unsteady-sate pore-scale simulator to investigate the effect of gas/oil IFT on k_r and interpret the results of a series of core flood experiments which had been previously performed for a gas/oil IFT range of 0.019 to 9.76 mNm^{-1}. The pore-scale model was suitably anchored to the experimental rock samples. The relative permeabilities calculated from the results of simulations were found to exhibit the same IFT sensitivity as the relative permeabilities calculated from experimental results. They concluded that as IFT decreased, the oil (wetting phase) k_r curve remained unaffected while the gas (non-wetting phase) k_r increased significantly.

Henderson et al. (1997) (1998) investigated the effect of flow rate and IFT on k_r in a gas condensate system using long sandstone cores at high pressure. The IFT range in their study was from 0.05 to 0.4 mNm^{-1}. They observed that gas (non-wetting) k_r was more sensitive to IFT changes than the condensate (wetting) k_r.

Chen et al. (1999) investigated the effects of IFT and flow rate on gas/oil k_r. They performed coreflood experiments under reservoir conditions using rock and fluid samples from two North Sea gas condensate reservoirs. They observed a greater change in k_{ro} than in k_{rg} when IFT decreased.

Blom et al. (2000) measured two-phase k_r curves for a binary fluid system of methanol/n-hexane at near-critical conditions. The fluid system exhibited a critical point at ambient conditions and could be representative of a near-critical gas/condensate or gas/volatile oil system. The measurements were done at IFT range from 0.10 to 0.51 mNm^{-1} and for different superficial velocities. They concluded that there was a strong dependency of k_r on IFT and superficial velocity. Their results showed that the non-wetting phase k_r was more affected by IFT reduction and the k_r to the wetting phase remained unaffected until IFT was reduced to below 0.06 mNm^{-1}.

Shen et al. (2006) performed a series of steady-state two-phase flow experiments to measure oil/water k_r at IFT range from 0.01 to 34 mNm^{-1}. They showed that there was a critical oil/water IFT value (of 3 mNm^{-1}) above which, IFT had little effect on k_r while below this critical value, k_r to both oil and water increased with a decrease in IFT. The results of their experiments showed that IFT variations have considerable impact on the water (wetting phase) k_r in comparison with the oil (non-wetting) k_r (Figure 5-2).

Calisgan et al. (2006) conducted unsteady state displacement experiments on a carbonate core using a binary gas condensate fluid sample at near-critical conditions. The experimental results showed a strong dependence of k_{rg} on IFT and superficial velocity. This dependency was more pronounced in the presence of immobile water.

Al-Wahaibi et al. (2006) investigated the behaviour of two-phase k_r at near-miscible conditions. They performed unsteady-state displacement in a linear two dimensional bead-pack. The results of experiments showed that k_r increased as IFT decreased from 24.2 to 0.03 mNm^{-1}. Furthermore, non-wetting phase k_r showed more rapid increase than the wetting phase k_r and had less hysteresis effect as IFT reduced.

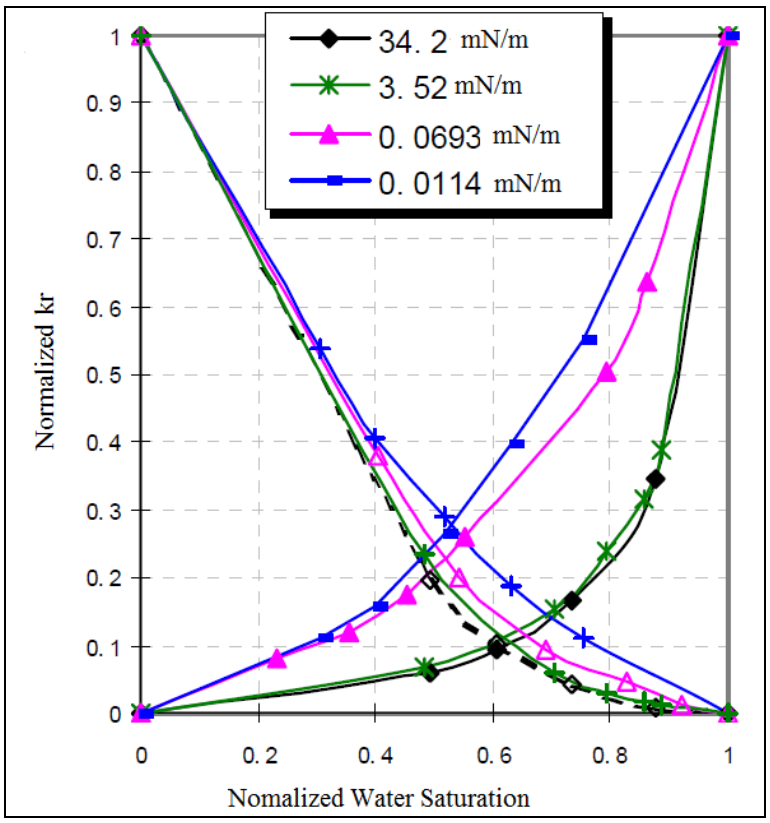

Figure 5-2: Oil and water relative permeabilities for different IFT values (after Shen et al. (2006)).

In contrast to the above literature, there are some research studies such as Delclaud et al. (1987) that did not report any significant change in two-phase k_r with IFT changes.

From the aformentioned literature (except the Delclaud's), it can be concluded that the IFT reduction increases the k_r of both phases but not necessarily equally. It has been observed that as the system moves from immiscible toward miscible conditions, the k_r increases, its curvature reduces, and less hysteresis effect is observed.

5.1.2 Effect of IFT on Three-Phase Relative Permeability

Although the effect of IFT on two-phase k_r has been extensively investigated, as expected, there are only very few research studies on the effect of IFT on three-phase relative permeabilities. According to the small amount of literature for three-phase systems, generally as IFT between one pair of phases, e.g. oil and gas changes, the relative permeabilities of all the three phases (gas, oil, and water) will be affected. It was observed (Cinar and Orr (2005)) that by reduction of gas/oil IFT, k_{ro} and k_{rg} increased but k_{rw} may remain unaffected. The degree of change in k_r of each phase and its dependency on its saturation and other fluid saturations should be further investigated at low IFT conditions. The following paragraph summarizes the results of available research in this area.

Delshad et al. (1987) measured steady-state two- and three-phase k_r for low IFT mixture of brine/oil/surfactant/alcohol in Berea sandstone cores at a constant capillary number of 10^{-2}. They concluded that in three-phase flow at low IFT conditions, the k_r of each phase was a function of its saturation.

Dria et al. (1993) reported steady-state three phase CO_2/oil/brine relative permeabilities in a water-wet dolomite core. They injected fluids at 71 ^oC and 1400 psia, to be representative of reservoir conditions. Their results also show that the k_r of each phase depends only on the saturation of that phase. However, the previous three-phase k_r measurements that had been performed with low-pressure N_2 gas or air showed that the k_r of each phase depended on two saturations. Therefore, they concluded that three-phase k_r behaves differently at low IFT (CO_2/oil) and high IFT (N_2/oil) conditions.

Cinar and Orr (2005) investigated the effect of IFT reduction on three-phase relative permeabilities for water-wet wettability condition using three-phase analogous liquid systems. The IFT between a pair of the phases could be varied in the analogous liquid systems while the IFT values between the other pairs of phases can be held roughly constant. They concluded that the water (wetting phase) k_r was not affected by IFT reduction but the k_r to oil (intermediate phase) and gas (non-wetting phase) were affected considerably.

Cinar et al. (2007) reported three-phase k_r measurements that included the combined effects of IFT variation and wettability. Similar to their previous study, they used an analogous liquid system for investigation of the effect of IFT variations at atmospheric pressure. Their results showed that, in the water-wet system, as gas/oil IFT decreased, relative permeabilities of these two phases increased but k_{rw} remained almost unaffected by IFT at any water saturation. However, in the oil-wet system, k_{rw} decreased with the reduction of gas/oil IFT only at low values of water saturation.

5.1.3 IFT Scaling Methods

5.1.3.1 Coats Method

Coats (1980) proposed an empirical treatment on k_r for IFT change which was not based on any theory or experimental results directly. However, it was based on the general idea that reduction in IFT must increase k_{ro} and k_{rg} towards straight lines that at the time was assumed to be the case for completely miscible fluids, such as alcohol and water in a pipe (rather than in a porous medium). This treatment was devised to show the

expected behaviour of k_r curves when IFT decreased. i.e., moving from immiscible conditions toward miscible conditions (reduction in IFT), the curvature of k_r decreases and residual oil saturation approaches zero. The Coats method was, in fact, an interpolation between immiscible and miscible relative permeabilities, using a weighting function with only one parameter (Equations 5-1 and 5-2). Other research work on the behaviour of k_r at near-miscible conditions for gas injection processes, and at near-critical conditions, for gas condensate reservoirs, showed that this flow function must depend on the ratio of viscous to capillary forces on a pore scale, known as capillary number (N_c). Therefore, several authors tried to modify the Coats equations by including the capillary number in the weighting function equation, residual saturation, and k_r at miscible conditions. As a consequence, the number of required parameters increased.

Fulcher et al. (1985) performed k_r measurements to determine the dependency of two-phase k_r on the capillary number and its constituents. They developed a k_r model based on the results of core experiments. The model is basically a Corey model with capillary number dependent coefficients. It requires seven parameters to predict residual saturation and Corey coefficient. Other authors tried to include the capillary number in the prediction of Corey coefficients differently with fewer parameters.

Blom and Hagoort (1998) reviewed and analysed fifteen different methods proposed for including the capillary number in the gas condensate k_r functions and categorized them into two groups: Corey functions with N_c-dependent coefficients and Interpolation functions between immiscible and miscible k_r with a N_c-dependent weighting factor. They mentioned that Corey functions were highly non-linear and could not accurately represent the convex-concave k_r shapes, and these are the main disadvantages of this category in comparison with Coats type of interpolation functions. They concluded that weighting factors introduced by Coats (1980) were one of the most appropriate factors.

The Coats (1980) method has been implemented in some commercial reservoir simulators, e.g. Eclipse and CMG for the purpose of IFT scaling for compositional simulations. It seems that since this method requires fewer parameters, in comparison with other methods, it has been selected for use in such more operational simulators. The suggested Coats' formula, for gas and oil relative permeabilities, is as follow:

$$k_{ri} = f(\sigma)k_{ri}^{immiscible} + [1 - f(\sigma)]k_{ri}^{miscible} \quad , i\text{=oil, gas} \qquad 5\text{-}1$$

where

$$f(\sigma)=\left(\frac{\sigma}{\sigma_o}\right)^{\frac{1}{nl}} \quad 5\text{-}2$$

$$k_{ri}^{miscible}=\frac{S_i-S_{ir}^*}{1-S_{wir}-S_{ir}^*} \quad 5\text{-}3$$

$k_{ri}^{immiscible}$ is the base k_r curve (measured values) for phase *i*, σ_o is the initial value of the interfacial tension for which k_{ro} and k_{rg} curves are available, σ is the interfacial tension at new conditions, *nl* is a tuning parameter between 4 and 10. $k_{ri}^{miscible}$ is the k_r curve for phase *i* at miscible conditions and S_i is the phase '*i*' saturation. As interfacial tension decreases the residual oil and gas saturation values (S_{org}, S_{gr}) approach zero, therefore the values of S_{org} and S_{gr} could be corrected at the current value of IFT as shown below:

$$S_{ir}^* = f(\sigma)S_{ir} \quad , i\text{=oil, gas} \quad 5\text{-}4$$

where, S_{ir}^* is residual (gas or oil saturation) at the new IFT value, σ. S_{ir} is the residual saturation at σ_o, the reference IFT, with $f(\sigma)$ defined by Eq. 5-2.

5.2 Experiments and History Matching

5.2.1 Two-Phase Flow Experiments

A series of two-phase gas/oil unsteady-state coreflood experiments were initially performed in the 1000 mD Clashach core on both water-wet and mixed-wet systems at two gas/oil IFT values of 2.7 (base IFT) and 0.04 mNm^{-1}. To explore the impact of interfacial tension (IFT) variation, another series of two-phase gas/oil coreflood displacement was performed on 65 mD mixed-wet Clashach core at IFT values of 2.7, 0.15 and 0.04 mNm^{-1} (Table 5-1). These experiments were unsteady-state gas injection into oil saturated core at irreducible water saturation. Pressure drop and production data for these experiments (performed at different gas/oil IFT values) were history matched using the developed computer program. As a result representative relative permeabilities for each phase, during its period of injection, could be obtained. The effect of IFT change on k_r was highlighted. The scaled capillary pressure curves (Figure 2-6 and Figure 2-7) were used for history matching of the experimental data.

Table 5-1: The two-phase (gas/oil) unsteady-state gas injection (i.e., drainage) experiments carried out on 1000 and 65 mD core samples in all of which S_g increased and S_o decreased.

Experiment	*Core Permeability/ mD*	*Wettability*	*$IFT_{g/o}$/mNm^{-1}*
1	1000	Water-Wet	2.7
2	1000	Water-Wet	0.04
3	1000	Mixed-Wet	2.7
4	1000	Mixed-Wet	0.04
5	65	Mixed-Wet	2.7
6	65	Mixed-Wet	0.15
7	65	Mixed-Wet	0.04

The results of history matching for the two gas injection tests performed at higher values of gas/oil IFT (0.15 and 2.70 mN.m^{-1}) are presented in Figure 5-3 and Figure 5-4. These figures depict the experimental data (production data and pressure drop across the core, shown by dots) and history matching results (shown by lines).

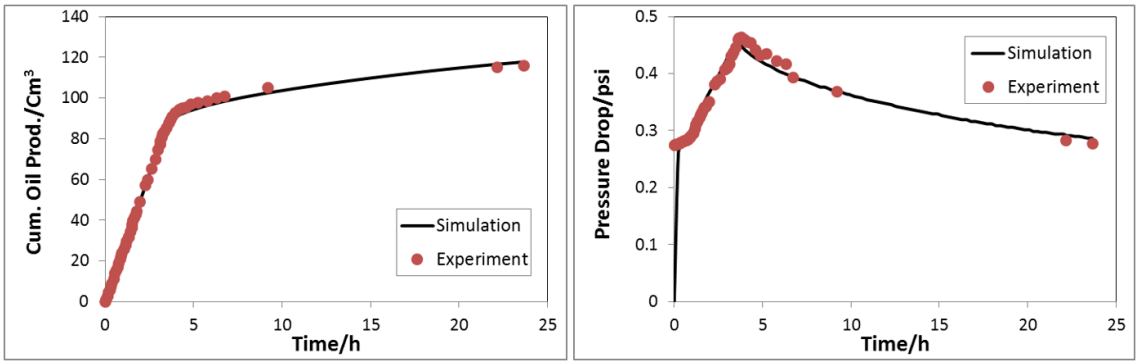

Figure 5-3: Experimental and history matched production data and pressure drop for the gas injection performed in 65 mD mixed-wet core at gas/oil IFT = 0.15 mN.m^{-1}.

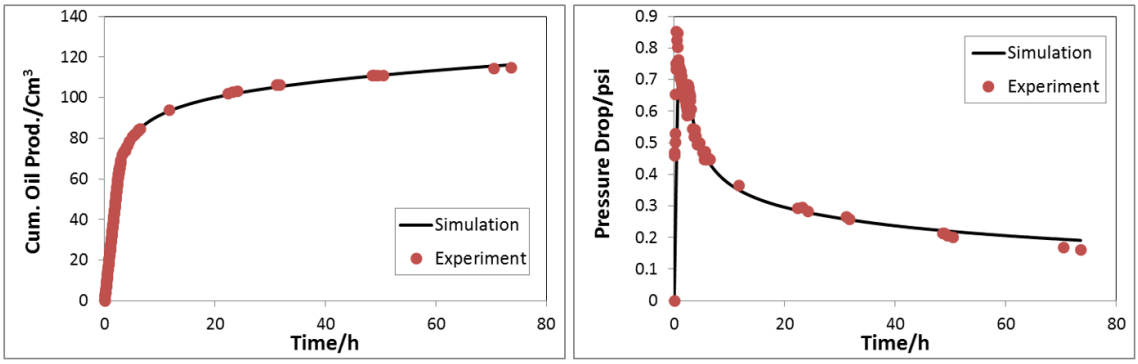

Figure 5-4: Experimental and history matched production data and pressure drop for the gas injection performed in 65 mD mixed-wet core at gas/oil IFT = 2.70 mN.m^{-1}.

5.2.2 Three-Phase Flow Experiments

Three WAG injection tests started with waterflooding (WAG-ID) were carried out at three different gas/oil IFT values of 0.04, 0.15 and 2.7. The 1st gas injection following the waterflooding was, in fact, a three-phase (gas/oil/water) flow experiment. The results of these experiments, e.g., pressure drop and production data were history matched to obtain the k_r for each phase during the period of injection. Although the gas/oil IFT for the case of the test performed at 1790 psia is as low as 0.15 mN.m^{-1}, the first gas injection does not significantly enhance the oil production, compared to the near-miscible gas injection (gas/oil IFT = 0.04 mN.m^{-1}). In fact, the performance during gas injection period at gas/oil IFT of 0.15 mN.m^{-1} is much closer to the case at immiscible condition (gas/oil IFT = 2.70 mN.m^{-1}), than it is to the recoveries of the near-miscible (0.04 mN.m^{-1}) case. Figure 5-5 and Figure 5-6 present the experimental data, cumulative oil production (left) and pressure drop across the core (right), and history matched results at the intermediate gas/oil IFT value of 0.15 mN.m^{-1} and at immiscible conditions (gas/oil IFT = 2.7 mN.m^{-1}). The history matching results for gas/oil IFT value of 0.04 mN.m^{-1} were presented in Chapter 3.

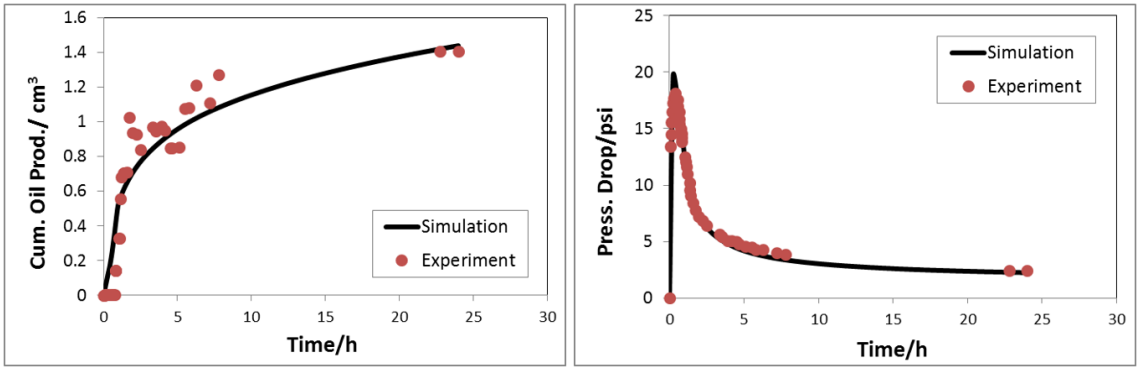

Figure 5-5: Experimental and history matched oil production and pressure drop data for the 1st gas injection period of the WAG performed in 65 mD mixed-wet core at $IFT_{g/o}$ = 0.15 mN.m^{-1}.

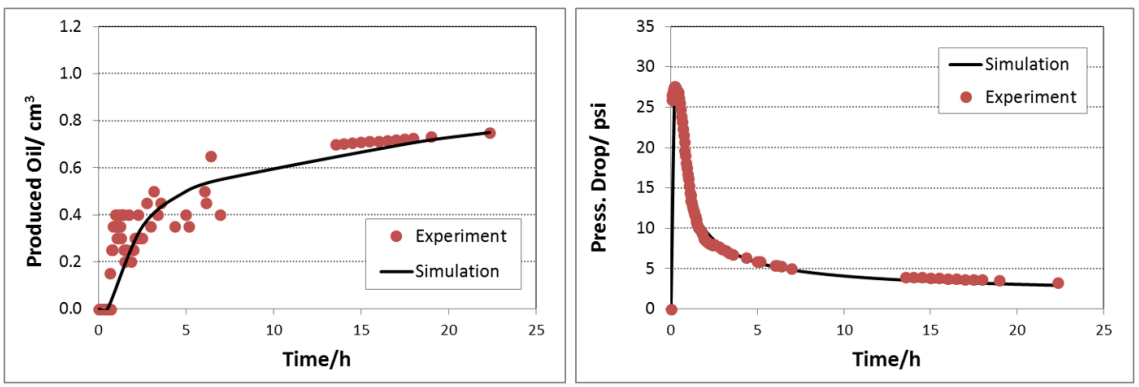

Figure 5-6: Experimental and history matched oil production and pressure drop data for the 1st gas injection period of the WAG injection performed in 65 mD mixed-wet core at $IFT_{g/o}$ = 2.70 mN.m^{-1}.

5.3 Results and Discussion

5.3.1 Two-Phase Relative Permeability

Figure 5-7 and Figure 5-8 compare the estimated relative permeabilities of gas and oil during the unsteady-state gas injections at two different IFT values of 0.04 and 2.7 mNm^{-1} in the 1000 mD, water-wet and mixed-wet cores respectively. No tests in the 1000 mD core at the intermediate IFT value of 0.15 mNm^{-1} were carried out. Figure 5-9 compares estimated relative permeabilities of gas and oil phases at three different IFT conditions (0.04, 0.15 and 2.7 mNm^{-1}) in the 65 mD mixed-wet core. All sets of relative permeabilities (1000 mD mixed-wet, 1000 mD water-wet, and 65 mD mixed-wet) are shown in the range of saturation change after the gas breakthrough. Results show that relative permeabilities for both gas and oil phases increase as the IFT value is decreased. The residual oil saturation (S_{org}) decreases (i.e., oil recovery increases) as the gas/oil IFT is reduced.

Although the intermediate IFT value of 0.15 mNm^{-1} appears to be very low compared to IFT of 2.7 mNm^{-1}, the improvements in gas and oil relative permeabilities are not substantial.

The k_r of gas, which is the non-wetting phase, was affected more by gas/oil IFT reduction in comparison with k_r of oil, which is the wetting phase, in the presence of gas. In another words, the k_r of gas increased in the entire range of its saturation, while oil k_r increased only within the range of its low saturation values. The following interpretation may be considered. As the non-wetting phase (gas) occupies the larger pores, it is affected by viscous forces more easily than the wetting phase (oil). As the gas/oil IFT decreases the capillary forces decrease, and gas can approach the small pores which were previously occupied by oil. Therefore, for ultra-low IFT conditions, oil can flow even at its low values of saturations (i.e., high gas saturations).

Comparison of the curvatures of the gas and oil k_r curves shows that they both decrease by reduction of gas/oil IFT, but they are still far from being straight lines, even at very low IFT value of 0.04 mNm^{-1}.

Comparing Figure 5-9 (65 mD core) with its corresponding results in the 1000 mD core Figure 5-8 shows that although qualitatively the effect of IFT variation is similar for the two cores, quantitatively the IFT effect is more pronounced for k_{ro} of the higher permeability rock. This observation is in line with the oil recovery curves of these two

cores, in which the effect of IFT variations is larger in the 1000 mD core. Comparison of the estimated gas and oil relative permeabilities at different IFT values shows that:

- The increase in either oil or gas k_r is not directly proportional to the value of IFT.
- The changes in oil and gas relative permeabilities are not identical.
- As the oil saturation decreases, the relative effect of IFT reduction becomes more significant.

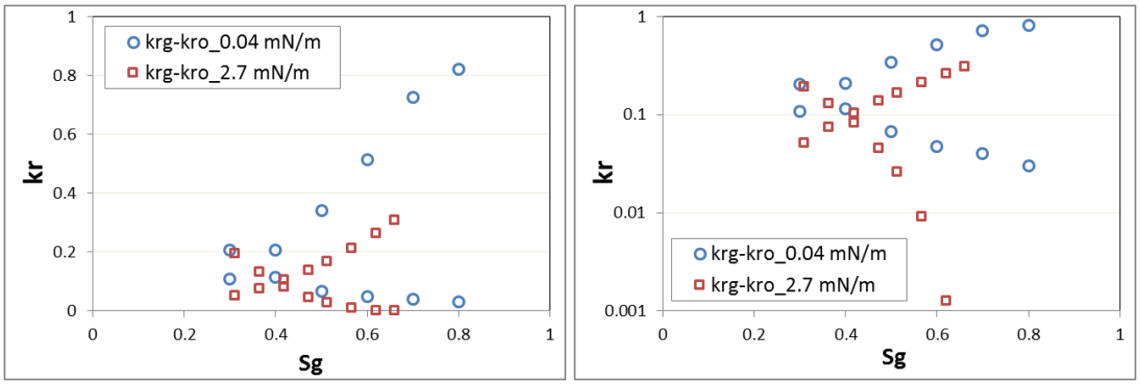

Figure 5-7: Gas and Oil relative permeabilities for the gas injections performed in 1000 mD water-wet core at different gas/oil IFT (IFT = 2.70 and 0.04 mN.m^{-1}).

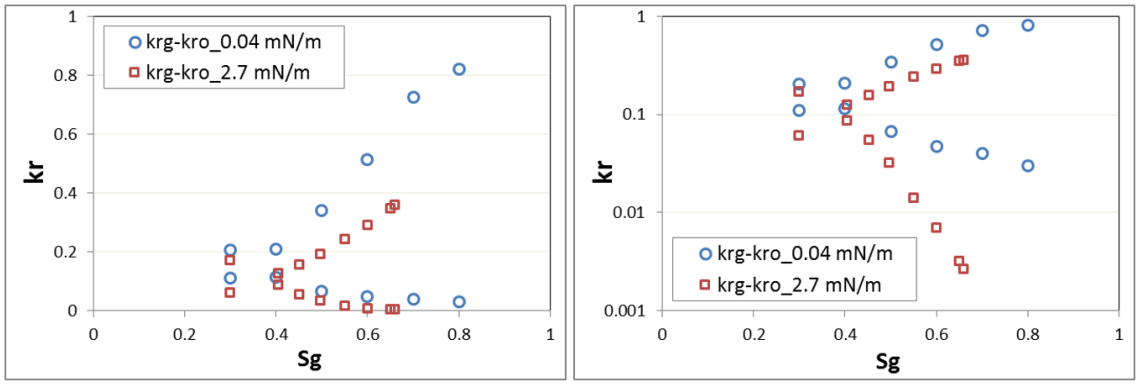

Figure 5-8: Gas and Oil relative permeabilities for the gas injections performed in 1000 mD mixed-wet core at different gas/oil IFT (IFT = 2.70 and 0.04 mN.m^{-1}).

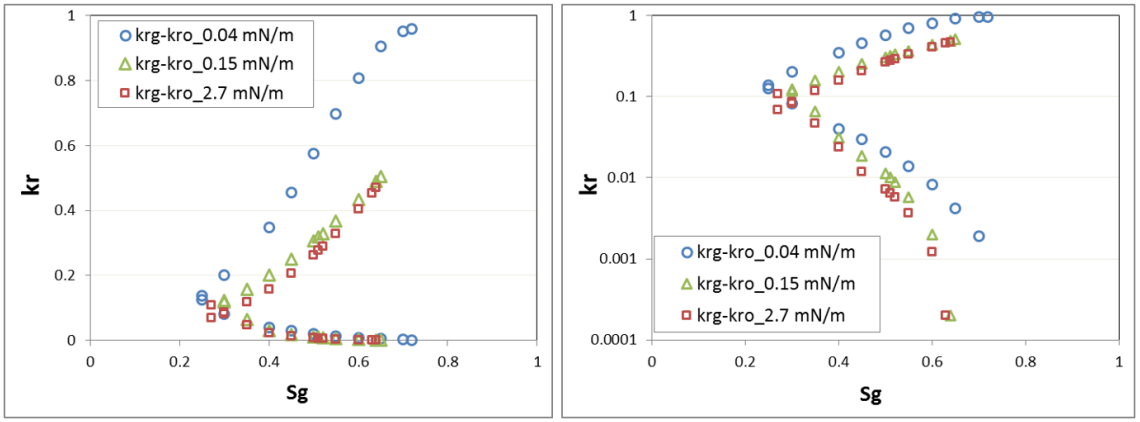

Figure 5-9: Gas and Oil relative permeabilities for the gas injections performed in 65 mD mixed-wet core at different gas/oil IFT (IFT = 2.70, 0.15 and 0.04 mN.m^{-1}).

5.3.2 Three-Phase Relative Permeability

To compare the estimated three-phase k_r curves at various IFT values, they have been plotted against their respective phase saturations, at various IFT values, in Figure 5-10 to Figure 5-12. These relative permeabilities, estimated from the 1st gas injection period of WAG injection, performed in 65 mD mixed-wet core, have been plotted for three different IFT values of 0.04, 0.15 and 2.7 mNm^{-1}. As the oil and water saturation values at the start of the gas injection period, and the residual saturations at the end of this period were different for the three IFT values, the estimated k_{ro} values at different saturation ranges do not necessarily agree with each other. A similar situation is valid for the estimated k_{rw} curves.

Although the saturation ranges for estimated oil relative permeabilities, at different IFT values, do not overlap, it can be observed that the three-phase k_{ro} increases with the reduction of gas/oil IFT. In other words, the residual oil saturation decreases with the reduction of gas/oil IFT. The increase in k_r and decrease in residual oil saturation are substantial when gas/oil IFT decreases to a very low value of $0.04mNm^{-1}$. As the gas/oil IFT decreases, gas tends to displace oil rather than water, and even oil that resides in tiny pores.

As Figure 5-11 shows, the gas/oil IFT reduction from 2.7 to 0.15 mNm^{-1} does not affect the k_{rg}, but the reduction of the IFT to the ultra-low value of 0.04 mNm^{-1} increases the k_{rg} significantly.

As shown in Figure 5-12, the three-phase k_{rw} at high and intermediate gas/oil IFT values are similar in shape and value. The k_{rw} at high values of water saturation is almost in the same range for all the three IFT values. As gas starts entering the core, it displaces both oil and water from large and intermediate pores. This is common among all three IFT values and as a result, the k_{rw} values are similar. However, as gas saturation increases and water saturation decreases, at IFT of 0.04 mNm^{-1}, gas mainly invades those pores which are occupied by oil and bypasses some water filled pores and therefore the k_{rw} values are less compared with the ones at high and intermediate IFT values.

Although the intermediate IFT value of 0.15 mNm^{-1} is rather low compared with 2.7 mNm^{-1} but their corresponding k_r curves are almost superposed for both gas and oil k_r curves. However, at ultra-low IFT value, of 0.04 mNm^{-1}, the k_r of all the three phases were affected by IFT reduction. At at ultra-low IFT value, gas and oil can flow together in the porous media which is the main reason behind the sharp increase in the oil and gas k_r at this conditions compared to the intermediate and high IFT conditions.

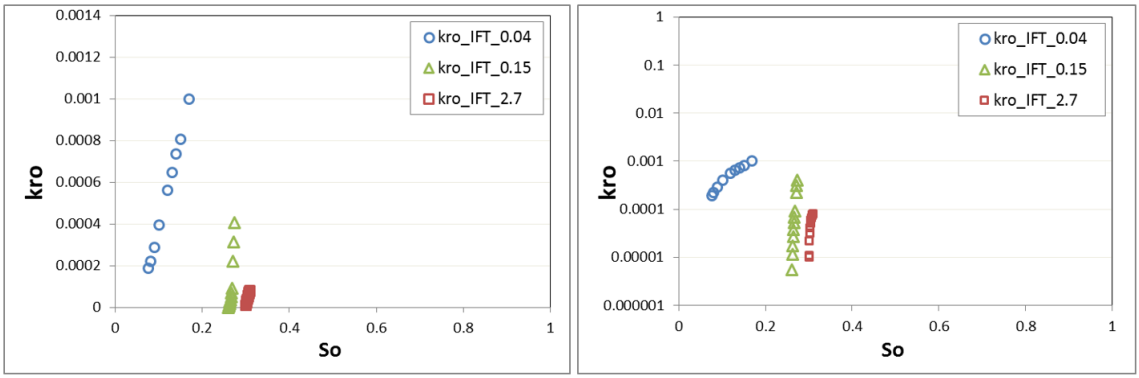

Figure 5-10: Oil relative permeabilities for the gas injections performed in 65 mD mixed-wet core at different gas/oil IFT (IFT = 2.70, 0.15 and 0.04 mN.m^{-1}).

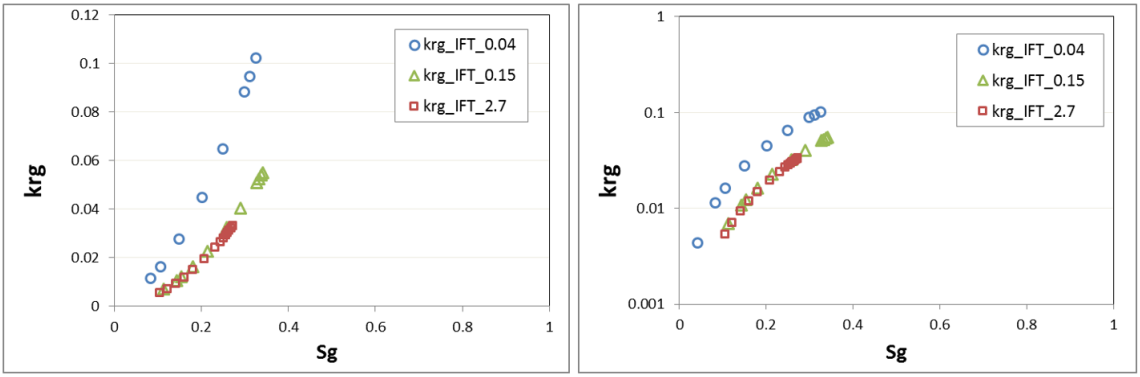

Figure 5-11: Gas relative permeabilities for the gas injections performed in 65 mD mixed-wet core at different gas/oil IFT (IFT = 2.70, 0.15 and 0.04 mN.m^{-1}).

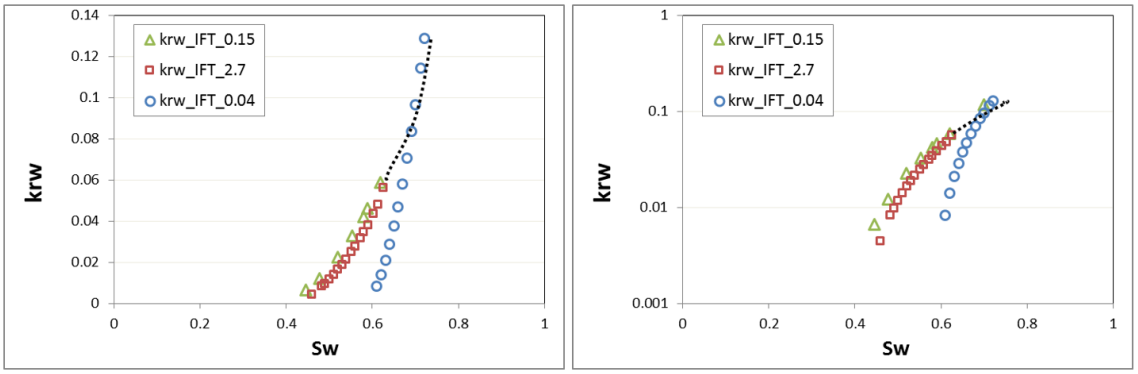

Figure 5-12: Water relative permeabilities for the gas injections performed in 65 mD mixed-wet core at different gas/oil IFT (IFT = 2.70, 0.15 and 0.04 mN.m^{-1}).

5.3.3 Two-Phase IFT Scaling Methods

The objective is to evaluate the application of Coats method (1980) which is currently used in reservoir simulators and to propose a possible modification when it is required to estimate the gas and oil relative permeabilities at low IFT conditions using the relative permeabilities at high IFT conditions.

The gas/oil relative permeabilities at a high value of IFT (e.g., 2.7 mNm^{-1}) have been calculated by history matching of the experimental results of a gas injection test, carried out in the lab. The experiment was conducted on the 1000 mD water-wet core at immiscible conditions (gas-oil IFT of 2.7 mNm^{-1}) at 1200 psia. The core initially

contain 92% oil and 8% irreducible water. The gas injection was performed at the rate of 200 cm^3h^{-1}. Figure 5-13 shows the calculated two-phase oil/gas k_r at high IFT of 2.7 mNm^{-1}. The blue arrow shows the saturation range of the experiment.

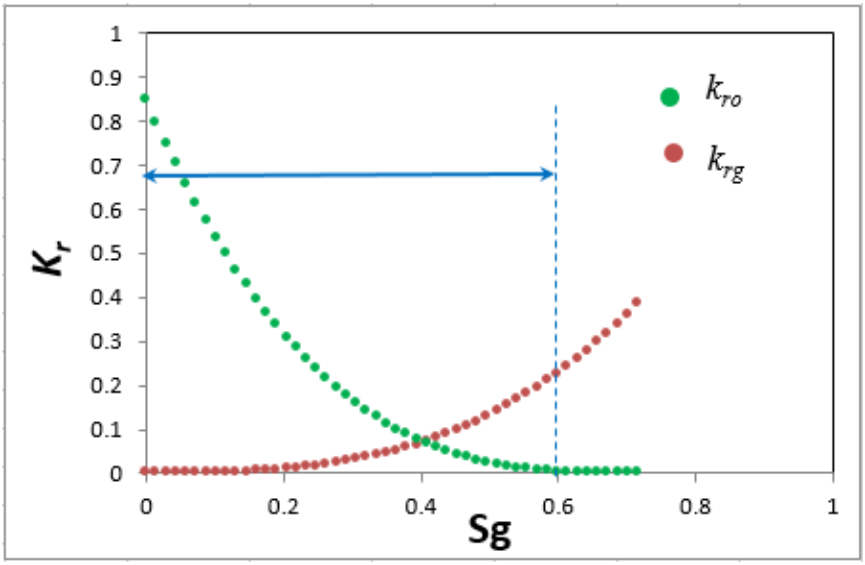

Figure 5-13: Measured gas and oil relative permeabilities 1000 mD mixed-wet core at IFT of 2.7 mNm^{-1}.

This set of k_r along with a numerical reservoir simulator (Eclipse) was used to perform a history match on a similar experiment (Experiment 4) but at low IFT conditions (0.04 mNm^{-1}). Initially, the measured k_r at a high IFT value was used directly in the numerical simulator - without any corrections - to simulate gas injection test at low IFT conditions, naturally expecting poor results. Then the correlations introduced by Coats were used to calculate modified k_{ro} and k_{rg} at a low IFT value explicitly. To do so the "*nl*" parameter in Eq.5-2 was used as the tuning parameter to find the best match between simulation and experimental results.

5.3.3.1 Using uncorrected k_r

To demonstrate the importance of accounting for the IFT effect in simulation, the results of an experiment, carried out at low IFT of 0.04 mNm^{-1} were compared with a simulation run of an experiment, using relative permeabilities of the same core obtained at high IFT of 2.7 mNm^{-1}, but ignoring the effect of IFT scaling. Obviously, the high IFT simulation results would not agree with the low IFT experimental results.

Figure 5-14 compares the oil recovery of an actual gas injection test at low IFT value of 0.04 mNm^{-1} (blue dotted curve) with the result of simulation in which no IFT scaling of k_r is used. As expected, there is a significant difference (25%) in the value of ultimate recovery between the experiment and simulation.

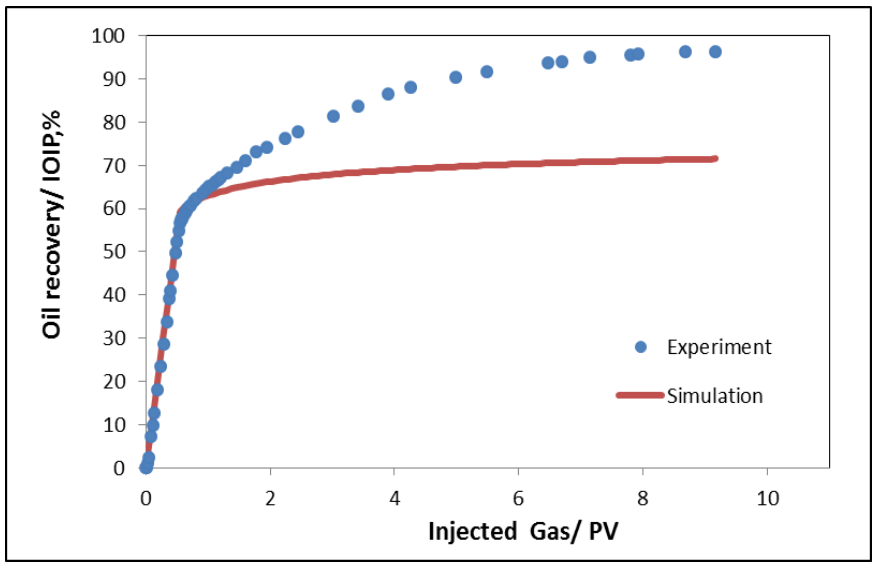

Figure 5-14: Comparison of oil recovery (%IOIP) between simulation while ignoring the effect of IFT and similar experiment performed at low gas/oil IFT of 0.04 mNm^{-1}.

Figure 5-15 shows that also the simulated pressure drop was significantly different from the experimental data. The results indicate that the effect of IFT on k_r must not be ignored.

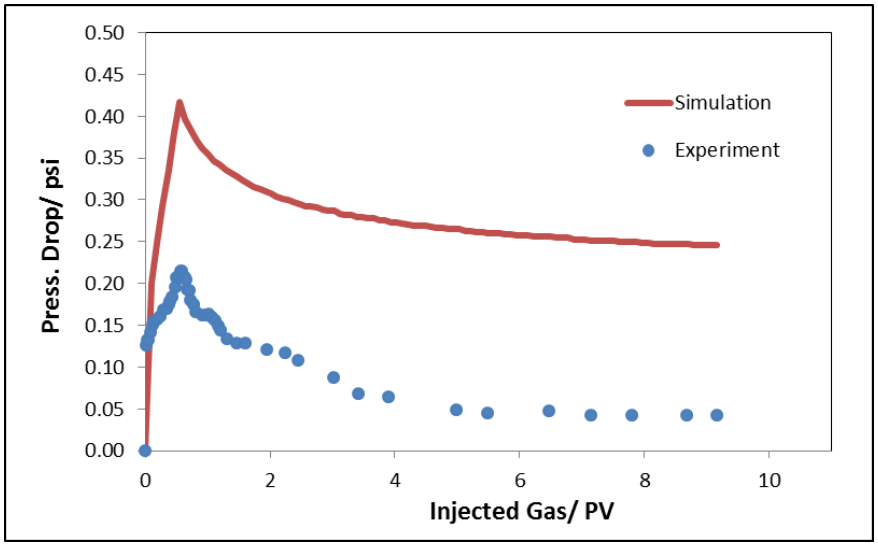

Figure 5-15: Comparison of pressure drop (psi) between simulation, while ignoring the effect of IFT and similar experiment performed at low gas/oil IFT of 0.04 mNm^{-1}.

5.3.3.2 Coats method of IFT scaling in Simulation

If the Coats method is used to scale the k_r curves of the low IFT case, from the high IFT k_r curves, the recovery and pressure drop curves are much closer to the experimental results, compared with the case mentioned above where no scaling corrections were used. To do so, the "*nl*" parameter in Eq. 5-2 was used as the tuning parameter to find the best match between simulation and experimental results, and the best match was obtained for *nl*=10 when $f(\sigma) = 0.66$. Figure 5-16 and Figure 5-17 compare the experimental data of gas injection test at low IFT values with the result of simulation

applying Coats method to the k_r at a high value of IFT. There is 11% difference in ultimate recovery between experiment and simulation. The recovery curve shows that although application of Coats method reduces the error in recovery and pressure drop the residual oil saturation and k_r curvature was not quite satisfactory by this method.

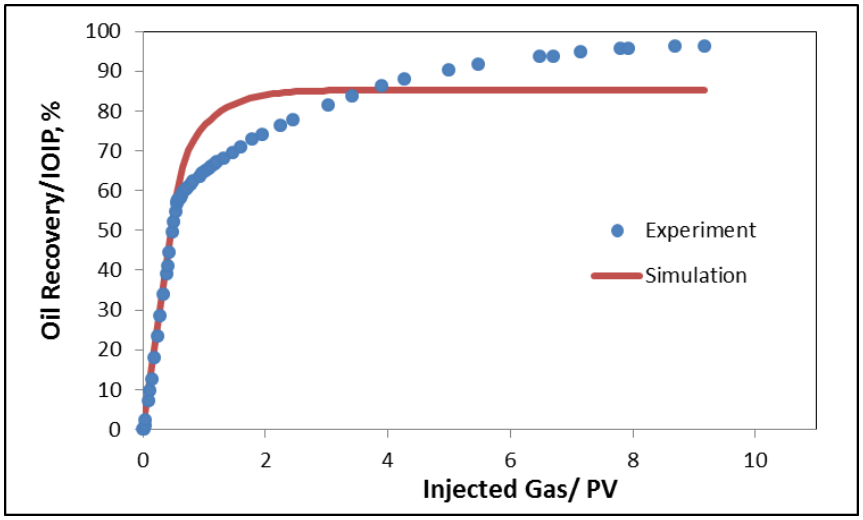

Figure 5-16: Comparison of oil recovery (%IOIP) between results of a simulation using Coats method and experiment at low gas/oil IFT of 0.04 mNm^{-1}.

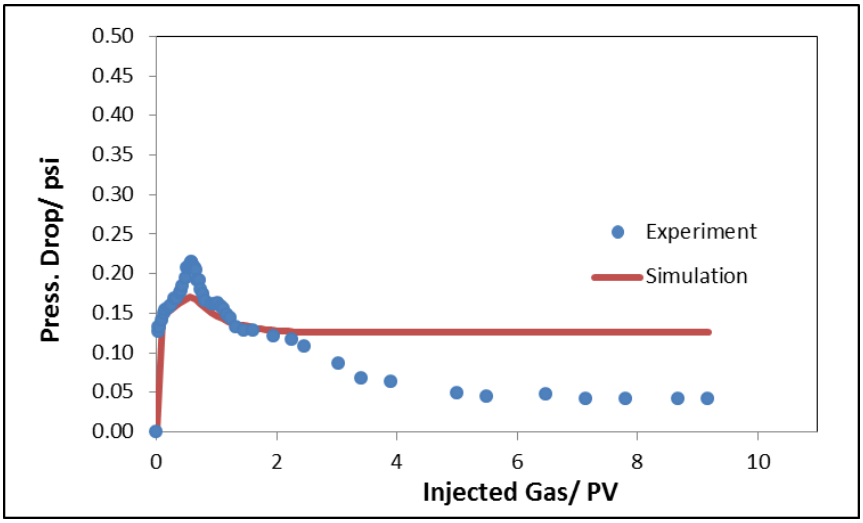

Figure 5-17: Comparison of pressure drop (psi) between results of a simulation using Coats method and experiment at low gas/oil IFT of 0.04 mNm^{-1}.

5.3.3.3 Proposed Modified Coats Method

As demonstrated in the above section, the Coats method could not satisfactorily predict the changes in the curvature of k_{ro} curve that occur due to the reduction in IFT. In Coats method the same value of $f(\sigma)$ is used for both oil and gas phases. According to the literature (Bardon and Longeron (1980), Harbert (1983)), the IFT reduction affects k_r of both phases, but not necessarily equally. As a general observation, as the system approaches the miscibility (i.e., IFT goes to zero), relative permeabilities increase and their curvature reduces. Some researchers (Bardon and Longeron (1980)) concluded that

the non-wetting phase k_r increases slightly as the IFT is reduced while others (Harbert (1983)) found that the wetting phase k_r remains completely unaffected by IFT reduction. To improve the performance, it was proposed to use the Coats formulation but with different values of *nl* for gas and oil in the weighting factors,

$$f_o(\sigma)=\left(\frac{\sigma}{\sigma_o}\right)^{\frac{1}{nl_o}} \text{ and } f_g(\sigma)=\left(\frac{\sigma}{\sigma_o}\right)^{\frac{1}{nl_g}}$$

For calculation of oil and gas k_r, respectively. "nl_o" and "nl_g" were introduced as separate tuning parameters for oil and gas phases and therefore the changes in curvature would be different for k_{ro} and k_{rg} curves. The best match was obtained for $f_g(\sigma)$ and $f_o(\sigma)$ of 0.62 and 0.84 respectively (compared with those mentioned above $f(\sigma)=0.66$ that was used for both k_{ro} and k_{rg} in the unmodified Coats method).

The error value between simulation and experimental results is obtained by applying standard error of estimate as below:

$$SSE=\sqrt{\frac{\sum_{i=1}^{n}\left(\frac{d_{Exp}-d_{Sim}}{d_{Exp}}\right)^2}{n-1}} \qquad 5\text{-}5$$

Where *SEE* is the percentage of standard error of estimate, *n* is number of data points and d_{Exp} and d_{Sim} are experimental and simulation results respectively. The calculated *SSE* for modified and unmodified Coats method are 54% and 56% respectively. Although the ultimate recovery calculated by simulation is still 15% less than the experimental result, the trends of oil recovery and pressure drop are relatively improved and are much more reasonable than in the unmodified Coats case (Figure 5-18 and Figure 5-19). The breakthrough time is critical for reservoir studies and an accurate estimate for this information is of great interest. The modified Coats method gives better results for the early times and also predicts the breakthrough time more accurately than the unmodified Coats method. In other words, using two separate weighting factors improved the curvature of the k_r curves adequately, but the predicted residual oil saturation still is not reasonable. Therefore, the modifications on the curvature of the k_r curves cannot capture the effect of IFT change on residual oil saturation. The physics behind the effect of IFT change on residual saturations should be investigated to propose a reliable model for predicting these parameters.

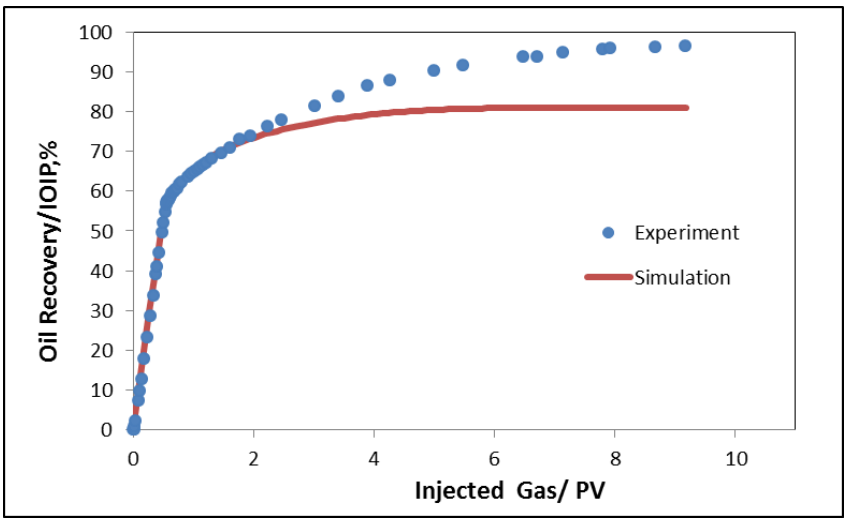

Figure 5-18: Comparison of oil recovery (%IOIP) between results of simulation using modified Coats method and experiment at low gas/oil IFT conditions

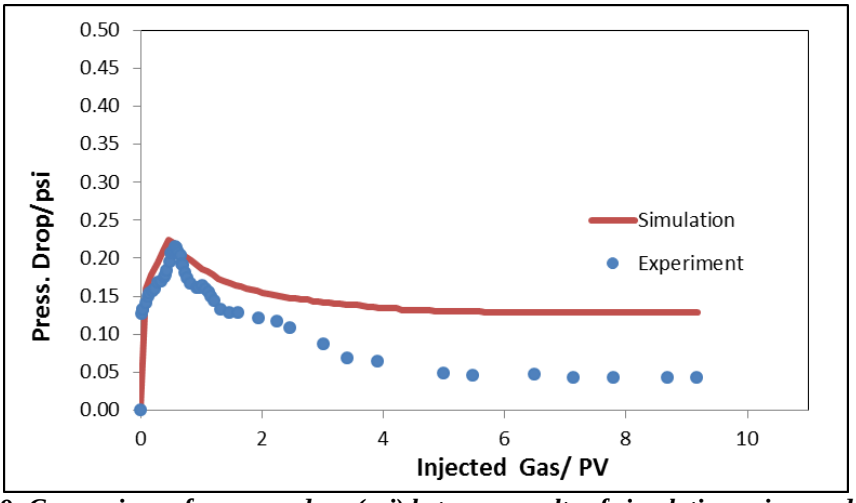

Figure 5-19: Comparison of pressure drop (psi) between results of simulation using modified Coats method and experiment at low gas/oil IFT conditions

5.4 Effect of Gas/Oil IFT on the Residual Oil Saturation in Water-Alternating-Gas (WAG) Injections at Laboratory Scale

The WAG injection was introduced and practiced in the oil industry to improve the sweep efficiency of the gas injection process. The WAG injection is intended to improve recovery by combining the microscopic displacement efficiency of gas flooding with macroscopic sweep efficiency of waterflooding. In the course of WAG injection it is possible not only to improve the displacement efficiency within the matrix of the rock (i.e., the microscopic displacement, similar to the process in laboratory core flooding), where both gas and water move, alternately, but also for these fluids to contact the unswept zones in the reservoir (i.e., macroscopic displacement) and improve the overall recovery. Review of WAG performance in 59 field applications shows an increased oil recovery of 5 – 10% of IOIP. Additional oil recovery by immiscible WAG

injection is usually less than the miscible WAG (Christensen et al. (1998)). Most of the field applications of WAG injection were reported as miscible WAG, and there are only a few field applications reported to be fully immiscible. The gas/oil IFT values can be representative of the types of WAG injection, which are miscible, near-miscible and immiscible. It was demonstrated that gas/oil IFT reduction improves both gas and oil relative permeabilities and results in lower residual oil saturation. The objective of this comparative study is to investigate the effect of gas/oil IFT on the reduction of residual oil saturation during the cyclic injections of gas and water (WAG). Several WAG experiments at different gas/oil IFT values (near-miscible to immiscible) have been performed in the Centre for EOR and CO_2 Solutions at Heriot-Watt University. There is limited detailed published research study in this area. Results of some of them have been collected and compared with the results obtained at Heriot-Watt University.

5.4.1 Summary of the results at HWU

Several WAG experiments at three gas/oil IFT values of 0.04 (near-miscible), 0.15 and 2.7 mNm^{-1} (immiscible) have been performed in the Centre for EOR and CO_2 Solutions at Heriot-Watt University. Table 5-2 summarizes different WAG experiments started with water (WAG-ID; I: imbibition & D:drainage) with the residual oil saturation after cyclic injection of water and gas for different gas/oil IFT values in 65 and 1000 mD water-wet and mixed-wet Clashach sandstone cores. Table 5-3 presents the WAG experiments started with gas (WAG-DI) and the residual oil saturation after cyclic injections for different gas/oil IFT values in 65 mD mixed-wet core. More details on these experiments can be found in Sohrabi et al. (2007), Fatemi et al. (2012), Fatemi and Sohrabi (2015).

The displacement process was denoted by G for gas injection and W for water flooding. The number behind the letter refers to the cycle number, i.e., G2 refers to gas injection in the second cycle. Figure 5-20 shows that the oil saturation in the 65 mD mixed-wet core, at $IFT_{g/o}$ of 0.15 and 2.7 mNm^{-1} conditions, decreased insignificantly after the secondary water flooding. This means during any of the subsequent cycles of WAG injection (i.e., end of G1, W2, G2, W3, and G3; the red curve) the residual oil saturation decreased due to the three-phase flow mechanism and the hysteresis effect but the reduction is limited while in the near-miscible conditions ($IFT_{g/o}$= 0.04mNm^{-1}) it decreased continuously even during the later stages of WAG injection. The similar continuous trend of reduction in residual oil saturation during the near-miscible WAG injection can be seen in the experimental results of the 1000 mD core. Figure 5-21

compares the reduction of oil saturation during WAG-DI injections at three different gas/oil IFT values. Unlike the WAG-ID results, WAG-DI at high gas/oil IFT value shows better performance than the intermediate IFT value. Similarly, the WAG-DI at near-miscible conditions had lower performance than WAG-DI at high IFT value, but the continuous reduction of residual oil during the cyclic injections at near-miscible conditions caused even better performance at the end of the fourth cycle. As a result, it can be concluded that in WAG-ID and DI injections at near-miscible conditions, the residual oil continuously decreased during the injections and the recovery was higher compared with the injections at intermediate and high gas/oil IFT values.

Comparing the results of WAG-ID and WAG-DI injections in the 65 mD mixed-wet core at immiscible conditions (0.15 and 2.7 mNm^{-1}) the performance of WAG injection was better when started with gas than when started with water. However, the near-miscible WAG-ID injection, especially in the first cycle, outperformed WAG-DI injection. Moreover, the performance of WAG in the mixed-wet system was much better than the water-wet system for the 65 mD core and still much better in the 1000 mD mixed-wet core (as expected).

Table 5-2: Residual oil saturations during WAG-ID injection in 65 and 1000 mD Clashach cores.

Rock	Wettability	IFTg/o	S_{oi}	S_{or} W1	S_{or} G1	S_{or}W2	S_{or} G2	S_{or}W3	S_{or} G3
1000 mD	MW	0.04	0.92	0.23	0.115	0.06	0.009	-	-
65 mD	WW	0.04	0.82	0.415	0.30	0.26	0.2	0.167	0.095
65 mD	MW	0.4	0.82	0.18	0.144	0.127	0.105	0.096	0.027
65 mD	MW	0.15	0.82	0.271	0.265	0.247	0.234	0.224	0.214
65 mD	MW	2.7	0.82	0.18	0.305	0.29	0.29	0.28	0.28

Table 5-3: Residual oil saturations during WAG-DI injection in 65 mD Clashach cores.

Rock	Wettability	IFTg/o	S_{oi}	S_{or} G1	S_{or} W1	S_{or} G2	S_{or}W2	S_{or} G3	S_{or}W3	S_{or} G4	S_{or}W4
65 mD	MW	0.04	0.82	0.29	0.19	0.16	0.14	0.11	0.095	0.07	0.05
65 mD	MW	0.15	0.82	0.305	0.168	0.153	0.141	0.133	0.124	0.113	0.105
65 mD	MW	2.7	0.82	0.35	0.089	0.082	0.068	0.064	0.06	0.06	0.057

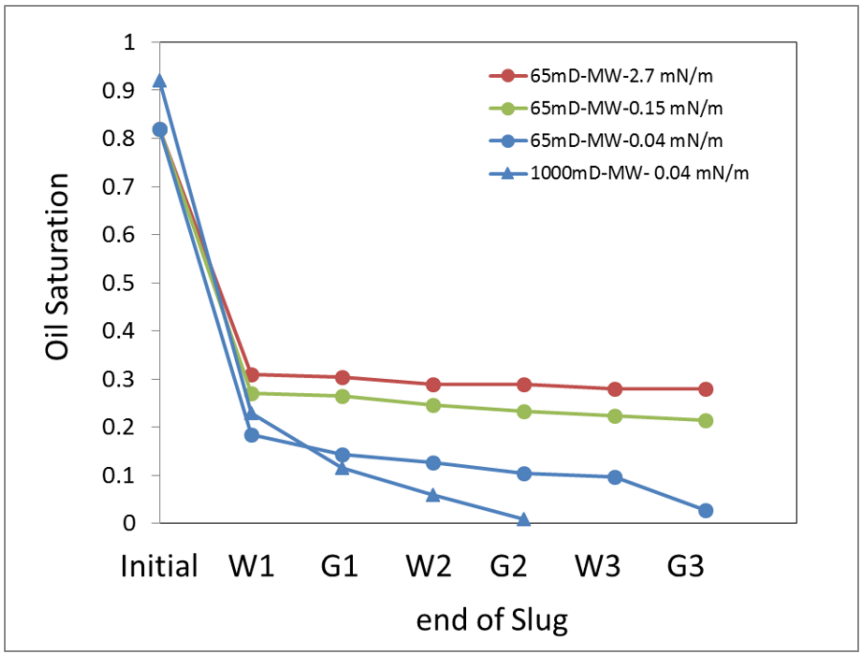

Figure 5-20: Residual oil saturation at the end of each flooding phase during WAG-ID injections in 65 and 1000 mD mixed-wet cores.

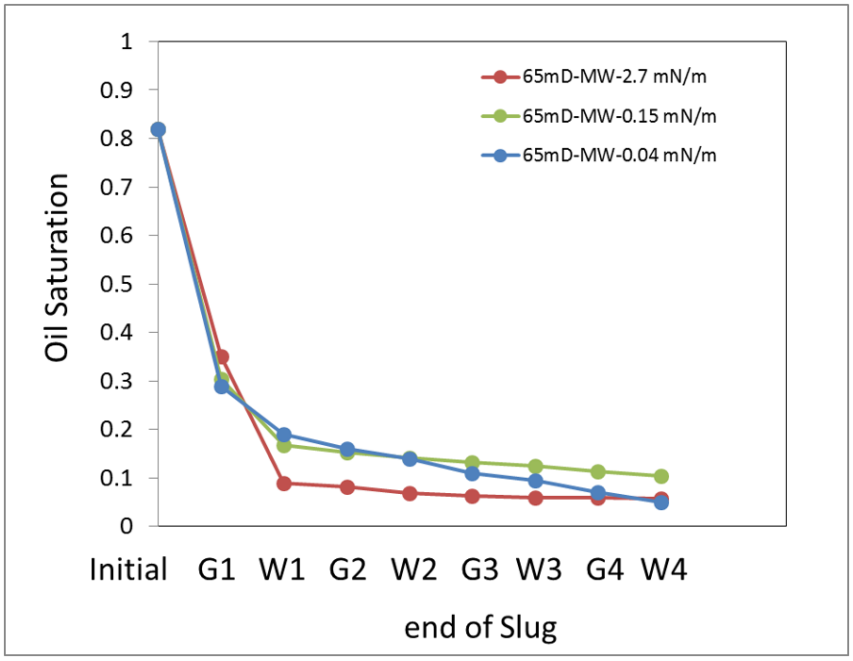

Figure 5-21: Residual oil saturation at the end of each flooding phase during WAG-DI injections in 65 mD mixed-wet core.

5.4.2 Published Literature

Skauge and Larsen (1994) conducted several immiscible WAG coreflood experiments on sandstone cores of outcrop Berea and the North Sea reservoir rocks (four different reservoirs) under different wettability conditions of water-wet, oil-wet and intermediate-wet. The wettability index measurements were performed at ambient conditions and it was noted that, for outcrop Berea sandstone, some changes in wettability occurred after a series of displacement tests at ambient or reservoir conditions. Modifying wettability

by silanization is a very questionable process, and does not result in a stable oil-wet or even mixed-wet rock, i.e., the wettability changes even during the short duration of the WAG test. In their tests, gas injection was performed on horizontal cores for Berea, silanized Berea and North Sea reservoir core 1 (R1) at constant differential pressure, but for the North Sea reservoir cores 2, 3 and 4 (R2, R3, and R4) the gas injection was in a gravity stable vertical displacement. For the reservoir cores, experiments were performed at approximately 100 °C and 300 bars, and the fluids were recombined reservoir oil and gas. For outcrop cores, synthetic fluids (mixtures of methane and decane) were used, and experiments were performed at a selected value of pressure but ambient temperature. For all cores, the initial water saturations were their irreducible values. They carried out tests on several cores from each of the North Sea reservoirs with different values of permeability. The permeabilities of the tested cores were as follows: R1:100-200 mD, R2: 30-300 mD, R3: 800-2000 mD and R4: 300-800 mD. No permeability information was reported for the Berea sandstone cores (but probably a range of 100-200 mD might be assumed, based on other Berea tests declared in the literature). Their results showed that the residual oil saturation could be significantly reduced by three-phase flow (immiscible) compared to two-phase waterflood or only gas injection, from initial conditions. Table 5-4 and Table 5-5 present the residual oil saturations and oil recovery, respectively, for different experiments including WAG-DI (started with gas injection) and WAG-ID (starting with water injection) injection scenarios. Figure 5-22 compares the changes in residual oil saturation for Berea and R1 cores during immiscible WAG-ID and DI injections. The residual oil saturations for two complete cycles of alternative gas and water injection were available only for these two cores. It is observed that for both set of cores, Berea, and the North Sea when the WAG processes started with gas injection it had higher oil recovery than those tests which began with water flooding.

Also, comparing the results obtained from the North Sea reservoir cores, Skauge and Larsen concluded that the performance of WAG in the mixed-wet system was much better than water-wet system whether it started with gas injection or water flooding. Similarly, according to the experimental results on 65 mD Clashach sandstone core, also, the performance of WAG in the mixed-wet system was better than that of the water-wet system.

Furthermore, in these immiscible WAG processes, the largest portion of recovery (decrease in oil saturation) occurred in the first cycle of injections and the decrease in residual oil saturation was not significant in the later injection periods.

Table 5-4: Residual oil saturation for each experiment, Skauge and Larsen (1994).

Rock	Orientation	Wettability	WAG-DI (starts with Gas)				WAG-ID (starts with Water)			
			S_{oi}	S_{or} G1	S_{or}W1	S_{or} G2	S_{oi}	S_{or} W1	S_{or} G1	S_{or} W2
Berea	Horizontal	WW	0.733	0.213	0.079	0.075	0.73	0.44	0.438	0.391
Silanized Berea*	Horizontal	NA	0.725	0.236	0.158	0.156	0.699	0.147	0.141	0.089
R1(North Sea)	Horizontal	WW	0.692	0.23	0.201	0.191	0.778	0.377	0.359	0.303
R2(North Sea)	Vertical	MW	0.64	0.35	0.16	-	0.63	0.28	0.18	-
R3(North Sea)	Vertical	MW	0.775	0.093	-	-	-	-	-	-
R4(North Sea)	Vertical	WW	0.381	0.191	0.145	-	0.489	0.218	-	-

** Wettability was initially altered to oil-wet by silanization but it changed from oil-wet to water-wet after series of experiments*

Table 5-5: Oil recovery(%) for different experiments, Skauge and Larsen (1994).

Rock	Orientation	Wettability	Secondary WAG	Tertiary WAG
Berea (B)	Horizontal	WW	89.7	46.4
Silanized Berea	Horizontal	NA	78.5	87.2
R1	Horizontal	WW	72.4	61.1
R2	Vertical	MW	75	71.4
R3	Vertical	MW	88	-
R4	Vertical	WW	61.9	55.4

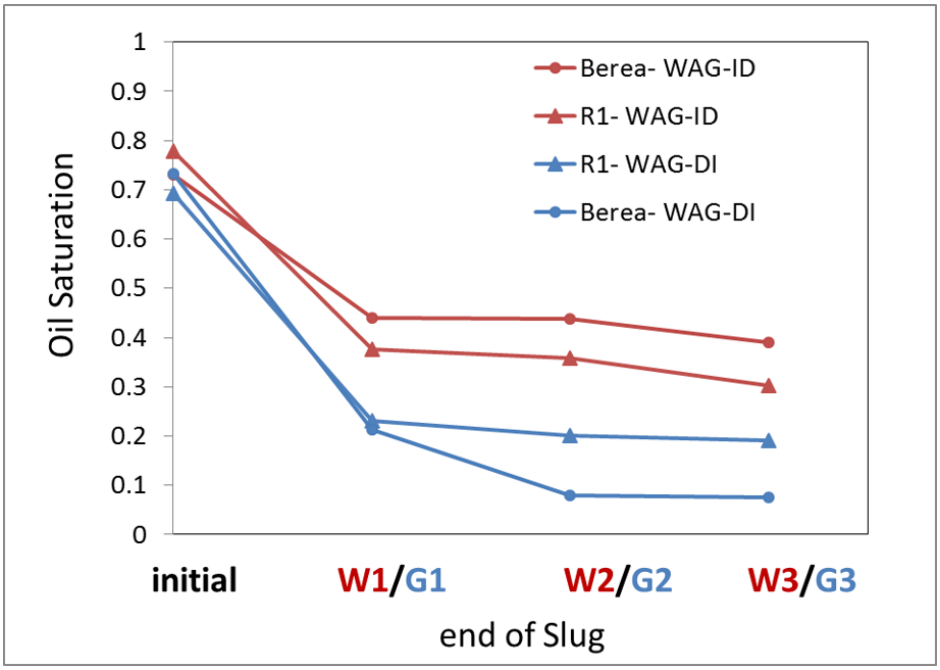

Figure 5-22: Residual oil saturation at the end of each flooding phase during WAG-DI (Blue) and WAG-ID (Red) for Berea Sandstone and R1 North Sea cores.

Minssieux and Duquerroix (1994) performed immiscible WAG experiments on an 80 cm composite sandstone core. The WAG experiments were performed after subsequent water flooding and started with gas injection. The core was water-wet with permeability and porosity of 130 mD and 0.11, respectively. The experiments were conducted at 80

°C with constant injection rates, and the core was horizontally oriented. Table 5-6 summarizes the results of their WAG experiments. They concluded that when oil was under-saturated, oil swelling in the presence of injected methane combined with gas trapping during imbibition helped to mobilize oil during the WAG injection. They also concluded that in the absence of oil swelling, three-phase hysteresis involved in WAG injection led to some extra but limited and slow oil production. As Figure 5-23 shows, the residual oil saturation could be significantly reduced by three-phase flow compared to two-phase waterflood.

Table 5-6: Results of Immiscible WAG experiments in water-wet sandstone core, Minssieux (1994).

Experiment	Swelling	S_{oi}	$S_{or\ WF}$	WAG S_{or}
WAG-ID	5% vol.	0.95	0.44	0.317
WAG-ID	13% vol.	0.56	0.325	0.152
WAG-ID	no Swelling	0.91	0.44	0.303
SWAG	no Swelling	0.78	0.467	0.387

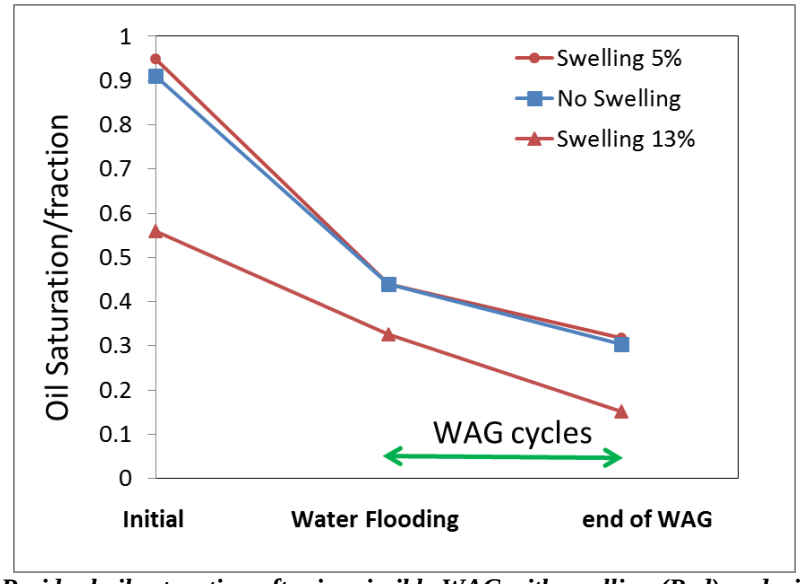

Figure 5-23: Residual oil saturation after immiscible WAG with swelling (Red) and without swelling (Blue) for a water-wet sandstone core.

The sequence of injections in the study by Minssieux and Duquerroix (1994) was similar to the most of the experiments that have been conducted at Heriot-Watt University. The results of their study for WAG injection with zero and 5% oil swelling were compared to the immiscible and near-miscible experiments that have been performed on 65 mD water-wet and mixed-wet cores (Figure 5-24). The results of both studies show that WAG injection at near-miscible conditions or with high oil swelling has higher recovery than immiscible WAG.

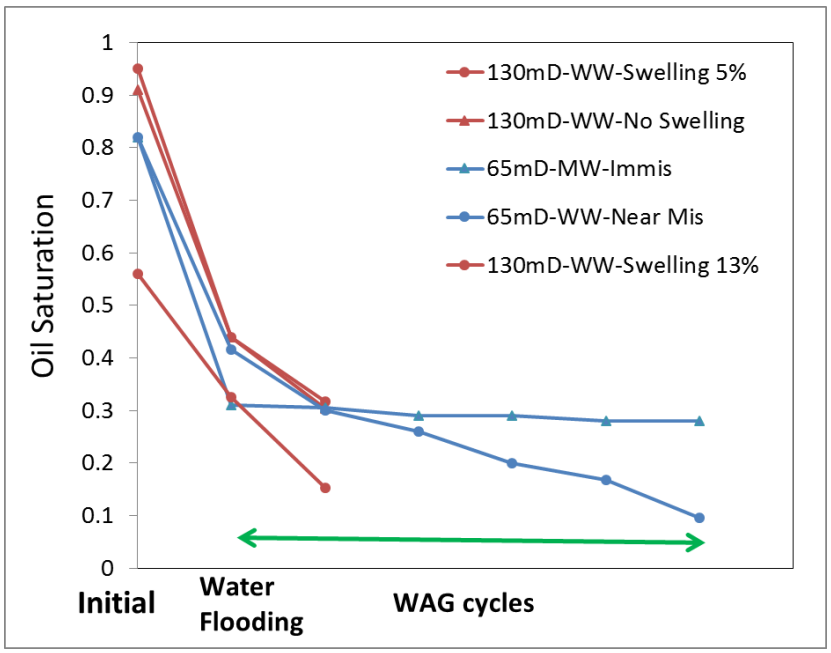

Figure 5-24: Comparison of residual oil saturation at the end of each flooding phase during WAG-ID experiments, performed by Minssieux (Red) and HWU (Blue).

Egermann et al. (2000) reported the results of a series of four cyclic gas and water injection experiments on a water-wet limestone core (φ=0.23, k=215 mD) with different initial saturations. In each series, there are two cycles and each cycle includes drainage (gas injection) and imbibition (water flooding) experiments. The drainage and imbibition experiments were at constant pressure and constant injection rate, respectively. To ensure that the displacement mode is the same in the whole core, each flooding test was pursued after the breakthrough of the injecting phase. The experiments were performed at ambient condition, and the core was horizontally oriented. The fluids used in these experiments were soltrol 70, brine (30 g/l NaCl) and nitrogen. The gas injections were immiscible or at high IFT conditions (IFT oil/gas =27 mNm^{-1}). Table 5-7 and Table 5-8 summarize the changes in residual oil saturation after cyclic gas and water injections in all series. For Series 1, the core was initially saturated with water but displaced by oil injection until no further water was produced (to establish irreducible water saturation S_{wir}). The cyclic gas and water injection was then performed. This experiment is equivalent to WAG-DI injection. In Series 2, the cyclic injections started after secondary water flooding where oil had reached to its residual value. For Series 3 and 4 by steady-state injection of oil and water, an intermediate value for oil saturation was established before starting the cyclic injections. These experiments are equivalent to WAG-ID injection. Whatever the establishment of the initial state was, the sequence of injection was drainage (gas injection) and imbibition (water injection). As depicted in Figure 5-25, the residual oil saturation can be considerably lower by three-phase flow compared to two-phase water flooding or gas injection. The majority of the oil recovery

took place during the first three injections, and no significant production was obtained after the subsequent injections. Although the lithology of the core used in this study (carbonate) is different from sandstone, almost the same trend in reduction of residual oil saturation was observed during immiscible WAG injection.

Table 5-7: Residual oil saturation during Series 1 (WAG-DI), Egermann et al. (2000).

Experiment	Initial S_o	S_{or} G1	S_{or}W1	S_{or} G2	S_{or}W2
S1 (S_{oi}=0.51, S_{wir}=0.49)	0.51	0.28	0.21	0.19	0.19

Table 5-8: Residual oil saturation during Series 2, 3, 4 (WAG-ID), Egermann et al. (2000).

Experiment	S_{or}W1 (initial)	S_{or} G1	S_{or}W2	S_{or} G3	S_{or}W3
S2 (S_{orw}=0.31, S_{wi}=0.69)	0.31	0.24	0.18	0.18	0.18
S3 (S_{oi}=0.39, S_{wi}=0.61)	0.39	0.25	0.19	0.18	0.18
S4 (S_{oi}=0.42, S_{wi}=0.58)	0.42	0.27	0.22	0.20	0.19

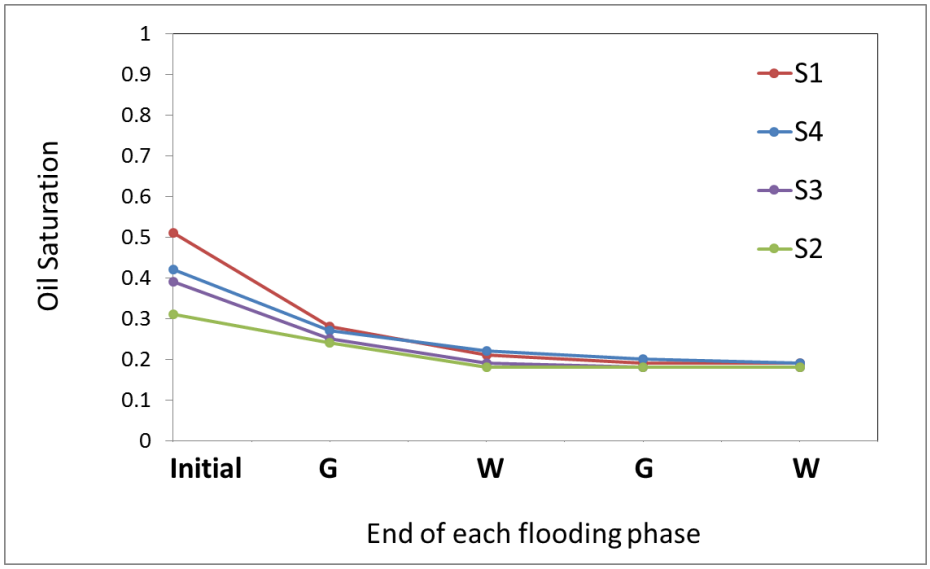

Figure 5-25: Residual oil saturation at the end of each flooding phase during WAG tests that started with different initial oil and water saturations.

Element et al. (2003) pursued a laboratory study on immiscible WAG-ID and DI floods in water-wet and mixed-wet (intermediate-wet) Berea sandstone cores. Water-wet and mixed-wet cores had the same porosity of 0.19 but gas permeability of 328 and 393 mD, respectively. Decane, distilled water, and nitrogen were the fluids used in their displacement experiments. The development of mixed wettability was done by aging the core with stock tank oil. The injections were performed vertically from the top of the core. The flooding sequences under the both wettability conditions started with water flooding for WAG-ID experiment and with gas for WAG-DI experiment. A higher recovery was achieved for water-wet and mixed-wet cores for WAG-DI (gas injection

before the first waterflood). The same conclusion has been made from research results of Skauge and Larsen (1994) and ours. Table 5-9 presents the residual oil saturation obtained after each drainage and imbibition process in a WAG-ID injection for the water-wet core. These data were the only published data in their paper. Figure 5-26 compares the results of tertiary WAG injection performed by Element et al. (2003) with WAG-ID and DI carried out by Skauge and Larsen (1994).

The results of WAG-ID experiment by Element et al. (2003) was compared with two most similar experiments performed at Heriot-Watt University; WAG-ID injection into 65 mD once with water-wet wettability at near-miscible conditions and once with mixed-wet wettability at immiscible conditions (Figure 5-27). The immiscible WAG injections for both studies showed very similar behaviour and no significant oil production was obtained after the first WAG cycle. However, the residual oil saturation at near-miscible conditions decreased considerably after the first cycle. Considering the trend of changes in residual oil saturation during WAG injections, it is revealed that, as expected, the recovery of WAG at near-miscible conditions is significantly higher than under immiscible conditions.

Table 5-9: residual oil saturation during immiscible WAG-ID injection for water-wet Berea sandstone core.

Experiment	S_{oi}	$S_{or}W1$	S_{or} G1	$S_{or}W2$	S_{or} G2	$S_{or}W3$	S_{or} G3	$S_{or}W4$	S_{or} G4
WAG (Secondary)	0.74	0.46	0.31	0.26	0.25	0.24	0.23	0.22	0.21

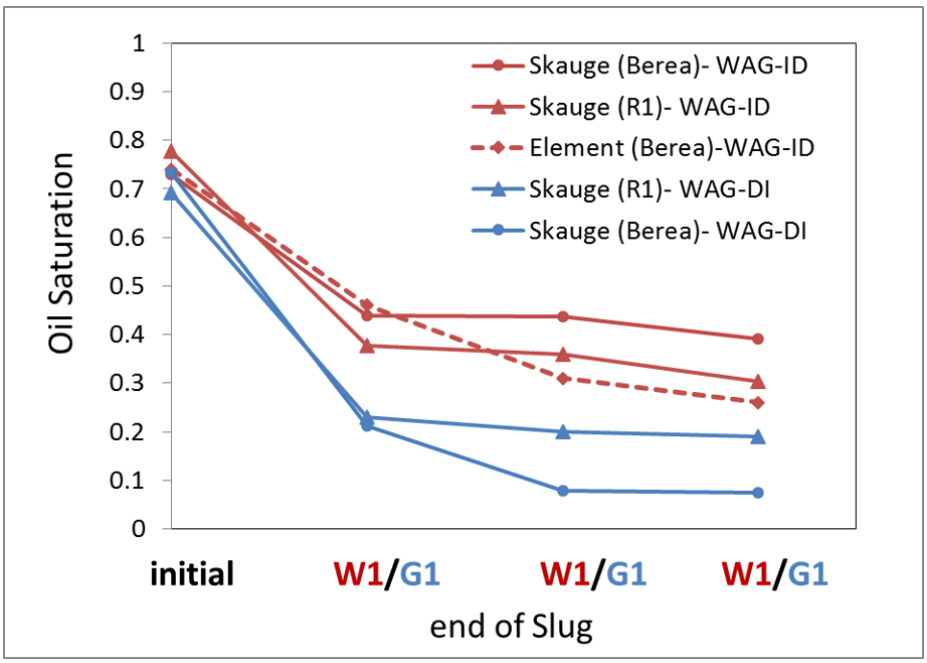

Figure 5-26: Residual oil saturation at the end of each flooding phase during WAG-DI (Blue) and WAG-ID (Red) WAG injections by Element et al. and Skauge & Larsen.

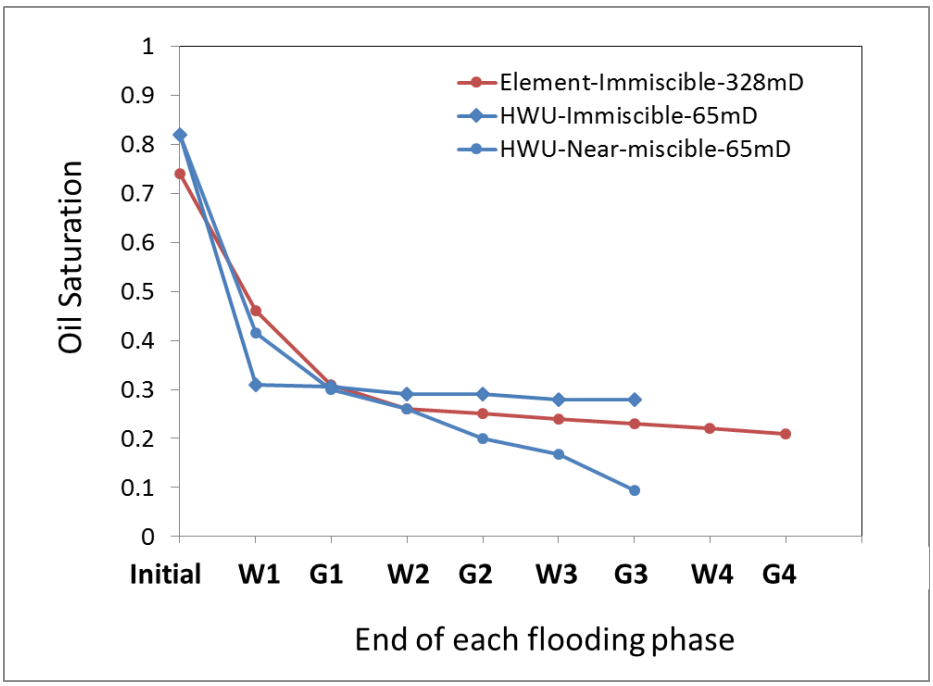

Figure 5-27: Residual oil saturation at the end of each flooding phase during WAG-ID injections by Element et al. (Red) and HWU (Blue).

5.5 Conclusions

In this study, the effect of gas/oil IFT reduction on two- and three-phase relative permeabilities has been investigated using the two- and three-phase coreflood displacement experiments. The current practice for two-phase k_r IFT scaling was examined using the measured data. Furthermore, the effect of gas/oil IFT on residual oil saturation change during WAG injections at immiscible (high gas/oil IFT) and near-miscible (very low gas/oil IFT) conditions in laboratory scale was evaluated. The following conclusions can be drawn from this study:

<u>Two-Phase Systems</u>

- The relative permeability of both phases increase as the IFT decreases, but not equally.
- As the system moves from immiscible toward miscible conditions, the relative permeability increases and its curvature reduces.
- The IFT reduction to the ultra-low value of 0.04 mNm^{-1} was more effective than 0.15 mNm^{-1}.
- The residual oil saturation decreased as the IFT decreased, particularly at the ultra-low IFT values.

- The wetting phase (oil) k_r was affected by IFT reduction mainly at low saturation values while the non-wetting phase (gas) k_r was impacted in the whole range of saturation.
- The effect of IFT reduction on k_{ro} and S_{or} was more pronounced for high permeability rocks.
- The measured relative permeability by a displacement experiment should be corrected for the effects of IFT if the IFT values of the experiment do not represent the IFT values of the reservoir. Using Coats method as the IFT scaling method should be done cautiously, and non-equal effects on k_{ro} and k_{rg} should be borne in mind.
- Application of separate weighing factor for oil and gas in the Coats method is recommended to alleviate the problem, although the method could not yet accurately estimate the residual fluid saturations.
- Application of the Coats method and the modified version proposed in this study will result in less error than using completely uncorrected k_r.

Three-Phase Systems

- The gas/oil IFT reduction affects the relative permeability of all three phases, $k_{ro,}$ and k_{rg} increase while k_{rw} decreases at low values of water saturation.
- The observed effect on the k_{rw} should be further investigated.
- Similarly to the two-phase system, the IFT reduction was more effective at ultra-low IFT conditions, with minor effects at intermediate values.
- Further investigations are required to understand the influence of gas/oil IFT variations on three-phase k_r.
- The residual oil saturation could be significantly reduced at three-phase flow compared to two-phase waterflood or only gas injection.
- In the most of the research studies on immiscible WAG injection, presented in this study, the major reduction in residual oil saturation is achieved in the first cycle, and further WAG cyclic injection does not have a significant contribution to oil recovery. The only exception is for near-miscible WAG (ultra-low gas/oil IFT) injection where the residual oil saturation keeps decreasing to the last injection cycle.
- Although there is not enough literature data on the performance of WAG injection at very ultra-low gas/oil IFT (near-miscible) conditions, based on the

data presented in this thesis, the performance of near-miscible WAG (ultra-low gas/oil IFT) is generally better than that of immiscible WAG (high gas/oil IFT).

- The immiscible WAG (high gas/oil IFT) experiments that started with gas injection (WAG-DI) have higher oil recovery than those starting with water flooding (WAG-ID) for both water-wet and mixed-wet systems.

5.6 References

Al-Wahaibi, Y. M., Grattoni, C. A. and Muggeridge, A. H. 2006. Drainage and Imbibition relative permeabilities at near miscible conditions. Journal of Petroleum Science and Engineering 53(3–4): 239-253.

Asar, H. and Handy, L. L., 1988. Influence of Interfacial Tension on Gas/Oil Relative Permeability in a Gas-Condensate System. SPE Reservoir Engineering 3(1): 257-264.

Bardon, C., Longeron, D. G., 1980. Influence of Very Low Interfacial Tensions on Relative Permeability", SPE Journal 20(5): 391-401.

Blom, S. M. P. and J. Hagoort, 1998. How to Include the Capillary Number in Gas Condensate Relative Permeability Functions? SPE Annual Technical Conference and Exhibition. New Orleans, Louisiana, 1998 Copyright 1998, Society of Petroleum Engineers Inc.

Blom, S. M. P., Hagoort, J., and Soetekouw, D. P. N., 2000. Relative Permeability at Near-Critical Conditions." SPE Journal 5(2): 172-181.

Calisgan, H., Demiral, B., and Akin, S., 2006. Near-Critical Gas/Condensate Relative Permeability of Carbonates. SPE/DOE Symposium on Improved Oil Recovery. Tulsa, Oklahoma, USA, Society of Petroleum Engineers.

Chen, H. L., Wilson, S. D. and Monger-McClure, T. G., 1999. Determination of Relative Permeability and Recovery for North Sea Gas-Condensate Reservoirs. SPE Reservoir Evaluation & Engineering 2(4): 393-402.

Christensen, J. R., Stenby, E. H. and Skauge, A., 1998. Review of WAG Field Experience. International Petroleum Conference and Exhibition of Mexico. Villahermosa, Mexico: 1998 Copyright 1998, Society of Petroleum Engineers, Inc.

Cinar, Y. and Orr Jr., F. M., 2005. Measurement of Three-Phase Relative Permeability with IFT Variation. SPE Reservoir Evaluation & Engineering, 8, pp. 33-43.

Cinar, Y., Marques, S. and Orr Jr., F. M., 2007. Effect of IFT Variation and Wettability on Three-Phase Relative Permeability. SPE Reservoir Evaluation & Engineering, 10, pp. 211-220.

Coats, K. H., 1980. An Equation of State Compositional Model. Society of Petroleum Engineers Journal 20(5): 363-376.

Delclaud, J., Rochon, J. and Nectoux, A. 1987. Investigation of Gas/Oil Relative Permeabilities: High-Permeability Oil Reservoir Application. SPE Annual Technical

Conference and Exhibition. Dallas, Texas, 1987 Copyright 1987, Society of Petroleum Engineers.

Delshad, M., Delshad, M., Pope, G. A., and Lake, L. W. 1987. Two- and Three-Phase Relative Permeabilities of Micellar Fluids. SPE Formation Evaluation 2(3): 327-337.

Dria, D.E., Pope, G.A. and Sepehrnoori, K. 1993. Three-Phase Gas/Oil/Brine Relative Permeabilities Measured Under CO2 Flooding Conditions. SPE Reservoir Engineering 8(2): 143-150.

Egermann, P., Vizika, O., Dallet, L., Requin, C. and Sonier, F., 2000. Hysteresis in Three-Phase Flow: Experiments, Modeling and Reservoir Simulations. SPE European Petroleum Conference. Paris, France: Copyright 2000, Society of Petroleum Engineers Inc.

Elemet, D. J., Masters, J. H. K., Sargent, N. C., Obe, A. J. J. and Goodyear, S. G., 2003. Assessment of Three-Phase Relative Permeability Models Using Laboratory Hysteresis Data. SPE International Improved Oil Recovery Conference in Asia Pacific. Kuala Lumpur, Malaysia: Society of Petroleum Engineers.

Fatemi, S. M. and Sohrabi, M., 2015. Mechanistic Study of the Effect of Gas/Oil IFT on the Performance of Gas, WAG and SWAG Injections in Mixed-Wet Systems. SPE Annual Technical Conference and Exhibition held in Houston, Texas, USA, 28–30 September 2015.

Fatemi, S. M., Sohrabi, M., Ireland, S. and Jamiolahmady, M. 2012. Recovery Mechanisms and Relative Permeability for Oil/Gas System at Near-miscible Conditions: Effects of Immobile Water Saturation, Wettability, Hysteresis and Permeability. SPE Improved Oil Recovery Symposium. Tulsa, Oklahoma, USA, Society of Petroleum Engineers.

Fatemi, S. M., Sohrabi, M., Jamiolahmady, M., Ireland, S. and Robertson, G., 2011. Experimental Investigation of Near-Miscible Water-Alternating-Gas (WAG) Injection Performance in Water-wet and Mixed-wet Systems. Presented at Offshore Europe,Aberdeen,6–8September.SPE-145191-MS. http://dx.doi.org/10.2118/145191-MS.

Fulcher Jr., R.A., Ertekin, T. and Stahl, C.D., 1985. Effect of Capillary Number and Its Constituents on Two-Phase Relative Permeability Curves. Journal of Petroleum Technology 37(2): 249-260.

Harbert, L. W., 1983. Low Interfacial Tension Relative Permeability. SPE Annual Technical Conference and Exhibition. San Francisco, California, 1983 Copyright 1983 Society of Petroleum Engineers of AIME.

Henderson, G. D., Danesh, A., Tehrani, D. H. and Peden, J. M., 1997. The effect of velocity and interfacial tension on relative permeability of gas condensate fluids in the wellbore region. Journal of Petroleum Science and Engineering 17(3–4): 265-273.

Henderson, G. D., Danesh, A., Tehrani, D. H., Al-Shaidi, S. and Peden, J. M., 1998. Measurement and Correlation of Gas Condensate Relative Permeability by the Steady-State Method. SPE Reservoir Evaluation & Engineering 1(2): 134-140.

McDougall, S. R., Salino, P. A. and Sorbie, K. S., 1997. The Effect of Interfacial Tension upon Gas-Oil Relative Permeability Measurements: Interpretation Using Pore-Scale Models. SPE Annual Technical Conference and Exhibition. San Antonio, Texas, 1997 Copyright 1997, Society of Petroleum Engineers, Inc.

Minsseieux, L., 1994. WAG Flow Mechanisms in Presence of Residual Oil. SPE Annual Technical Conference and Exhibition. New Orleans, Louisiana: Society of Petroleum Engineers.

Shen, P., Zhu, B., Li, X. B., and Wu, Y. S., 2006. The Influence of Interfacial Tension on Water/Oil Two-Phase Relative Permeability. SPE/DOE Symposium on Improved Oil Recovery. Tulsa, Oklahoma, USA, Society of Petroleum Engineers.

Skauge, A. L. and Johne A., 1994. Three-Phase Relative Permeabilities and Trapped Gas Measurements Related to WAG Processes. International Symposium of the Society of Core Analysts, Stavanger, Norway.

Sohrabi, M., Tehrani, D. H. and Al-Abri, M., 2007. Performance of Near-Miscible Gas and SWAG Injection in a Mixed-Wet Core. Oral presentation of paper SCA2007-26 given at the International Symposium of the Society of Core Analysts, Calgary, 10–12 September.

Cinar, Y., Marquez, S. and Orr Jr, F. M., 2007. Effect of IFT Variation and Wettability on Three-Phase Relative Permeability. SPE Reservoir Evaluation & Engineering 10(3): pp. 211-220.

Chapter 6 – Gas/Oil Relative Permeability Normalization

Relative permeability (k_r) is usually measured in the laboratory. Measuring k_r under conditions involving mixed-wet rocks and low interfacial tension (IFT) fluids are particularly difficult and requires special equipment. The question is how to predict k_r for a mixed-wet rock using existing k_r data measured for a water-wet rock. Generally, how do we predict k_r for a new rock/fluid conditions (such as permeability, wettability, and IFT) using existing k_r data measured at different conditions?

The objective is to apply k_r normalization techniques on available gas/oil k_r data for one condition to calculate gas/oil k_r for another condition and to examine the effect of absolute permeability, wettability, and IFT on the results of this technique.

6.1 Introduction

The relative permeabilities (k_r) are crucial flow functions governing the fluid distribution within and production from the petroleum reservoirs under various oil recovery methods. To obtain these vital reservoir parameters, conventionally, it is required to take rock samples from the reservoir and perform appropriate laboratory measurements. Although k_r is expressed as a function of fluid saturation, it is now well-known that k_r values are affected by pore structure and distribution, absolute permeability, wettability, IFT, and saturation history. These rock/fluid properties often change from one region of the reservoir to another, but it would be impossible to perform k_r measurements for all areas of a reservoir. Performing experiment on a core with higher permeability is faster and easier than a low permeability rock. Therefore, assuming all other parameters such as wettability, IFT, and displacement direction are the same for two rocks with different permeability, the question is, how to estimate the k_r of a rock with lower permeability from available (measured) k_r of a higher permeability rock? How to account for wettability and IFT differences? A normalization technique has been proposed to remove the effect of irreducible water and trapped saturations, which would be different under different conditions. The relative permeabilities can then be denormalized and assigned to different regions (rock types) of the reservoir based on their own irreducible water and trapped saturations.

The objective of this study is to predict the gas/oil k_r for a new rock/fluid conditions (such as permeability, wettability, and IFT) using existing gas/oil k_r data measured at different conditions. By use of measured data from coreflood experiments, it was shown that by applying an appropriate normalization technique one can adequately predict k_r of rocks with different permeability and wettability conditions in two-phase gas/oil flow. To improve the methodology, a new hypothesis is introduced and proposed here based on Dynamic Trap Saturation. Finally, the aim is to devise ways and means of estimating relative permeabilities, using available k_r data of one set of rocks and relevant fluid conditions, for different rocks and conditions. The two-phase gas/oil relative permeabilities for two Clashach sandstone cores with similar pore size distribution and absolute permeability of 65 mD and 1000 mD, under mixed-wet (MW) and water-wet (WW) conditions, with low and high gas/oil IFT have been measured. The experimental data together with the computer program presented in Chapter 3 were used to obtain two-phase k_r for the two cores and at different conditions.

6.2 Theory & Methodology

Generally, one could define relative permeability as the ratio of the conductance of a continuous phase, in a connected path filled by that phase, to the total conductance of the porous media. Therefore, the relative permeability of one phase represents the contribution of the flow of that phase to the total flow. Having said that in the displacement processes, some parts of existing phases are not mobile, and they do not have any contribution to flow until they join a continuous-flowing path. Therefore, in any phase distribution, there are two types of saturations; mobile and immobile saturations. Of course, only the mobile fluids contribute to flow and production. The critical parameters that affect relative permeability are absolute rock permeability, wettability, IFT, and hysteresis, which control the fluid distribution within the porous media. The immobile fluids within the pore space of the rock restrict the path available for fluid flow of the mobile fluids. Therefore, immobile fluid saturation is a key parameter in defining relative permeability. Eq. 6-1 describes this fact, in which immobile saturation of any fluid is expressed as a function of other fluid saturations (*S*), absolute rock permeability, wettability, IFT, and hysteresis behaviour.

$$S_{immobile} = S_{immobile}\left(S, k, wettability, IFT, hysteresis\right) \qquad 6\text{-}1$$

Normalization techniques have been proposed to account for the effect of irreducible water and trapped saturations, which would be different under different conditions. The traditional normalization technique (Mawla & Al-Saadoon (1978)) can be presented as

$$S_{in} = \frac{S_i - S_{ir}}{1 - S_{wr} - S_{or} - S_{gr}} \quad , i\text{=oil, gas, water} \qquad 6\text{-}2$$

Where S_{in} is the normalized saturation for phase *i*, S_i is the phase saturation at any time, and S_{ir} is the residual (immobile) saturation for each phase attained at the end of displacement.

In this study, it is assumed that using the normalized saturation and the relevant irreducible and residual saturations the k_r under new conditions could be estimated from existing k_r at different conditions.

Improved Normalization Technique

To improve the current normalization technique, this study proposes a new hypothesis based on the concept of *Dynamic Trapped Saturation*. At any time, the total saturation

of each phase is the sum of immobile and mobile components of that phase's saturation, where:

$$S_i = S_i^{mobile} + S_i^{immobile} \quad 6\text{-}3$$

For example, in the two-phase flow process of water displacing gas, at any point in time, the in-situ gas has two parts, one mobile, and the rest is immobile. Both mobile and immobile saturations change as the displacement progresses (Land (1968) and Carlson (1981)). At the end of the water injection (when no more gas is produced) the mobile portion is zero, and the immobile portion is equal to the final trapped gas. This final trapped gas is equivalent to the possible maximum trapped gas for that system. It is visualized that initially, at the start of water injection, the trapped (immobile) gas saturation is zero, but as the injection proceeds, it increases. In other words, the trapped component of the gas is dynamic and increases during the process of displacement. It is called 'dynamic trapped gas saturation'. This concept is applied to any non-wetting phase that is being displaced by a wetting phase (i.e., in imbibition processes). In the conventional normalization technique, the maximum trapped saturation, which is also called residual saturation is used, Eq. 6-2. A modified version of that equation, replacing the final trapped saturation values by dynamic ones, is:

$$S_{in}^{dynamic} = \frac{S_i - S_{irt}}{1 - S_{wrt} - S_{ort} - S_{grt}} \quad 6\text{-}4$$

Here the subscript *i* refers to a non-wetting phase (gas in the example mentioned above), *t* for dynamic trapped saturation or trapped saturation of each phase at corresponding S_i.

To estimate the immobile portion of fluid at any point in the flow process, several researchers have proposed trapping models such as Land (1968) and Spiteri et al. (2008) models. Spiteri et al. (2008) demonstrated in their research work that the Land model was only applicable to water-wet systems. They proposed a new model that apply to any wettability condition. The relationship between the initial saturation and trapped saturation in their model is defined as

$$S_{gt}\left(S_{gi}\right) = \alpha S_{gi} - \beta S_{gi}^2 \quad 6\text{-}5$$

Where, subscript *i* is for initial, and *t* stands for maximum trapped (not dynamic) gas saturation corresponding to an initial gas saturation and α and β correspond to the initial slope and the curvature of the curve of S_{gt} versus S_{gi} respectively. The flowing gas saturation at any value of S_g is calculated from the following equation.

$$S_{gf} = \frac{1}{2\beta}\left[(\alpha - 1) + \sqrt{(\alpha - 1)^2 + 4\beta\left(S_g - S_{gt} + \gamma\left(S_g - S_{gt}\right)\left(S_g - S_{gi}\right)\right)}\right] \quad 6\text{-}6$$

where γ is a tuning parameter for oil-layer drainage mechanism.

They have optimized α and β parameters using the pore-network simulation data. The optimization was performed for all contact angles and resulted in the following constraints; $0 \leq \alpha \leq 1$ *and* $\beta \geq 0$. They have plotted the optimal parameters α and β as functions of the intrinsic contact angle which is shown in Figure 6-1.

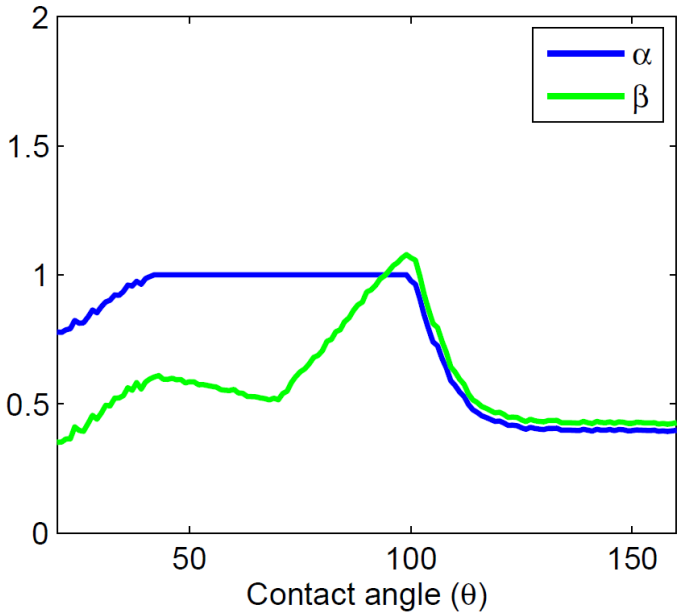

Figure 6-1: Optimal parameters α and β as functions of the intrinsic contact angle (after Spiteri et al. 2005).

Although, these models have been developed for imbibition process and for estimating trapped-fluid saturation of the non-wetting phase in a two-phase system, Spiteri et al. (2008) model, which was designed for all ranges of wettability, was used for calculating trapped saturations for drainage experiments too.

6.3 Experiments

To assess the validity of the normalization procedure (Eq. 6-2), the two-phase gas/oil experiments summarized in Table 6-1 were used. Six gas injections were performed on 65 and 1000 mD water-wet and mixed-wet core at two IFT conditions of 0.4 and 2.7 mNm^{-1}. More details on each experiment are provided in the following subsections and can be found in Sohrabi et al. (2007) and Fatemi et al. (2012 & 2015).

Table 6-1: summary of two-phase unsteady-state coreflood experiments.

Experiment No.	*Core Permeability /mD*	*Wettability*	*IFT g/o /mNm^{-1}*	*Initial Saturations*	*Maximum Residual Oil Saturation*
1	65	Water-Wet	0.04	S_{oi}=0.82, S_{wir}=0.18	S_{or}=0.14
2	65	Mixed-Wet	0.04	S_{oi}=0.82, S_{wir}=0.18	S_{or}=0.16
3	1000	Water-Wet	0.04	S_{oi}=0.92, S_{wir}=0.08	S_{or}=0.034
4	1000	Mixed-Wet	0.04	S_{oi}=0.92, S_{wir}=0.08	S_{or}=0.046
5	1000	Water-Wet	2.7	S_{oi}=0.92, S_{wir}=0.08	S_{or}=0.11
6	1000	Mixed-Wet	2.7	S_{oi}=0.92, S_{wir}=0.08	S_{or}=0.25

***Experiments 1 and 2**:*

The experiments were conducted on the 65 mD water-wet and mixed-wet cores respectively under near miscible conditions (gas/oil IFT of 0.04 mNm^{-1}) at 1840 psia. The gas injection started at the rate of 50 cm^{3}h^{-1}, and the injection rate was increased to 100 cm^{3}h^{-1} until the end of the test. The reason for increasing the injection rate (bumped flood) in this and other tests was basically to increase the range of saturation for which relative permeability can be obtained from history matching of these displacement experiments.

***Experiments 3and 4**:*

These experiments were conducted on the 1000 mD water-wet and mixed cores under near miscible conditions. The core initially contains 92% oil and 8% irreducible water. The gas injection was performed at the rate of 200 cm^{3}h^{-1}.

***Experiments 5 and 6**:*

These experiments were conducted on the 1000 mD water-wet and mixed-wet cores under immiscible conditions (gas/oil IFT of 2.7 mNm^{-1}) at 1215 psia. The gas injection was performed at the rate of 200 cm^{3}h^{-1}.

6.4 Results & Discussion

The k_r at two different conditions of interest were measured and the residual saturations for each experiment were calculated based on material balance. Eq. 2 and the relevant residual saturations were used to present relative permeability for condition 1 based on normalized saturation. To estimate k_r for condition 2, the saturation should be de-normalized using the corresponding residual saturations. In this study, as the measured

k_r at condition 2 is available, it is possible to compare the estimated versus measured relative permeabilities and evaluate the performance of normalization technique.

6.4.1 Effect of absolute permeability

The aim in this subsection is to use a normalization technique and estimate k_r for a low permeability core from the measured kr of a high permeability core. The wettability and IFT conditions are the same between two cores.

6.4.1.1 Water-wet and Low IFT conditions

The gas/oil k_r were obtained from the two gas injection tests (Experiments 1 and 3) performed on the 65 mD and 1000 mD water-wet cores saturated with oil and irreducible water at low gas/oil IFT conditions. The two-phase relative permeabilities were obtained after history matching the experimental data. Figure 6-2(a) shows the relative permeabilities versus gas (non-wetting phase) saturation obtained from history matching for both tests on a semi-log plot. Then, the k_r from 1000 mD core is used, and the normalization technique is applied to estimate k_r for 65 mD core. Figure 6-2(b) and Table A-1 (Appendix A) compare the estimated and measured gas/oil k_r for the 65 mD core which presents a reasonable match between them. In other words, if the only available k_r data is for 1000 mD water-wet rock at IFT of 0.04 mNm^{-1}, and the k_r data of 65 mD for water-wet conditions and at the same IFT value is required for the reservoir simulation purposes, the above method can be used to obtain a rough, but reasonable estimate of the required relative permeabilities. These will definitely be much better than any other guess made for input to the simulator.

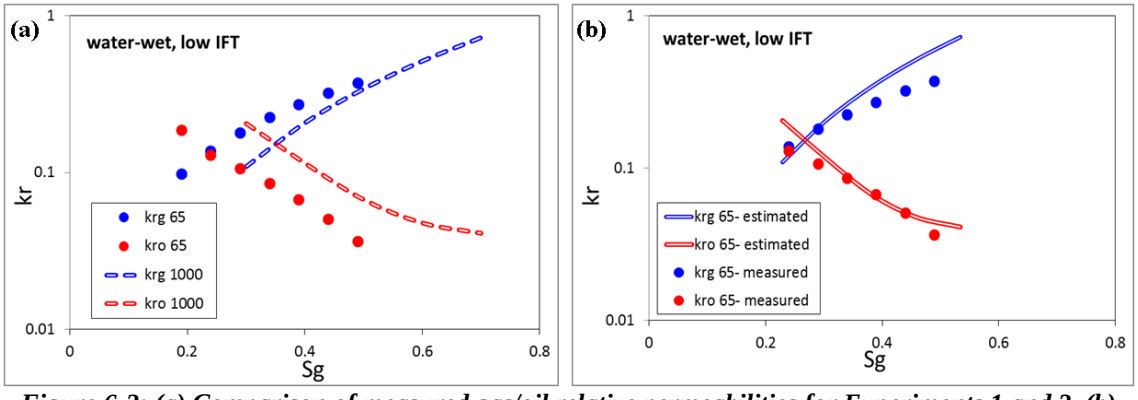

Figure 6-2: (a) Comparison of measured gas/oil relative permeabilities for Experiments 1 and 3. (b) Comparison between measured and estimated gas/oil relative permeabilities for 65 mD water-wet core. Measured gas/oil relative permeabilities of 1000 mD water-wet core were used in estimation.

Mixed-wet and Low IFT conditions

The comparison between measured gas/oil k_r for two gas injection tests (Experiments 2 and 4) conducted on 65 mD and 1000 mD cores, under mixed wettability and low gas/oil IFT conditions is presented in Figure 6-3(a). By applying the normalization technique, it was possible to estimate k_r for the 65 mD mixed-wet core from the measured k_r of 1000 mD mixed-wet core. Figure 6-3(b) and Table A-2 (Appendix A) compare the measured and estimated k_r for 65 mD core. In other words, in the complete absence of gas/oil k_r curves for the 65 mD core, one could use the said normalization technique to obtain a rough, but reasonable, estimate for relative permeabilities using the available k_r curves of the 1000 mD core.

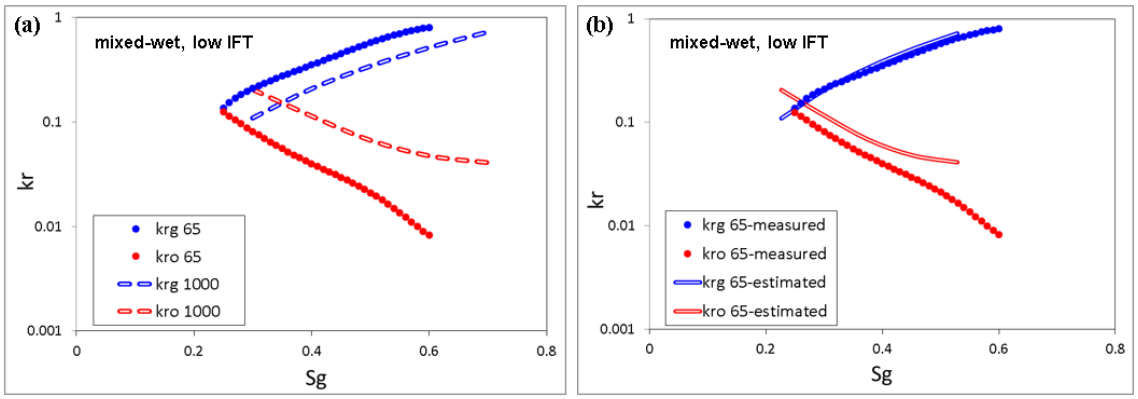

Figure 6-3: (a) Comparison of measured gas/oil relative permeabilities for Experiments 2 and 4. (b) Comparison between measured and estimated gas/oil relative permeabilities for 65 mD mixed-wet core. Measured gas/oil relative permeabilities of 1000 mD mixed-wet core were used in estimation.

6.4.2 Effect of wettability

The normalization technique is used to estimate k_r for a mixed-wet core from measured kr of a water-wet core while the permeability and IFT conditions are the same for the two cores.

65 mD and Low IFT conditions

Figure 6-4(a) depicts measured gas/oil relative permeabilities for 65 mD core at two different wettability conditions of water and mixed-wet (Experiments 1 and 2). Using normalization, gas/oil k_r at mixed-wet condition was estimated from k_r of water-wet core and as Figure 6-4(b) and Table A-3 (Appendix A) show there is a reasonable agreement between measured and estimated relative permeabilities.

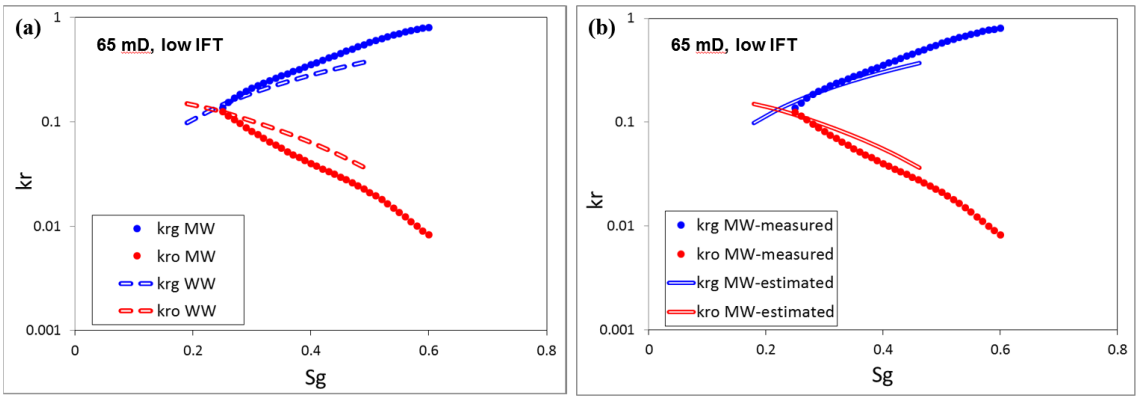

Figure 6-4: (a) Comparison of measured gas/oil relative permeabilities for Experiments 1 and 2. (b) Comparison between measured and estimated gas/oil relative permeabilities for 65 mD mixed-wet core. Measured gas/oil relative permeabilities of 65 mD water-wet core were used in estimation. MW =mixed-wet; WW=water-wet.

1000 mD and Low IFT conditions

The relative permeabilities obtained from history matching of experimental data for both tests (Experiments 3 and 4) are in very close agreement (Figure 6-5). These results highlight that at high permeability and low IFT conditions the effect of wettability on the flow of fluids in porous media can be less pronounced because the capillary force at pore scale is very minimal which leads to insignificant residual saturation. Hence, the k_r of the water-wet core is also representative of that of the mixed-wet core for low IFT and high permeability systems. In other words, if the rock is highly permeable, and the reservoir is operated at high pressure (i.e., the gas/oil IFT value is low), one could neglect the effect of wettability and use the relative permeabilities obtained under one wettability condition for another one, without incurring significant errors.

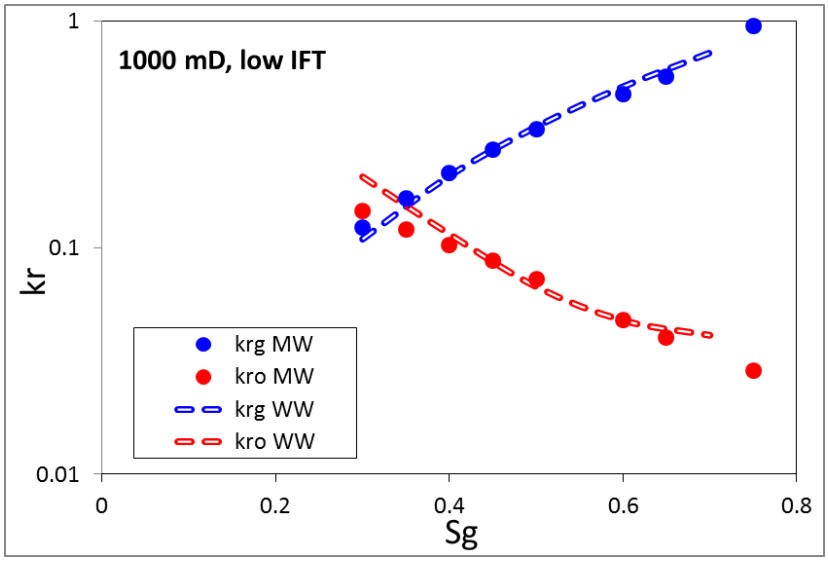

Figure 6-5: Comparison of measured gas/oil relative permeabilities for Experiments 3 and 4. MW = mixed-wet; WW = water-wet.

1000 mD and High IFT conditions

Although gas/oil relative permeabilities for 1000 mD core at low IFT conditions were almost identical for water-wet and mixed-wet wettability conditions, at high IFT conditions (Experiment 5 and 6) there is a considerable difference between relative permeabilities at different wettabilities (Figure 6-6(a)). Applying the normalization technique, the k_r at mixed-wet conditions were estimated from the k_r at the water-wet condition with a good agreement to the measured k_r (Figure 6-6(b) and Table A-4).

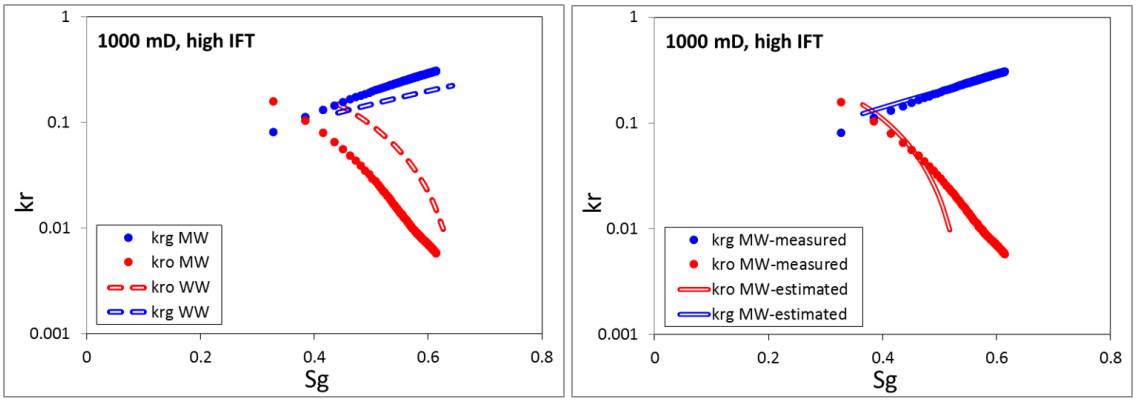

Figure 6-6: (a) Comparison of gas/oil relative permeabilities for Exp#5 and 6. (b) Comparison between measured and estimated gas/oil relative permeabilities for 1000 mD mixed-wet core. Measured gas/oil relative permeabilities of 1000 mD water-wet core were used in estimation.

6.4.3 Effect of gas/oil IFT

The effect of IFT on k_r has been studied by several researchers and different results, and conclusions have been published in the literature which has been presented in Chapter 5. Moreover, the current state of the art for IFT scaling has been presented in Chapter 5. The normalization technique is used to estimate k_r at low IFT conditions from measured k_r at high IFT conditions while the permeability and wettability are the same between two cores.

1000 mD and water-wet wettability

The gas/oil relative permeabilities measured by conducting two experiments (Experiments 3 and 5) on a 1000 mD water-wet core saturated with oil and irreducible water at different IFT conditions (0.04 and 2.7 mNm-1). Figure 6-7(a) compares these relative permeabilities. The normalization technique was used to estimate k_r at low IFT conditions from the k_r at high IFT conditions, but the result was not promising (Figure 6-7(b)). For 1000 mD mixed-wet core, the same practice was performed between relative permeabilities of low and high IFT conditions but normalization technique was not able to estimate k_r at different IFT conditions. As it was concluded in Chapter 5, gas/oil IFT affects both relative permeabilities and their curvatures but not equally. This

can be one of the reasons that normalization technique did not work to capture the effect of IFT.

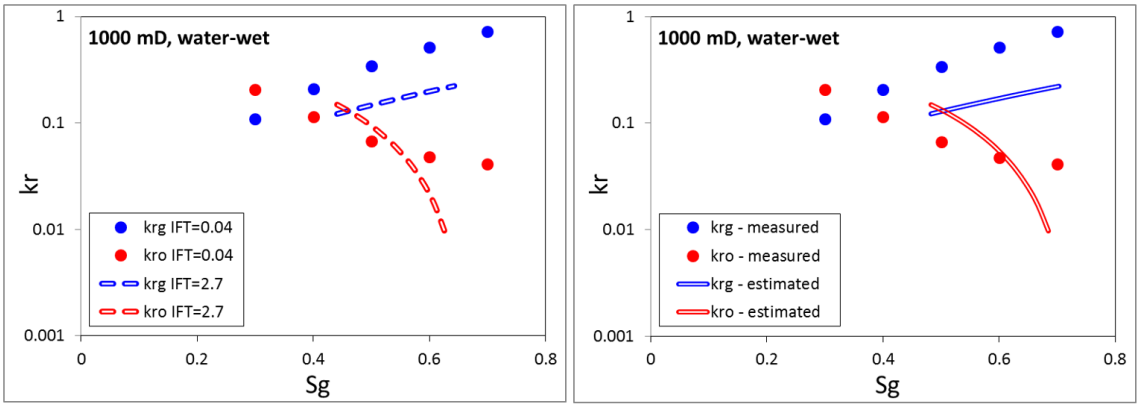

Figure 6-7: (a) Comparison of gas/oil relative permeabilities for Experiments 3 and 5. (b) Comparison between measured and estimated gas/oil relative permeabilities for 1000 mD water-wet core at low IFT. Measured gas/oil relative permeabilities of 1000 mD water-wet core at high IFT were used in estimation.

6.4.4 Application of Dynamic Trap Saturation

The normalization method using dynamic trapped saturation would be beneficial if the maximum trapped saturation is significant, which would result in considerable variation in trapped saturation at different times during the displacement process. To assess the validity of the above method using dynamic trapped saturation in normalisation equation (Eq.6-2), those experiments which exhibit high maximum trapped saturation at the end of displacement were selected. The two-phase experiments used in this investigation are Experiments 1 and 2. The following equation was used for calculating dynamic normalization of the gas saturation.

$$S_{gn}^{dynamic} = \frac{S_g}{1 - S_{wir} - S_{ort}} \qquad 6\text{-}7$$

Since the wettability varies in the above-selected sets of experiments, the Spiteri et al. (2008) trapping model is used as it has been proposed for all types of wettability conditions (not limited to water-wet). According to the introduced optimal value for α as the function of contact angle, for a water-wet rock, this parameter should be around 1. The β parameter was calculated 0.99 from Eq. 6-5 and γ parameter was tuned to 1.1 using Eq. 6-6 and the maximum trapped saturation value of 0.14 for the water-wet core. Figure 6-8(a) shows the calculated trapped oil saturation during the displacement experiment in the water-wet core. The calculated dynamic trapped saturation has been used in the normalization formula and k_r for mixed-wet core estimated accordingly. Figure 6-8(b) depicts much better agreement between measured and estimated relative

permeabilities when the dynamic trapped saturation was used in the normalization technique. More experimental data are required to perform a comprehensive evaluation of the proposed method.

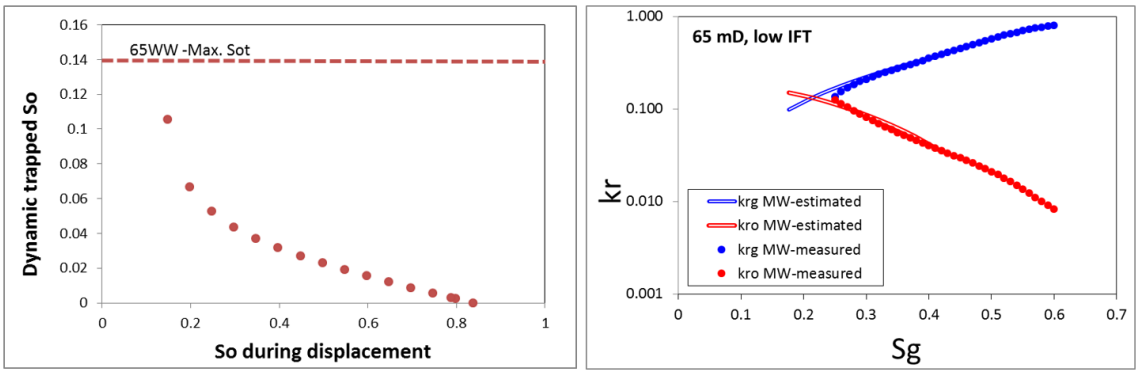

Figure 6-8: (a) Dynamic trapped oil saturation versus oil saturation for Experiments 1 and 2. (b) Comparison between measured and estimated gas/oil relative permeabilities for 65 mD mixed-wet core. Measured gas/oil relative permeabilities of 65 mD water-wet core and dynamic trap saturations were used in estimation.

6.5 Conclusions

The main conclusions drawn from this study for two-phase gas/oil systems are as follows:

1. The results of two-phase gas/oil systems confirm that the two-phase gas/oil k_r of a high permeability rock (1000 mD) may predict the performance of two-phase gas injection test in a lower permeability (65 mD) rock. Hence, if there is no directly measured two-phase k_r available on a low permeability rock but it is available for a higher permeability rock (of similar lithology), the two-phase k_r of the high permeability rock could be used instead, as an approximation. In this case, it would be preferable to express the high permeability k_r data in terms of normalized saturation and use the results for the low permeability rock if reasonably accurate estimates of irreducible water and trapped fluid saturations are available. This practice would be recommended for the case with different wettability.
2. However, the effect of gas/oil IFT change cannot be captured using conventional normalization technique. Application of modified Coats (1980) method which was presented in Chapter 5 can help to capture the effect of gas/oil IFT on k_r.
3. Applying modified normalization method (based on dynamic trap model) predicts relative permeability more accurately for some cases. An extensive set

of experimental data is required to evaluate the performance of this method properly.

4. In general, the normalization technique can provide a simple tool to a practicing reservoir engineer to have a better estimate for the k_r curves which there is no laboratory measurement.

6.6 References

Carlson, F. M., 1981: "Simulation of Relative Permeability Hysteresis to the Nonwetting Phase". SPE Annual Technical Conference and Exhibition. San Antonio, Texas, Society of Petroleum Engineers of AIME.

Coats, K. H., 1980: "An Equation of State Compositional Model", SPE Journal 20(5): 363-376.

Fatemi, S. M., Sohrabi, M., Jamiolahmady, M. Ireland, S., and Robertson, G., 2011. Experimental Investigation of Near-Miscible Water-Alternating-Gas (WAG) Injection Performance in Water-wet and Mixed-wet Systems, SPE Offshore Europe Oil and Gas Conference and Exhibition, Aberdeen, UK, Society of Petroleum Engineers.

Fatemi, S. M., Sohrabi, M., Ireland, S., and Jamiolahmady, M., 2012. Recovery Mechanisms and Relative Permeability for Oil/Gas System at Near-miscible Conditions: Effects of Immobile Water Saturation, Wettability, Hysteresis and Permeability, SPE Improved Oil Recovery Symposium. Tulsa, Oklahoma, USA, Society of Petroleum Engineers.

Fatemi, S. M. and Sohrabi, M., 2015. Mechanistic Study of the Effect of Gas/Oil IFT on the Performance of Gas, WAG and SWAG Injections in Mixed-Wet Systems. SPE Annual Technical Conference and Exhibition held in Houston, Texas, USA, 28–30 September 2015.

Land, C. S., 1968. Calculation of Imbibition Relative Permeability for Two- and Three-Phase Flow from Rock Properties", presented at SPE 42nd Annual Fall Meeting held in Houston, Texas, Oct. 1-4, 1968.

Mawla, R. A. and Al-Saadoon, F. T., 1978. Normalization Techniques and Interpretive Practices of Relative Permeability Curves of Reservoir Rocks. SPWLA Nineteenth Annual Logging Symposium, June 13-16, 1978. Society of Petrophysicists and Well-Log Analysts.

Sohrabi, M., Tehrani, D. H., and Al-Abri, M., 2007. Performance of Near-Miscible Gas and SWAG Injection in a Mixed-Wet Core. International Symposium of the Society of Core Analysts, SCA2007-26, Calgary, Canada.

Spiteri, E. J., 2005. Relative Permeability Hysteresis: A new Model and Impact on reservoir Simulation. Master Thesis.

Spiteri, E. J., Juanes, R., Blunt, M. J., and Orr, F. M., 2008. A New Model of Trapping and Relative Permeability Hysteresis for All Wettability Characteristics, SPE Journal 13(3): pp. 277-288.

Chapter 7-Conclusions, Recommendations, and Future Works

Relative permeability and capillary pressure are two crucial parameters in multiphase flow which describe the distribution and flow of each fluid in porous media. The importance of these flow functions will be even more significant for three-phase flow systems. This thesis attempted to address three key questions.

(i) How to accurately obtain multi-phase flow functions?

A methodology was devised for calculating k_r values and in particular three-phase k_r from unsteady-state experiments. The effort was extended to simultaneously calculating capillary pressure from the same coreflood experiment.

(ii) What are the physical parameters which can affect flow functions?

There are different physical parameters which can affect flow functions. Effect of gas/oil interfacial tension ($IFT_{g/o}$) on two and three-phase relative permeability and also on residual saturation during alternative water and gas injections was studied.

(iii) How to predict flow functions?

It was attempted to predict two-phase relative permeability for a certain rock and fluid conditions when there is no available measured data for that conditions. A methodology was introduced to use available data for different conditions than the conditions of interest and estimate relative permeability reasonably well.

In this chapter, a summary of the drawn conclusions from previous chapters and some recommendations for possible future research works are presented.

Chapter 3

A computer program was developed as an optimization tool to obtain two- and three-phase k_r from unsteady-state coreflood experiments. An optimization algorithm was implemented to minimize the differences between the experimental data and the results of numerical simulation through a process of a history matching. The main purpose was to provide an automatic history matching tool for researchers, practicing reservoir engineers, and petrophysicists to obtain two- and three-phase relative permeabilities from the corresponding two- and three-phase coreflood experiments. To the best of our knowledge, the current commercial softwares work for two-phase experiments, and

there is no commercial software in the oil industry for calculating three-phase relative permeabilities from unsteady-state coreflood experiments. Two and three-phase unsteady-state coreflood experiments were history matched successfully, and the estimated two and three-phase relative permeabilities were presented in this thesis.

Using this approach, some of the limitations of analytical methods like JBN has been overcome. P_c can be included in the process of k_r calculation, and its associated effects are accounted. Moreover, as the developed tool is linked to a commercial reservoir simulator, all the state of the art formulations available in the current commercial simulators can be used for properly simulating the coreflood experiments.

The tool is equipped with a global optimizer and appropriate and flexible functional representations of k_r. GA has been employed in the optimizer which minimizes the possible trapping of the best solution in the local minimum solutions. In addition to the power-law model, the versatile model of LET was employed for kr curves.

Chapter 4

A new methodology was introduced to estimate k_r and P_c using the results of a coreflood experiment and assuming that k_r was interrelated with P_c. The P_c was defined as a function of saturation with some tuning parameters, and the k_r was then calculated from this P_c. For comparison, the conventional approach of simultaneous estimation of k_r and P_c was also utilized. In the conventional approach k_r and P_c are two independent functions and, to reduce the uncertainty, some in-situ measurements are included in the history matching. The results of the new method were compared with the conventional approach. The results demonstrated that simultaneous P_c and k_r estimation through the interrelated approach introduced in this work improves the accuracy of estimated k_r and P_c. The number of tuning parameters decreased in the history matching when k_r is assumed to be related to P_c. Having fewer tuning parameters in the history matching may help to reduce the non-uniqueness problem associated with the history matching process,

The simultaneous estimation of k_r and P_c has a high degree of uncertainty and to reduce this, it would be recommended to use as much data as possible in the process of history matching. Inclusion of in-situ measurements, e.g. saturation profile in the process of history matching will reduce the degree of uncertainty, and the estimated flow functions will be more accurate.

Chapter 5

The effect of gas/oil IFT reduction on two- and three-phase relative permeabilities has been investigated using our two- and three-phase coreflood displacement experiments. In a two-phase system, the relative permeability of both phases increases as the IFT decreases, but not equally. As the system moves from immiscible toward miscible conditions, the relative permeability increases, the residual oil saturation decreases, and the k_r curvature reduces. The k_{ro} was affected by IFT reduction mainly at low saturation values while the k_{rg} was affected in the whole range of saturation. In a three-phase system, the gas/oil IFT reduction affects the relative permeability of all three phases, $k_{ro,}$ and k_{rg} increase while k_{rw} decreases at low values of water saturation.

The current practice for two-phase k_r IFT scaling was examined using the measured data. Using Coats method as the IFT scaling method should be done cautiously, and non-equal effects on k_{ro} and k_{rg} should be considered. Application of separate weighing factor for oil and gas in the Coats method is recommended to alleviate the problem, although the method still could not accurately estimate the residual fluid saturations.

Furthermore, the effect of gas/oil IFT on residual oil saturation change during WAG injections at immiscible (high gas/oil IFT) and near-miscible (very low gas/oil IFT) conditions in laboratory scale was evaluated. There is little information in the literature concerning the performance of WAG injection at ultra-low gas/oil IFT (near-miscible) conditions. However, based on data gathered in this thesis, the performance of near-miscible WAG (ultra-low gas/oil IFT) is generally better than that of immiscible WAG (high gas/oil IFT). In the majority of the research studies on immiscible WAG injection, presented in this study, the main reduction in residual oil saturation is achieved in the first cycle, and further WAG injection cycles do not have a significant contribution to oil recovery. Moreover, the immiscible WAG-DI experiments have higher oil recovery than WAG-ID for both water-wet and mixed-wet systems.

Chapter 6

A new methodology was introduced based on normalization concept to predict the gas/oil k_r for a new rock/fluid conditions (such as permeability, wettability, and IFT) using existing gas/oil k_r data measured at different conditions. Using of measured data from coreflood experiments, it was shown that one can adequately predict k_r of rocks with different permeability and wettability conditions in two-phase gas/oil flow.

Application of dynamic trap saturation in normalization technique has improved the methodology.

The results of two-phase gas/oil systems confirm that the two-phase gas/oil k_r of a high permeability rock (1000 mD) may predict the performance of two-phase gas injection test in a lower permeability (65 mD) rock. Hence, if there is no directly measured two-phase k_r available on a low permeability rock but it is available for a higher permeability rock (of similar lithology), the two-phase k_r of the high permeability rock could be used instead, as an approximation. This practice would be recommended for the case with different wettability. However, the effect of gas/oil IFT change cannot be captured using conventional normalization technique. In general, the normalization technique can provide a simple tool to a practicing reservoir engineer to have a better estimate for the k_r curves which there is no laboratory measurement.

Recommendations and Future Works

- The estimated three-phase k_r from unsteady-state coreflood experiments should be compared against measured k_r from steady-state experiments for similar saturation direction, fluid and rock system.
- The performance of the automatic history matching depends on the simulator, functional form of flow function (e.g., k_r) and the optimization method. Global optimization methods are strongly recommended to be used for the history matching purpose. In this study, we have used GA, which is a global optimizer. However, it is recommended to evaluate the performance of stochastics methods such as Ensemble Kalman based methods. Ensemble smoother with Multiple Data Assimilation (MDA) is one of the promising optimization methods among ensemble-based methods. Using Stochastic methods leads to obtaining a confidence interval for the estimated flow functions.
- A set of laboratory measured P_c is required to investigate the concept of dynamic P_c properly. The significance of differences between dynamic and static P_c should be elaborated.
- In general, the simultaneous estimation of k_r and P_c is practical when capillary forces are significant in comparison with viscous forces during a dynamic corefood experiment. Therefore, the physical and experimental conditions in which this method can be applied should be investigated.

- The application of the simultaneous estimation of interrelated k_r and P_c should be evaluated for imbibition processes and different wettability conditions as well.
- Further investigations are required to understand the influence of gas/oil IFT variations on three-phase k_r.
- The existing IFT scaling models for two-phase systems should be improved based on the correct understanding of effect of IFT on each k_r curve (curvature and residual saturation) separately.
- The Normalization Technique has been evaluated for gas/oil two phase system. It is required to extend this evaluation to gas/water and oil/water system.
- The application of Normalization Technique should be investigated for three-phase flow systems. Most of the existing three-phase k_r models are not capable of predicting relative permeability and it is worth to investigate the capability of normalization technique.
- The application of dynamic trapping in Normalization Technique can be evaluated having more measured relative permeability data.

APPENDICES

Appendix A: Measured and Estimated k_r in Chapter 6

Table A-1: Comparison between measured and estimated gas/oil relative permeabilities for 65 mD water-wet core. Measured gas/oil relative permeabilities of 1000 mD water-wet core were used in estimation.

	Measured		Estimated	
Sg	krg	kro	krg	kro
0.240	0.138	0.129	0.124	0.192
0.290	0.179	0.106	0.188	0.133
0.340	0.224	0.085	0.269	0.093
0.390	0.270	0.067	0.361	0.065
0.440	0.319	0.050	0.474	0.052
0.490	0.371	0.036	0.603	0.045

Table A-2: Comparison between measured and estimated gas/oil relative permeabilities for 65 mD mixed-wet core. Measured gas/oil relative permeabilities of 1000 mD mixed-wet core were used in estimation.

	Measured		Estimated	
Sg	krg	kro	krg	kro
0.250	0.137	0.125	0.140	0.177
0.260	0.154	0.114	0.153	0.165
0.270	0.169	0.105	0.166	0.153
0.280	0.184	0.096	0.179	0.141
0.290	0.198	0.088	0.192	0.129
0.300	0.211	0.081	0.205	0.117
0.310	0.223	0.075	0.222	0.110
0.320	0.236	0.069	0.240	0.104
0.330	0.248	0.064	0.257	0.097
0.340	0.261	0.060	0.275	0.091
0.350	0.275	0.056	0.293	0.085
0.360	0.289	0.052	0.311	0.078
0.370	0.303	0.048	0.328	0.072
0.380	0.319	0.045	0.347	0.067
0.390	0.335	0.043	0.370	0.064
0.400	0.352	0.040	0.393	0.062
0.410	0.370	0.038	0.416	0.059
0.420	0.389	0.035	0.439	0.056
0.430	0.409	0.033	0.461	0.054
0.440	0.431	0.031	0.484	0.051
0.450	0.453	0.030	0.507	0.049
0.460	0.476	0.028	0.533	0.047
0.470	0.499	0.026	0.561	0.046
0.480	0.524	0.024	0.589	0.045
0.490	0.549	0.023	0.617	0.045
0.500	0.574	0.021	0.645	0.044
0.510	0.600	0.019	0.673	0.043
0.520	0.625	0.018	0.701	0.042

Table A-3: Comparison between measured and estimated gas/oil relative permeabilities for 65 mD mixed-wet core. Measured gas/oil relative permeabilities of 65 mD water-wet core were used in estimation.

	Measured		Estimated	
Sg	krg	kro	krg	kro
0.250	0.137	0.125	0.159	0.118
0.260	0.154	0.114	0.168	0.113
0.270	0.169	0.105	0.176	0.108
0.280	0.184	0.096	0.186	0.103
0.290	0.198	0.088	0.195	0.099
0.300	0.211	0.081	0.204	0.094
0.310	0.223	0.075	0.214	0.090
0.320	0.236	0.069	0.223	0.086
0.330	0.248	0.064	0.233	0.082
0.340	0.261	0.060	0.243	0.078
0.350	0.275	0.056	0.253	0.074
0.360	0.289	0.052	0.263	0.070
0.370	0.303	0.048	0.273	0.066
0.380	0.319	0.045	0.283	0.063
0.390	0.335	0.043	0.294	0.059
0.400	0.352	0.040	0.304	0.056
0.410	0.370	0.038	0.314	0.052
0.420	0.389	0.035	0.325	0.049
0.430	0.409	0.033	0.336	0.046
0.440	0.431	0.031	0.347	0.043
0.450	0.453	0.030	0.358	0.040
0.460	0.476	0.028	0.369	0.037

Table A-4: Comparison between measured and estimated gas/oil relative permeabilities for 1000 mD mixed-wet core. Measured gas/oil relative permeabilities of 1000 mD water-wet core were used in estimation.

	Measured		Estimated	
Sg	krg	kro	krg	kro
0.385	0.112	0.104	0.132	0.127
0.415	0.131	0.080	0.149	0.093
0.436	0.145	0.065	0.160	0.072
0.450	0.155	0.056	0.169	0.058
0.463	0.165	0.049	0.176	0.047
0.473	0.173	0.043	0.183	0.039
0.482	0.179	0.039	0.189	0.032
0.496	0.191	0.032	0.198	0.022
0.502	0.196	0.030	0.202	0.018
0.512	0.205	0.026	0.209	0.013
0.521	0.213	0.023	0.215	0.009
0.531	0.222	0.019	0.222	0.004
0.542	0.232	0.016	0.230	0.001
0.544	0.234	0.016	0.232	0.000

Appendix B: Sample Eclipse Data File for Coreflood Simulation Model

```
================================================================
RUNSPEC
================================================================

TITLE
THREE-PHASE GAS INJECTION

LAB
-- Cartesian system
CART

--Phases involved
OIL
WATER
GAS

FULLIMP

-- Stack size
NSTACK
 10 /

-- Dimension of the model is 100x1x1 gridblock
--        NX      NY      NZ
--        --      --      --
DIMENS
          100     1     1  /

TABDIMS
-- max no.   max. no.   max. no. max. no.    max. no.
--satn tab   pvt tab   satn node   pres node   FIP region

     1          1          200          50      3  8* 1
/

WELLDIMS
-- MAXWEL      MAXCON      MAXGRP   MAXWGP
-- max no.    max. no.    max. no.    max. no.
-- of well   connection    group well/gp

   20          50          10      3 /

MESSAGES
2* 10 6* 10000 /

-- Simulation start date
START
1 'SEP' 2012 /

-- Unified input and output files
UNIFIN
UNIFOUT
```

```
================================================================
GRID
================================================================
-- Request for Output geometry and rock properties
-- Size of each cell in X, Y and Z directions

EQUALS
DX    0.6/
DY    4.5/
DZ    4.5/

TOPS  1 /
/


-- Permeability in X, Y and Z directions for each cell

PERMX
100* PERMEABILITY/

PERMY
100* PERMEABILITY /

PERMZ
100* PERMEABILITY /


-- Porosity of each cell
PORO
100* POROSITY /


-- Output file with geometry and rock properties (.INIT)
INIT

================================================================
--- THE PROPS SECTION DEFINES THE REL. PERMEABILITIES, CAPILLARY
--- PRESSURES, AND THE PVT PROPERTIES OF THE RESERVOIR FLUIDS
================================================================

PROPS

--         Pref          Cr
ROCK
           125.17         1E-10 /

--
--         Oil        Water       Gas
DENSITY
            0.4       1.0000       0.2 /

PVTW
--Pref          Bw       Comp      Vw      Cv
  125.17      1.000      0      0.6819    0.0 /
```

```
PVDG
-- Dry Gas PVT Properties (No Vapourised Oil)
125.17     1                0.02
130        0.9999           0.02
/

PVDO
--
-- Dead Oil PVT Properties (No Dissolved Gas)
--
125.17     1                0.04
130        0.9999           0.04
/

INCLUDE
'kr.txt'/

--==============End props section==============================
REGIONS
=================================================================
SOLUTION
=================================================================
PRESSURE
 100*125.17 /

SGAS
 100*0 /

SWAT
100*0.50/


RPTRST
basic=2           NORST=1  VGAS VOIL  SOIL SGAS KRO KRG /

--=================================================================
SUMMARY
--=================================================================
RPTONLY
--Cumulative Oil Production
FOPT

--Cumulative Water Production
FWPT

--Cumulative Gas Production
FGPT

--Pressure at outlet (Production) and inlet (Injection)
WBHP
 /

-- Create Excel readable Run Summary file (.RSM)
RUNSUM
EXCEL
```

```
================================================================
SCHEDULE
================================================================
-- Location of wellhead and pressure gauge
--       Well  Well    Location    BHP     Pref.
--       name  group    I     J   datum    phase
--      -----  ----     -     -   -----    -----
WELSPECS
         PROD    G1    100   1     1*     OIL     /
         INJG     G2     1   1     1*     GAS     /

  /


-- Completion interval
--       Well    Location  Interval  Status  Trans
--       name     I    J    K1  K2   O or S
--       ----     -    -    --  --   ------  ------
COMPDAT
         PROD   100   1     1  1    O       1*     7845.465/
         INJG   1     1     1  1    O        1*   7845.465/

  /


-- Injection control (q1 is the injection and production rate)
--  Well  Fluid  Status  Control   Surf   Resv    Voidage   BHP
--  NAME  TYPE           mode     rate   rate  frac flag  limit
--  ----  -----  ------  -------   ----   ----  ---- ----  -----
WCONINJE

    INJG     GAS       OPEN    RESV     1*  q1    /

   /

WCONPROD

PROD  OPEN  RESV  4*   q1  1/
/

TSTEP

50*0.092
/


END
```